RETROACTIVITY TO THE OUTPUT OF TRANSCRIPTION DEVICES: QUANTIFICATION AND INSULATION

by

Shridhar Jayanthi

A dissertation submitted in partial fulfillment
of the requirements for the degree of
Doctor of Philosophy
(Electrical Engineering: Systems)
in The University of Michigan
2012

Doctoral Committee:

Professor James S. Freudenberg, Co-Chair
Associate Professor Domitilla Del Vecchio, Co-Chair
Professor Jessy W. Grizzle
Professor Alex J. Ninfa

To the *atithi* that may build upon these results.

ACKNOWLEDGEMENTS

I would like first to thank my advisor Prof. Domitilla Del Vecchio whose support, vision, incredible patience and remarkable intellectual brilliance were essential in providing the wonderful and pleasant environment I experienced during the course of this investigation.

I would also like to thank Prof. Alex Ninfa for teaching me how to conduct biological experimentation with the attention, patience, discipline and ethics required for productive science and for providing and a place for me to learn.

I would also like to thank my Prof. Jessy Grizzle and Prof. James Freudenberg for the feedback provided as members of my committee. I thank also Prof. Demosthenis Teneketzis and Prof. Ron Weiss for providing insight that was very helpful in my work.

I also thank my labmate Kayzad Nilgiriwala for helping me and keeping me sane during the long and often frustrating hours in the laboratory and my colleagues Rajeev Verma, Koushil Sreenath, Michael Hafner and Alessandro Colombo for giving me much valuable insights for the price of a beer.

I would also to thank Becky Turanski, Ann Pace and Beth Lawson from at the University of Michigan and Mieke Moran and Joe Gaken at the Massachusetts Institute of Technology for their kind assistance.

I must also mention Claudia Favaro, Ana Mattos, Mariko Burgin, Alexis Frank, Moises Escudero, Breno Braga, Jenny Lin, Emily Vogtmann, Higor Sales, Elizabeth

Christian, Daniel Schultz, Lucas Heitzmann and Kerin O'Toole for being amazing people and making sure I always had a smile on my face during the past 7 years.

Finally, I would like to thank my parents Kasi Annapurna and Udaya Bhaskaram, my brothers Shriram and Krishna and their wives, Poliana and Vanessa, whose continued and selfless support made this dissertation possible.

TABLE OF CONTENTS

LIST OF FIGURES

Figure

ABSTRACT

RETROACTIVITY TO THE OUTPUT OF TRANSCRIPTION DEVICES: QUANTIFICATION AND INSULATION

by
Shridhar Jayanthi

Co-chairs: James Freudenberg and Domitilla Del Vecchio

Traditional engineering often relies on hierarchical design techniques to build complex systems from simpler subsystems. This technique requires *modularity*, a property that states that the input/output characteristics of a system are not affected by interconnections. In this work we investigate *retroactivity*, an impedance-like effect in biomolecular systems that makes the behavior of a system change upon interconnection. We show, through analysis and experiments, that retroactivity in synthetic biology circuits is responsible for substantial changes in a system dynamic response. In order to construct circuits modularly, we propose the design of insulation devices, which, similar to insulating amplifiers in electronics, attenuate retroactivity effects and recover modular behavior. Our technique is based on a novel disturbance attenuation approach based on singular perturbation theory.

CHAPTER I

Introduction

Hierarchical design is a technique used in the design of complex systems in several engineered systems. In this technique, one designs a complex system as a composition of several subsystems which, in its turn, can be composed of even simpler subsystems. The subsystems with simplest specifications are then designed directly. Besides simplifying the design process, this method has the additional advantage that these atomic components may be reused in different contexts [1].

This methodology is based on the principle of breaking a complex design problem into several simpler problems. However, the integration of the sub-solutions into an integrated design may not be trivial if the sub-solutions are context sensitive. An example of challenges in this integration appears in dynamic programming algorithms, in which the impact of an optimal sub-solution on the optimality of the partial solution must be assessed in every iteration [2]. In engineering, integration becomes trivial when each part is *modular*, i.e., if the part obeys its specifications in a context-independent fashion. In software engineering, for example, modularity of components is achieved through the object-oriented paradigm [3]. In analog electrical circuits, modularity is achieved through careful design of low impedance output stages [4] while in digital electronics, suppliers state operating fan-out limitations for

modular behavior of parts [5].

Synthetic Biology is a field whose goal is to build biological machines employing engineering tools [6]. In this field, organisms are programmed using *biological circuits*, networks of genes, proteins, regulatory DNA elements and other signalling elements arranged to perform a specific task. The complexity of design of most elementary components in this domain is high and the hierarchical approach has been popular in the design of *biological parts* [7, 8, 9]. As such it is important to understand how modular are these biological parts and what are their limits [10]. It has been suggested that lack of modularity is responsible for differences in the behavior between *in vivo* and *in vitro* systems, which ultimately cause failures in biological design [11]. This lack of modularity can be caused by several reasons such as toxicity of recombinant proteins, non specific crosstalk between circuit and native elements or interference in the global metabolism.

In this work, we focus on the lack of modularity stemming from the nature of signalling elements responsible for carrying information. These elements, usually transcription factors or signalling proteins, suffer from the presence of loads in the form of DNA binding sites, other signalling proteins or substrates. These loads affect the signal carrier via binding interactions. This effect, which in biomolecular circuits is called *retroactivity* [12, 13], is illustrated in Figure 1.1a. When an upstream system is connected to a downstream system, perturbations on the upstream system may occur due to how the connection takes place. This retroactivity perturbation can be modelled as an additional signal from the downstream system to the upstream system. Retroactivity is unlike feedback because it is tied to the flow of information and therefore cannot be disconnected.

This type of effect from downstream systems to upstream is not unique to molec-

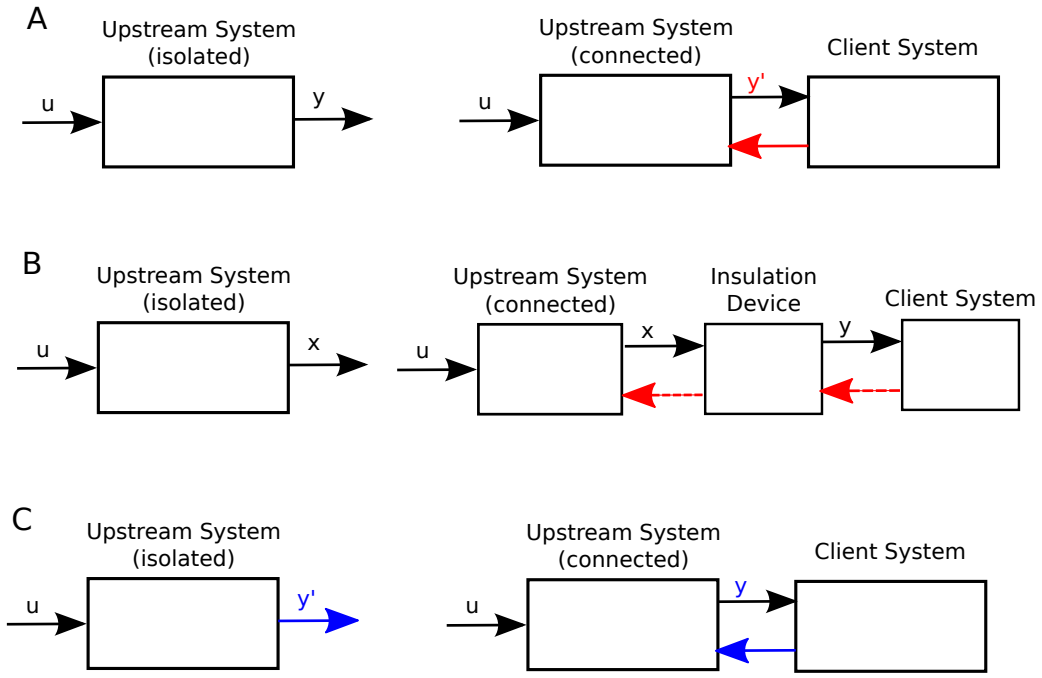

Figure 1.1: **Parasitic effect of retroactivity and strategies to mitigate its effect.** Assume there exists in a complex design two connected subsystems: an upstream system required to give an output signal y whenever input is u and and a client system that expecting input y. (A) Due to retroactivity, designing the upstream system assuming a non-existing modularity may lead to unexpected results as retroactivity may alter the output of the upstream system from y to y'. (B) One strategy to prevent this problem is by designing an insulation device, a device sitting in the interconnection. The insulation device relays the signal without generating retroactivity to the upstream system and mitigating retroactivity from the client. In this case, the design of the upstream is independent of any potential retroactivity from a downstream load. (C) Another solution to this problem is to design the upstream system in a manner that "pre-compensates" for retroactivity. In this case, retroactivity from a load becomes a part of the design of the upstream system. In this case, the re-usability of the upstream system becomes compromised since it is susceptible to retroactivity, and therefore, not modular.

ular biology systems. In electrical circuits, for example, flux of information is tied to current flows. Current demands of a downstream system can greatly impact the upstream, an effect that is is captured by the output impedance of a system. A version of retroactivity in fluid mechanics and in engine design also appears in the form of back pressure.

There are two mechanisms of handling problems from retroactivity-type phenomenon in engineering. The first method is the design of *insulation devices*, buffering elements that sit between the upstream and the downstream system and ensures signal propagation with mitigated retroactivity, as shown in Figure 1.1b. Examples of this approach include amplifier-based output stages [4] and buffer tanks in HVAC systems [14]. A second approach, illustrated in Figure 1.1c, is to carefully design the system to operate under the presence of the disturbance. Examples of this approach include impedance matching in high frequency electrical circuits [15] and exhaust design to prevent back pressure in engines [16]. This approach may not be as robust as the one employing insulation devices and does not provide modularity. However, design constraints, such as high energy flow or efficiency may require this second approach.

In this work we show how to adequately model retroactivity caused by connections between synthetic biology devices employing transcription factors as an output. We begin by analysing the effects of retroactivity in a simple "toy model" for a transcription system. Employing principles from this analysis, we show how to design a biomolecular circuit taking retroactivity into account by analysing a theoretical model for an activator-repressor oscillator. Then a framework for insulation devices is introduced. Finally, experimental results validating the predicted analytical results presented in this dissertation are presented.

The last section contains a summary of the technical results presented in this thesis.

1.1 Literature Review

Th models for retroactivity in biomolecular systems used in this work follows the definition provided in [12]. There, retroactivity is defined as a failure of modularity that occurs when the connection between two functional modules is not unidirectional. This concept was structured in the framework of systems theory in [13]. In this work, retroactivity is defined as a signal that flows in a direction opposite to the natural flow of information, as illustrated in Figure 1.1a. This paper also suggests circuits that are robust to retroactivity to the output and, therefore, can act as insulation devices. The insulation devices suggested in [13] are inspired in low output-impedance buffers used in electrical circuits, and are able to reject disturbances to the output by implementing large input amplification and strong negative feedback on the output. The large gains from such systems are exploited analytically by employing Tikhonov's singular perturbation theorem biomolecular systems [17].

Another technique for model reduction in biomolecular circuits that employs a singular perturbation arguments is given in [18]. Here, instead of using Lyapunov stability arguments to show convergence to the slow manifold, contraction theory tools are employed. While stronger assumptions may be needed for the application of these results, it is possible to obtain explicit bounds on the convergence rate between full and approximate systems.

The idea of applying concepts from electrical circuit design to study retroactivity in synthetic biology are illustrated in the two following works. The first one is inspired by the analog electrical circuits theorems of Thevenin and Norton [19]. This result

offers a mathematical model that provides the retroactivity to the output to any nodes in devices with composed of a complex networks. Another approach, based on limitations of digital circuits, a specification for synthetic biology parts analog to fan-out [20].

Another view for retroactivity in biomolecular circuits comes from the perspective of Systems Biology. For example, [21] studies retroactivity in the context of long signalling cascades based on post-translational modifications, and show that long signalling cascades such as the MAPK are able to attenuate retroactivity. Another study analysing retroactivity in MAPK signalling networks shows that downstream sites may even induce oscillations [22] in natural systems.

Recent work experimentally validated several of predicted effects of retroactivity. A study shows that substrate modulates upstream systems in the MAPK pathway because modified signalling molecules are protected by the substrate from dephosphorylation, affecting development of *D. melanogaster* embryos [23]. Studies employing reconstituted *in vitro* systems have shown the impact of retroactivity in post-transcriptional signal networks. Reduction of the sensitivity on the steady state characteristics as well as a reduction in the bandwidth of the system was observed due to presence of the load [24, 25]. These also show that large amplification and feedback gains are capable of mitigating retroactivity. Another *in vitro* study, dealing with RNA circuits, show that retroactivity may impact the functionality of oscillators and show that an insulation device is capable of protecting the upstream oscillator from retroactivity [26].

Since the biochemical mechanism by which retroactivity impacts the system is the binding between signal carriers and load, it is important to mention protein sequestration studies, a research program that has a different aim but has several

points of convergence nevertheless. It has been shown [27, 28] that protein titration can impact drastically the sensitivity of a system, with several follow-up studies confirming these results. Of note, [29] shows that DNA binding sites can generate this same response and [30] suggests that, in principle, this effect depends how much protection the DNA binding sites give to the sequestered protein. These studies focus on steady state responses and noise characteristics of the stationary random processes at its dynamic equilibrium.

In this study we illustrate how retroactivity may affect the behavior of an oscillator based on an *activator repressor* motif. This clock is comprised by an activator module that activates itself and a repressor module, which in its turn represses the activator. Interesting theoretical discussion on this biological topology can be found in [31, 32, 33, 34, 35, 36, 37]. In particular, it was shown that the key parameters for such systems to provide oscillations are the appropriate sensitivity [31, 33, 37] and the difference between activator and repressor timescales [**?**, 31, 32].

This design, was first shown to be a viable biomolecular synthetic oscillator *in vivo* in [38]. An implementation of this clock in mammalian cells was shown in [39] and is considered one of the most complex synthetic circuits in mamalian cells. Another implementation in prokaryotes, that allows for tuning and synchronization was published in [40, 41, 42]. This pattern has also been shown to be present in several natural systems [43, 35], including in the human circadian clocks [44]. Another result of note presented in [45] show DNA binding sites changing the behavior of an activator repressor clock.

1.2 Thesis Organization

Chapter II gives an description of the mechanisms by which a transcription component becomes susceptible to retroactivity. We show the impact of retroactivity to the dynamic and the steady state behavior. We also show that the effect depends on changes on the stability of the transcription factor when bound to the DNA. A final section in this same chapter illustrates how retroactivity can generate a qualitative change in the periodic behavior of a biological oscillator. Analytical tools employed in this section include singular perturbation arguments to reduce the order of a system and bifurcation studies with a Hopf parameter related to retroactivity that changes the stability of the fixed point.

Chapter III provides a strategy to design insulation devices based on timescale separation. This chapter also provides tools to verify the stability of the slow manifolds reached by the fast dynamics. We also comment on the potential tradeoffs between insulation capacity and noise.Analytical tools employed in this section include nested application of singular perturbation to a generalized structure of for insulation devices and stochastic models for the systems such as the Master Equation, and Langevin and Fokker-Planck approximations.

Chapter IV describes experimental results that the support some of the results presented in Chapter II. We describe a realization of a system susceptible to retroactivity to the output and give results of *in vivo* experiments. A mechanistic model of this system is also given.

Finally, Chapter V gives a summary of the results, a discussion commenting how the results presented here compare with current literature and offer suggestions of future work.

CHAPTER II

Retroactivity to a Transcription Component

In order to study the effect of retroactivity to the output due to employing a transcription factor in the output stage, we will analyse the *transcription component*, illustrated in Figure 2.1. This device relays information from the input to the

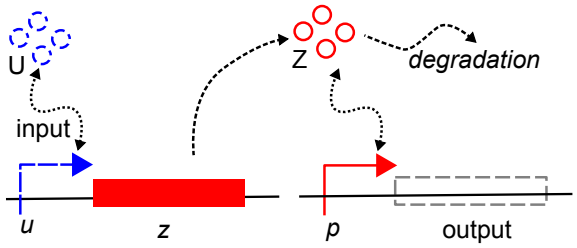

Figure 2.1: **Diagram of the transcriptional component.** An input species U regulates expression of the gene z by interacting with the promoter u. Protein Z, expressed from gene z, interacts with promoter p regulating expression downstream to its promoter. Additionally, protein Z suffers from degradation either through protease mediated degradation or due to dilution resulting from cell growth.

output through transcriptional regulation. Input to this systems occurs when species U interacts with the input promoter u to regulate the expression of the gene z. Expression of this gene in its turn leads to transcription of protein Z which, regulates the expression from promoter p. This mechanism for regulation depends on the binding of protein Z to the promoter p which increases or decreases the RNA polymerase activity depending on whether Z is an activator or repressor, respectively. A client system can then be connected to the output Z of the transcription device through

an input gene inserted downstream to p. Note however that the presence of p, at the same time that enables the connection to between the transcription and client modules to relay information, may potentially act as a load to the output protein Z due to the interaction via binding.

In this chapter, we study how the the connection of the transcriptional device to clients impacts the its performance. Our goal is to compare the behavior of the system when the promoter p is not present (*isolated*) with the behavior when it is present (*connected*). Since it was found that the stability of transcription factors when bound to the complex affects qualitatively the effect of retroactivity, we also investigate the sensitivity of the observed changes to a complex stability parameter.

In the Section 2.1 we introduce the ODE model for this device and exploit the presence of a singular parameter in the system that can be used to obtain a reduced order model. In Section 2.2 we analyse the impact of retroactivity on the dynamic response of this system. Section 2.2.2 shows how retroactivity on a transcription factor can affect a biomolecular oscillator and how proper modelling may be employed to take retroactivity effects into account.

2.1 Transcriptional Component Model

Consider a transcription component, that takes as input a transcription factor or inducer u and gives Z as the output transcription factor. When this system is connected to a downstream transcription component, Z binds to promoter sites q in the downstream system to either repress or activate the promoter. Let Z·q denote the complex of Z with downstream promoter sites q and let p denote the promoters that express Z. This system can be modelled through chemical reactions:

$$\mathrm{p} \xrightarrow{k(u)} \mathrm{Z} + \mathrm{p}, \quad \mathrm{Z} \xrightarrow{\delta} \emptyset, \quad , \mathrm{q} + \mathrm{Z} \underset{k_{\mathrm{off}}}{\overset{k_{\mathrm{on}}}{\rightleftharpoons}} \mathrm{Z} \cdot \mathrm{q}, \quad \mathrm{Z} \cdot \mathrm{q} \xrightarrow{\rho\delta} \mathrm{q},$$

in which $k(u)$ is a standard Hill function [46] with normalized input activator u,

$$k(u) = \alpha \frac{u^n}{(1+u^n)},$$

k_{on} and k_{off} are, respectively, the association and dissociation rates between Z and p, and δ models the protein decay due to natural dilution or degradation. We assume protein Z is also subject to decay when bound to the DNA. However, since it is possible for that the degradation rate when bound to the promoter to be smaller due to a protection effect [30] we introduce a "degradation efficiency" parameter $0 \leq \rho \leq 1$. This leads to a degradation of the complex Z·q at rate $\rho\delta$.

Let Z denote the concentration of free protein Z, and C denote the concentration of the complex Z·q. Let $q_T := q + C$ be a constant denoting the total concentration of promoters to which Z binds in the downstream system and let p_T denote the total concentration of promoters expressing Z. The ordinary differential equation ODE model, in the state space for this system is given by

$$\begin{aligned} \frac{dZ}{dt} &= p_T k(u) - \delta Z - k_{\text{on}} Z(q_T - C) + k_{\text{off}} C \\ \frac{dC}{dt} &= k_{\text{on}} Z(q_T - C) - k_{\text{off}} C - \rho\delta C. \end{aligned} \tag{2.1}$$

Here, $s = -k_{\text{on}} Z(q_T - C) + k_{\text{off}} C$ models the effect of retroactivity to the output. The isolated system configuration that does not present retroactivity to the output ($s = 0$) is trivially given by

$$\dot{Z} = p_T k(u) - \delta Z.$$

To study the effect of s on the response of Z to u, it is useful to normalize the concentrations by the amount of promoter p_T and the time t in terms of the decay rate δ. Consider the state-space normalization $(z, c) := (Z, C)/p_T$ and the nondimensional time $\tau := \delta t$. Consider additionally, the nondimensional parameters $\lambda := \frac{q_T}{p_T}$, $\kappa(u) :=$

$k(u)/\delta$, $\kappa_{\text{on}} := p_T k_{\text{on}}/\delta$ and $\kappa_{\text{off}} = k_{\text{off}}/\delta$. The resulting differential equation system is given by

$$\begin{aligned} \frac{dz}{d\tau} &= \kappa(u) - z - \kappa_{\text{on}} z(\lambda - c) + \kappa_{\text{off}} c \\ \frac{dc}{d\tau} &= \kappa_{\text{on}} z(\lambda - c) - \kappa_{\text{off}} c - \rho c. \end{aligned} \tag{2.2}$$

In this system, $0 < \rho < 1$ describes the amount of protection against degradation provided to the transcription factor by the DNA, with $\rho = 0$ modelling perfect protection and $\rho = 1$ providing no protection. Parameter λ models the amount of downstream system promoters relative to that of the upstream system and thus is responsible for controlling the amount of retroactivity to the output. The isolated system can be modelled by setting $\lambda = 0$ to obtain

$$\frac{dz}{d\tau} = \kappa(u) - z. \tag{2.3}$$

In general, association reactions are very fast when compared to production and decay [46]. In the nondimensionalized model, this can be modelled by assuming $\kappa_{\text{on}} \gg 1$. In what follows, the dot notation will be used to denote derivation with respect to the nondimensional time τ.

2.1.1 Effect of retroactivity on the steady state.

By identifying the equilibrium z^* reached by system (2.2) under a constant input $\kappa^* := \kappa(u^*)$, one can identify the impact retroactivity will have as a function of parameter λ. Let $k_d := \kappa_{\text{off}}/\kappa_{\text{on}}$ denote the dissociation constant of Z. Define $k_m = k_d + \rho/\kappa_{\text{on}}$ as a shorthand. The steady state value of z for a constant input $z^* = \kappa(u^*)$ is given by

$$z^* = \frac{\kappa^* - k_m - \rho\lambda + \sqrt{(\kappa^* - k_m - \rho\lambda)^2 + 4\kappa^* k_m}}{2}. \tag{2.4}$$

This equation shows that the effect of retroactivity on the steady state characteristic is observed when the DNA does not confer protection to the protein. When $\rho \neq 0$, a connected system ($\lambda > 0$) reaches a lower steady state concentration of free protein z^* than the isolated system ($\lambda = 0$).Note additionally that when there is full protection to the complex ($\rho = 0$), there is no change in the steady state value of free output due to retroactivity.

2.2 Dynamic Impact of Retroactivity

2.2.1 Model Reduction.

In order to compare the one dimensional dynamics of the isolated system with the two dimensional dynamics of the connected system, we reduce the order of the connected system employing a singular perturbation argument based on a natural timescale separation in the system. The association rate is usually a very fast reaction compared to the other processes in the system. This can be modelled by making the nondimensional rate $\kappa_{\text{on}} \gg 1$. In this section we assume the case in which $\kappa_{\text{off}} = O(\kappa_{\text{on}})$ as well. A treatment of the *high affinity* case, in which letting $\kappa_{\text{off}} \ll \kappa_{\text{on}}$ will be treated later as a special case. Let $\epsilon := \kappa_{\text{on}}^{-1}$ be a small parameter and, $k_d = \kappa_{\text{off}}/\kappa_{\text{on}}$ as defined previously. Considering the change of coordinates $y := z + c$ be a slow variable, (2.2) can be rewritten in the standard singular perturbation form as

$$\begin{aligned} \dot{y} &= \kappa(u) - y + (1-\rho)c \\ \epsilon\dot{c} &= (y-c)(\lambda - c) - K_d c - \epsilon\rho c \end{aligned} \tag{2.5}$$

The slow manifold obtained by setting $\epsilon = 0$ is given by

$$\bar{c} = \phi(y) = \frac{y + \lambda + k_d - \sqrt{(y+\lambda+k_d)^2 - 4y\lambda}}{2}. \tag{2.6}$$

We can verify the stability of this manifold by verifying that

$$\frac{\partial}{\partial c}\{(y-c)(\lambda-c)-k_d c-\epsilon\rho c\}\Big|_{c=\phi(y)} = -\lambda - y - k_d - \epsilon\rho + 2\phi(y) < 0. \tag{2.7}$$

Define $\bar{z} = y - \phi(y)$ and the inverse mapping $y := \mu(\bar{z})$. Let

$$\psi(\bar{z}) := \phi(\alpha(\bar{z})) = \frac{\bar{z}}{\bar{z}+k_d}\lambda.$$

The dynamics for $\bar{z}$ obeys the ODE

$$\frac{d\bar{z}}{d\tau} = \left(1+\frac{\partial\psi(\bar{z})}{\partial\bar{z}}\right)^{-1}\frac{dy}{dt} = \frac{1}{1+k_d\lambda(k_d+\bar{z})^{-2}}\left(\kappa(u)-\bar{z}-\rho\frac{\bar{z}\lambda}{\bar{z}+k_d}\right). \tag{2.8}$$

Since from the singular perturbation theorem [47], $z(\tau)-\bar{z}(\tau) = O(\epsilon)\ \forall\tau\in[\tau_0,\tau_f]$ for some $\tau_0 > 0$ arbitrarily small, one can measure the effect of retroactivity to the order of ϵ by comparing the one dimensional systems (2.8) and (2.3).

2.2.2 Step Inputs

To quantify the impact of retroactivity in the response to step inputs, we employ the following Lemma which compares two unidimensional systems with identical initial conditions and asymptotic behavior by comparing their vector field.

Lemma 1 (Response to Step Input)**.** *Let $\dot{x} = f(x)$ and $\dot{y} = g(y)$, $x\in\mathbb{R}$, $y\in\mathbb{R}$, f and g Lipschitz continuous, define two scalar initial value problems with $x(0) = y(0) = a$, and let the unique solutions be $x(\tau)$ and $y(\tau)$. Additionally, assume $\exists b\neq a$ such that $f(b) = g(b) = 0$. Define the set $L := \{a\}\cup\{x\in\mathbb{R}|\min\{a,b\} < x < \max\{a,b\}\}$ and assume that $\forall c\in L, f(c)/(b-a) > g(c)/(b-a) > 0$. Then, $x(\tau):\mathbb{R}_+\to L$ and $y(\tau):\mathbb{R}_+\to L$ are invertible functions and that for all $c\in L$ $x^{-1}(c) < y^{-1}(c)$.*

Proof. In order to show $x(\tau)$ is invertible, consider the auxiliary variable $\xi = (x-a)/(b-a)$. From this definition, the initial value problem becomes $\dot{\xi} = f(x)/(b-a)$

with $\xi(0) = 0$. From the fact $f(x)$ is Lipschitz continuous, $\exists M > 0$ such that for any $x \in (a, b)$, $|f(x)| \leq M|x - b|$. This implies that $f(x)/(b - a) \leq M(b - x)/(b - a)$. Since

$$\xi(t) = \int_0^\tau f(x(s))/(b - a)ds \leq \int_0^\tau M(1 - \xi(s))ds$$

from the Gronwall-Bellman Lemma, $\xi(t) \leq 1 - e^{-M\tau} < 1$. Due to the fact $\forall \xi \in [0, 1)$, $\dot{\xi}(\tau) > 0$, $\xi(\tau)$ is a strictly monotonically increasing function of τ. But since $\xi(\tau) < 1$, $\lim_{\tau\to\infty} \xi(\tau) = 1$. We can therefore conclude that the function $\xi : \mathbb{R}_+ \to [0, 1)$ is bijective and therefore invertible. This implies that $x : \mathbb{R}_+ \to L$ is invertible as well, since $x \to \xi$ is an affine transformation. Let the inverse function be $\theta_x := x^{-1}$ with domain L and image $\mathbb{R}_+$. These results are trivially extended for the function $y(t)$; let $\theta_y := y^{-1}$ be the inverse mapping. From the inverse function theorem, we know that $\dfrac{d\theta_x(z)}{dz} = \dfrac{1}{f(z)}$ and $\dfrac{d\theta_y(z)}{dz} = \dfrac{1}{g(z)}$ and therefore for any $x \in L$,

$$\theta_x(c) - \theta_y(c) = \int_a^c \frac{g(z) - f(z)}{g(z)f(z)}dz = \int_{\min\{a,c\}}^{\max\{a,c\}} \frac{|b - a|}{g(z)f(z)} \frac{g(z) - f(z)}{b - a}dz < 0,$$

which proves the last statement in the lemma. □

This lemma provides a method to compare two scalar systems with same initial conditions and asymptotic behavior by comparing their vector fields. We show next how this can be applied to study the difference in the response of isolated and connected systems to step inputs.

Consider first the induction problem with saturating input, modelled by a positive step in which for $\tau < 0$, $\kappa(\tau) = 0$ ($u(\tau) = 0$) and for $\tau \geq 0$, $\kappa = \kappa^* = \alpha/\delta$ ($u(\tau) \to \infty$). Recall from (2.4) that the isolated and connected systems may reach different equilibrium values. Thus, in order to apply Lemma 1 we normalize system (2.8) by setting $w = z/z^*$, in which z^* is a function of λ and κ^* as defined in (2.4).

The resulting initial value problem is given by

$$\frac{dw}{dt} = \frac{1}{1 + k_d\lambda(k_d + z^*w)^{-2}} \left[\frac{\kappa^*}{z^*} - w - \rho\frac{\lambda w}{z^*w + k_d}\right], \tag{2.9}$$

for the connected system and

$$\frac{dw}{dt} = 1 - w, \tag{2.10}$$

for the isolated system. It is easy to show that (2.9) and (2.10) satisfy the conditions of Lemma 1 with $w(0) = 0$ and $\lim_{\tau\to\infty} w(\tau) = 1$ in both systems. Let $w_i(t)$ and $w_c(t)$ be the solutions to the isolated and to the connected initial value problem, respectively. Define

$$f(w, \lambda) = \frac{1}{1 + \lambda k_d(k_d + z^*w)^{-2}} \left[\frac{\kappa^*}{z^*} - w - \rho\frac{\lambda w}{z^*w + k_d}\right],$$

and $g(w) = 1 - w$. it is easy to check that $g(w), f(w, \lambda) > 0$ for all values of $0 \leq w < 1$. From (2.4), one can obtain the value of κ^* in terms of z^* as

$$\kappa^* = z^*\frac{z^* + k_d + \rho\lambda}{z^* + k_d} \tag{2.11}$$

Substituting (2.11) and comparing the vector fields, we obtain

$$g(w) - f(w, \lambda) = \frac{\lambda(1 - w)k_d[(1 - \rho w)z^* + k_d(1 - \rho)]}{[(k_d + z^*w)^2 + k_d\lambda](z^* + k_d)} > 0,$$

for all $\lambda > 0$ and as a result these initial value problems satisfy the conditions from Lemma 1. Thus, for all $w^* \in (0, 1)$, $w_i^{-1}(w^*) < w_c^{-1}(w^*)$ which shows that the load decreases the speed of the response to positive step inputs.

We will consider now a de-induction experiment from saturating conditions. To model this, let the input be the step function such that for $\tau < 0$, $\kappa(\tau) = \kappa^* = \alpha/\delta$ ($u(\tau) \to \infty$) and for $\tau > 0$, $\kappa(\tau) = 0$ ($u(\tau) = 0$), and let the initial conditions be $z(0) = z^*$, where z^* is the steady state for saturating input k^* defined in (2.4). In

both cases, the connected and the isolated systems go to the equilibrium $z = 0$, but the initial conditions are different. In order to apply Lemma 1, we employ an approach similar to the one above by defining $w = z/z^*$. The resulting initial value problem becomes

$$\frac{dw}{d\tau} = \frac{-1}{1 + k_d\lambda(k_d + z^*w)^{-2}}\left[w + \rho\frac{\lambda w}{z^*w + k_d}\right],$$

for the connected system and $dw/d\tau = -w$ for the isolated one. These two systems satisfy conditions of Lemma 1, since $w(0) = 1$ and $\lim_{\tau\to\infty} w(\tau) = 0$. Let

$$f(w, \lambda) = \frac{-1}{1 + k_d\lambda(k_d + z^*w)^{-2}}\left[w + \rho\frac{\lambda w}{z^*w + k_d}\right]$$

and let $g(w) = -w$, it is easy to check that $g(w), f(w, \lambda) < 0$ for all values of $0 < w \leq 1$. The comparison of the vector fields in this case gives

$$g(w) - f(w, \lambda) = \frac{\lambda w[-k_d + \rho(k_d + wz^*)]}{[(k_d + z^*)^2 + k_d\lambda]}. \tag{2.12}$$

In a negative step input for this system, the impact of the response will depend on the protection efficiency ρ. If there the DNA provides no protection ($\rho = 1$ the connected system responds faster. On the other hand, if the DNA provides full protection ($\rho = 0$) the connected system becomes slower than the isolated one. In particular, since $w < 1$, a slower response is guaranteed if

$$\rho < \frac{k_d}{k_d + z*}. \tag{2.13}$$

Figure 2.2 validates the results shown above. Retroactivity to a transcription component slows the response to induction when compared to the isolated system in both situations. In contrast, in a de-induction experiment the response depends on the protection level. When the DNA provides protection to the DNA ($\rho = 0$), the response is slower than in the isolated system. In contrast, when there is no protection ($\rho = 1$), the response becomes faster.

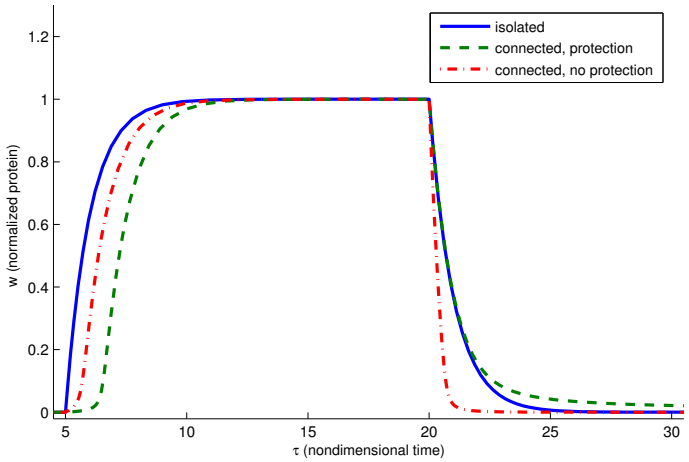

Figure 2.2: **Retroactivity effect on step responses.** The plot shows a simulation of isolated system (2.3) and connected system (2.2) to step inputs under levels or protein protection. When there is no protection, the system is slower to both inputs. In contrast, when there is protection, the response is slower to induction but faster to de-induction. In this simulation, an induction ($\kappa(u) = \kappa^*$) at time $\tau = 5$ is followed by a de-induction ($\kappa(u) = 0$) at time $\tau = 20$. The simulations was normalized by the maximum amount of protein. Values used in this simulation were $\kappa^* = 20$, $\kappa_{\text{on}} = 100$ and $\kappa_{\text{off}} = 10$. For the isolated system, $\lambda = 0$. For the connected system with protection, $\lambda = 30$ and $\rho = 0$. For the connected system with no protection, $\lambda = 10$ and $\rho = 1$.

2.2.3 Frequency Response

Another characteristic of interest in studying signalling system is its frequency response. This information gives the limits of the system in terms of the bandwidth of the signals it is capable of transmitting. In order to analyse this, proceed by setting an input $\kappa(\tau) = \kappa_0 + \tilde{\kappa}(\tau)$ in which $\tilde{\kappa}(\tau)$ is a signal with small amplitude. Define z_0 to be the equilibrium reached for a constant input κ_0 obtained by setting $\kappa^* = \kappa_0$ in expression (2.4). The Jacobian of system (2.8) with input $\kappa = \kappa_0$ is given by

$$J(z_0) = -\frac{1 + \rho\lambda k_d (k_d + z_0)^{-2}}{1 + \lambda k_d (k_d + z_0)^{-2}}. \tag{2.14}$$

Define $\tilde{z} = z - z_0$ and $\tilde{\kappa} = \kappa - \kappa_0$. If the amplitude of signal $\tilde{\kappa}(\tau)$ is small, (2.8) can be well approximated by

$$\frac{d\tilde{z}}{d\tau} = \frac{1}{1 + \lambda k_d (k_d + z_0)^{-2}} \tilde{\kappa} - \frac{1 + \rho\lambda k_d (k_d + z_0)^{-2}}{1 + \lambda k_d (k_d + z_0)^{-2}} \tilde{z}. \tag{2.15}$$

The resulting transfer function from input to output is

$$G(s) = \frac{Z(s)}{K(s)} = \frac{R}{s + QR}, \tag{2.16}$$

in which

$$R = \frac{1}{1 + \lambda k_d (k_d + z_0)^{-2}} \text{ and } Q = 1 + \rho \lambda k_d (k_d + z_0)^{-2}.$$

The resulting system is a first order system with DC gain $G(0) = Q^{-1}$ and cut-off frequency $-QR$.

Note that for frequency inputs, ρ behaves as a tradeoff parameter between amplitude loss and bandwidth. For example, in the system with no protection ($\rho = 1$), the bandwidth is not affected by retroactivity, but the amplitude decreases. However, when the DNA offers perfect protection ($\rho = 0$), the value of the cut-off frequency decreases with an increase in λ, but the DC gain is not affected by retroactivity. This results is illustrated in Figure 2.3. In these plots, we adjust the input κ_0 in each system so that the bias output level z_0 is constant.

2.2.4 Transcription factors with high affinity

There are several situations in which the affinity between the promoter and the transcription factor is so strong that the dissociation rate is of the same order of magnitude or slower than the decay rate. Since this is a special case of the general system, the above results apply. However, these systems merit special treatment due to their high incidence. These *high affinity* cases can be modelled by setting $\kappa_{\text{off}} \ll 1$ in our models.

The impact of retroactivity on the steady state in this situation can be obtained by noticing that k_m becomes insignificant in (2.4) when compared to any meaningful non-null input κ^*. In this situation, the steady state of the connected system is well

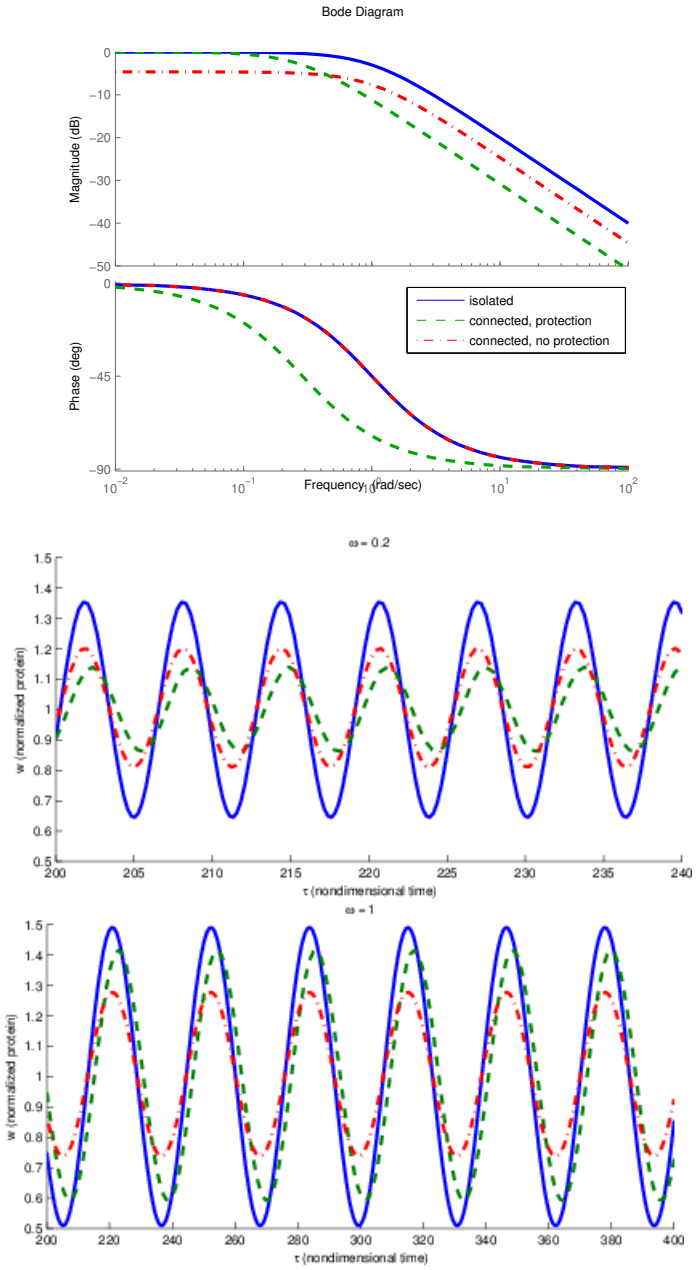

Figure 2.3: **Protein protection as a tradeoff parameter in the frequency response of transcription components.** The top figure shows the Bode plot of the linearized system shown in (2.15). The system in which DNA binding sites confer protection to the protein leads to change in the cutoff frequency. On the other hand, in a system in which no protection is provided, there are no changes on the cutoff frequency and, consequently, no phase changes between the isolated and the connected. However, there is a loss of amplitude over all frequencies. The bottom two figures shows simulations of the output of systems (2.2) and (2.3) to sinusoidal input $\tilde{k}appa(\tau) = 0.5\cos\omega\tau$, with the middle plot having input $\omega = 1$ rad/s and the bottom plot having $\omega = .2$ rad/s. Note that, as predicted by the crossover found in the amplitude graph of the bode plot of the linearized system, for slower inputs, the system with protection has a lower attenuation whereas at faster outputs, the system with no protection has lower attenuation.

approximated by

$$z^* = \begin{cases} 0 & \text{if } 0 \leq y < \lambda \\ \kappa^* - \rho\lambda, & \text{if } y \geq \lambda. \end{cases} \tag{2.17}$$

Note that, due to the high affinity, if the amount of free proteins is $z^* = 0$ unless the total amount of proteins is large enough ($y > \rho\lambda$). From the above solution, we can determine u_{50}, the value of input that results in an output equivalent to half of the maximum. The maximal value of $z^*_{max} = \alpha/\delta - \rho\lambda$, so that

$$u_{50} = \left(\frac{\alpha/\delta + \rho\lambda}{\alpha/\delta - \rho\lambda}\right)^{1/n}, \tag{2.18}$$

in which for $\lambda = 0$ we obtain $u_{50} = 1$ for the isolated system and, as λ increases, the value of u_{50} increases. To obtain the reduced model employed in the dynamic analysis, one can assume $k_d = O(\epsilon)$ in (2.5), and as a result the slow manifold obtained setting $\epsilon = 0$ becomes

$$\bar{c} = \phi_d(y) = \begin{cases} y & \text{if } 0 \leq y < \lambda \\ \lambda & \text{if } y \geq \lambda. \end{cases}$$

It is easy to verify that the non-smooth manifold is the limit case of the smooth manifold $\phi(y)$ from (2.6), since $\lim_{k_d \to 0} \phi(y) = \phi_d(y)$ and that this manifold is also stable. However the $\phi_d : \mathbb{R}_+ \to [0, \lambda]$ map is not injective. As a consequence, $\bar{z} := y - \phi_d(y)$ is non-invertible map, and therefore the approximation (2.8) is not valid. The approximate dynamics can still be obtained in terms of y. Let $\bar{z} := y - \phi_d(y)$ as

$$\frac{d\bar{z}}{d\tau} = \left(1 - \frac{\partial \phi_d(y)}{\partial y}\right)\frac{dy}{d\tau} = \begin{cases} 0 & \text{if } 0 \leq y < \lambda \\ \kappa(u) - \bar{z} - \rho\lambda & \text{if } y \geq \lambda. \end{cases} \tag{2.19}$$

in which y is the solution of

$$\frac{dy}{d\tau} = \begin{cases} \kappa(u) - \rho y & \text{if } 0 \leq y < \lambda \\ \kappa(u) + \lambda(1-\rho) - y & \text{if } y \geq \lambda. \end{cases} \tag{2.20}$$

This system has an intuitive interpretation. When the affinity between the transcription factor and DNA is very strong, there will be no free protein available ($\bar{z} = 0$) until the total amount of protein y becomes larger than the number of binding sites λ.

In the induction experiment, assuming an input u such that $\kappa > \rho\lambda$, since $y_0 = 0$, $y(t) = \kappa(1 - e^{-\rho\tau})$. Therefore, system (2.19) can be written as the non-homogeneous system

$$\frac{dz}{d\tau} = \begin{cases} 0 & \text{if } 0 \leq \tau < \tau_d \\ \kappa(u) - z - \rho\lambda & \text{if } \tau \geq \tau_d, \end{cases} \tag{2.21}$$

in which

$$\tau_d = \frac{1}{\rho} \ln \frac{\kappa}{\kappa - \rho\lambda}$$

for $\rho \neq 0$ and $\tau_d = \lambda/\kappa$ for $\rho = 0$. This shows the delay in the response, since soon after the induction and until $\tau = \tau_d$, $\dot{z} = 0$. This effect is a result of the fact that every generated transcription factor binds to the sites q. Additionally, $\rho\lambda$ reduces the right hand side of the ODE slowing down the response to induction as per Lemma 1.

To model the de-induction (wash) experiment, one can set $\kappa = 0$ in (2.19) to obtain the non-homogeneous system

$$\frac{dz}{d\tau} = \begin{cases} -z - \rho\lambda & \text{if } z > 0 \\ 0 & \text{if } z = 0. \end{cases} \tag{2.22}$$

which, for $z(0) > 0$ has solution is thus given by

$$z(\tau) = z(0)e^{-\tau} - \rho\lambda(1 - e^{-\tau}).$$

If both isolated and connected systems have same initial amount of free protein, it is clear from Lemma 1 that the connected system will respond faster to the de-induction. That is also the case if we instead assume that prior to the experiment,

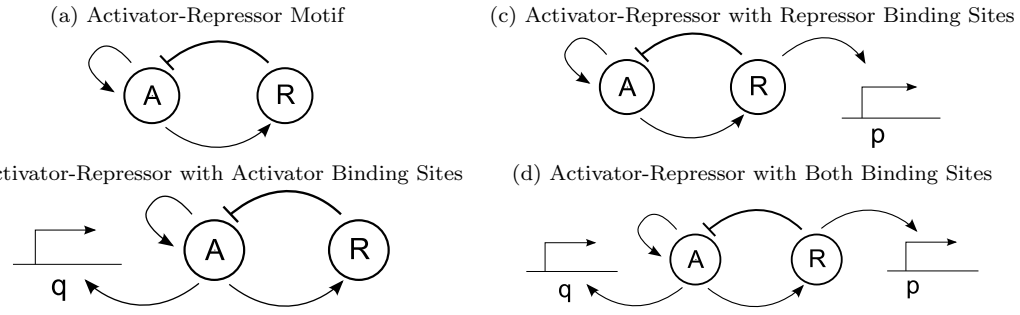

Figure 2.4: **Illustration of the systems analysed in this section.** Diagram (a) illustrates the activator-repressor motif. Diagram (b) and (c) illustrate the systems after the addition of DNA binding sites with affinity to the activator and the repressor, respectively. Diagram (d) illustrates the case in which both types of DNA binding sites are present.

both isolated and connected systems have the same amount of inducer u^*. This can be seen by evaluating the time of depletion $\tau_e := z^{-1}(0)$ as the time in which the amount of free protein becomes zero. By letting $\kappa^* = \kappa(u^*)$, the initial conditions are given by $z(0) = \kappa^* - \rho\lambda$ and as a result $z(\tau) = ke^{-\tau}$. For the connected system, depletion occurs at finite time, since $\tau_e = ln\dfrac{\kappa + \rho\lambda}{\kappa - \rho\lambda}$, while in the isolated system, $\tau_e \to \infty$. When there is perfect protection of the complex ($\rho = 0$), there is no effect of retroactivity in the response in the high affinity case.

2.3 Employing Retroactivity to Tune Clocks

In this Section we give an example of a system design that inserts retroactivity effects in the model of the system.

Consider a model for a two-component clock incorporating both positive and negative feedback loops based on the activator-repressor configuration of [48] and illustrated in Figure 2.4a. Oscillations for activator-repressor clocks often arise from Hopf bifurcation, wherein a stable equilibrium point bifurcates into an unstable equilibrium and a stable periodic orbit when a key parameter is changed [49, 36, 31, 50, 39]. In the models surveyed in the literature, the fundamental mechanism responsible for

this oscillatory behavior is well captured by a reduced two-dimensional model that describes the rate of change of the activator and repressor concentrations. This model is obtained by taking into account that the period of oscillations occurs in a timescale slower than the dynamics of multimerization, binding and dissociation interactions, so that quasi-steady state approximations can be made. Additionally, it has been shown that transcription and translation can be lumped into a one-step expression model with no impact to the dynamics of interest. Based on these prior work, we focus on a reduced two-dimensional model.

In the system of Figure 2.4a, activator protein A promotes its own expression as well as the expression of repressor protein R. Protein R, in turn, represses expression of protein A. In what follows we introduce a nondimensional model for the activator repressor clock. A detailed derivation of this system is given in the Appendix.

Let K_{m1} be the apparent dissociation constant between the activator protein and its DNA binding site and K_{m2} be the apparent dissociation constant between repressor protein and its DNA binding site [51]. Consider the concentration of A and R given in units of their respective dissociation constants $a := A/K_{m1}$ and $r := R/K_{m2}$. Considering a one-step model for protein expression, the dynamics for this system can be represented by

$$\begin{aligned} \dot{a} &= -\delta_A a + f_1(a, r) \\ \dot{r} &= -\delta_R r + f_2(a), \end{aligned} \tag{2.23}$$

in which δ_A and δ_R model protein decay (due to either dilution or degradation) and functions f_1 and f_2 model expression rates and take the form of the standard Hill functions [46]

$$f_1(a, r) = \frac{\beta_1 a^m + \beta_2}{1 + a^m + r^n} \text{ and } f_2(a) = \frac{\beta_3 a^m + \beta_4}{1 + a^m}, \tag{2.24}$$

in which β_1 and β_3 are the maximal expression rates, β_2 and β_4 represent the basal expression, and m and n are the Hill coefficients of the affinity between the proteins A and R and their respective binding sites. The mathematical derivation of this reduced nondimensional model is given in the Appendix. In the sequel, we refer to system (2.23) as the *isolated system*.

We assume that the values of the parameters are such that system (2.23) has a unique equilibrium point. We give conditions for which this assumption holds when either $m = 1$ or $m = 2$ in the Appendix. In particular, it is shown that when $m = 1$, the system always presents a unique and stable equilibrium and, therefore, no oscillatory behavior can be observed. When $m = 2$ the uniqueness of the equilibrium is guaranteed under the following conditions: (i) the value of β_2 must be sufficiently smaller than the maximal expression rate of the activator, which is proportional to β_1; (ii) β_2 must be non-zero; (iii) the maximal expression rate of the repressor must be larger than the maximal expression rate of the activator; (iv) the smaller β_2 becomes, the smaller β_4 must be. In the general case ($m > 2$), results related to existence and uniqueness of equilibria require a case by case analysis, which is out of the scope of this work. The results in this section, do not explicitly impose conditions on the Hill coefficients m and n and only assume the uniqueness of the equilibrium (a^*, r^*) for system (2.23).

Since system (2.23) is a two-dimensional system, Poincaré-Bendixson theorem [52] can be employed to obtain conditions for the existence of a periodic orbit. Specifically, one must show that the trajectories of the system are bounded in a compact set and that the equilibrium point is unstable and not locally a saddle.

The following proposition shows that the trajectories of system (2.23) are bounded in a compact set.

Proposition 1. *There exists a constant $D \in \mathbb{R}_+$ such that the set $K = \{(a, r) \in \mathbb{R}^2_+ | a^2 + r^2 \leq D^2\}$ is a positively invariant set under the vector field defined by system (2.23) and its equilibrium $(a^*, r^*) \in K$.*

Proof. Note that $f_1(a, r)$ and $f_2(a)$ are positive bounded functions in the domain $\mathbb{R}^2_+$. Let $M_1 = \sup_{(a,r)\in\mathbb{R}^2_+}\{f_1(a, r)\}$ and $M_2 = \sup_{a\in\mathbb{R}_+}\{f_2(a)\}$. First, notice that for $a = 0$, $\dot{a} > 0$ according to (2.23). Similarly, for $r = 0$, $\dot{r} > 0$. The quadrant $\mathbb{R}^2_+$ is, therefore, a positively invariant set. Define $\delta^* := \min\{\delta_A, \delta_R\}$ and $M := \max\{M_1, M_2\}$. Consider the positive definite function $v(a, r) = a^2/2 + r^2/2$. Using the chain rule, we obtain

$$\begin{aligned}\frac{dv(a, r)}{dt} &= -\delta_A a^2 - \delta_R r^2 + a f_1(a, r) + r f_2(a)\\ &\leq -\delta^* a^2 - \delta r^2 + aM + rM\\ &= -\delta^*\left(a - \frac{M}{2\delta^*}\right)^2 - \delta^*\left(r - \frac{M}{2\delta^*}\right)^2 + \frac{M^2}{2(\delta^*)^2}.\end{aligned}$$

From the above, it is clear that $\dot{v}(a, r) < 0$ on the exterior of a circle with center $(M/2\delta^*, M/2\delta^*)$ and radius $\sqrt{2}M/2\delta^*$. Thus, for any $D > \max\{\sqrt{2}M/\delta^*, a^*, r^*\}$, $\dot{v}(a, r) < 0$ along the arc defined by the boundary of K. Hence, K is a positively invariant set that contains the equilibrium (a^*, r^*). □

To show that the equilibrium point is unstable and not locally a saddle, consider the Jacobian matrix of system (2.23) calculated at the equilibrium:

$$J_0 = \begin{bmatrix} -\delta_A + \dfrac{\partial f_1(a^*, r^*)}{\partial a} & \dfrac{\partial f_1(a^*, r^*)}{\partial r} \\ \dfrac{\partial f_2(a^*)}{\partial a} & -\delta_R \end{bmatrix}, \tag{2.25}$$

and denote by $\mathrm{tr}(J_0)$ and $\det(J_0)$ the trace and the determinant of J_0, respectively. The eigenvalues of the Jacobian are given by

$$\lambda_{1,2} = \frac{\mathrm{tr}(J_0) \pm \sqrt{\mathrm{tr}(J_0)^2 - 4\det(J_0)}}{2},$$

hence the equilibrium point is unstable and not locally a saddle if $\mathrm{tr}(J_0) > 0$ and $\det(J_0) > 0$. Given the specific expression of the Jacobian in (2.25), the equilibrium (a^*, r^*) of system (2.23) is unstable and not locally a saddle if the following conditions are fulfilled:

$$\textit{(i)}\ \delta_R\left(\delta_A - \frac{\partial f_1(a^*, r^*)}{\partial a}\right) - \frac{\partial f_1(a^*, r^*)}{\partial r}\frac{\partial f_2(a^*)}{\partial a} > 0\ (\det(J_0) > 0);$$

$$\textit{(ii)}\ \frac{\partial f_1(a^*, r^*)}{\partial a} - \delta_A - \delta_R > 0\ (\mathrm{tr}(J_0) > 0).$$

System (2.23) satisfying conditions *(i)* and *(ii)* presents periodic orbits and will be referred to as *Functional Clock*.

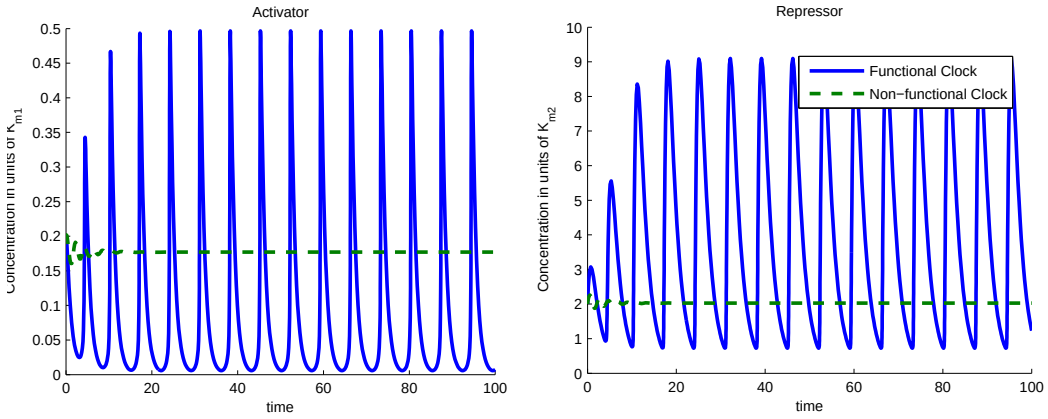

Figure 2.5: **Effect of the trace of the Jacobian on the stability of the equilibrium.** The above plots illustrate the trajectories of system (2.23) for both Functional and Non-Functional Clocks. The parameters in the simulation were $\beta_1 = \beta_3 = 100$, $\beta_2 = .04$, $\beta_4 = .004$ and $\delta_A = 1$. In the Functional Clock, $\delta_R = 0.5$ whereas in the Non-Functional Clock, $\delta_R = 1.5$. Parameters β_1 and β_3 were chosen to give about 500-2000 copies of protein per cell for activated promoters. Parameters β_2 and β_4 were chosen to give about 1-10 copies per cell for non-activated promoters.

Condition *(ii)* highlights a crucial design principle for the activator-repressor clock. In fact, assume that $\dfrac{\partial f_1(a^*, r^*)}{\partial a} - \delta_A > 0$, which is satisfied if the self activation is sufficiently strong. Then, condition *(ii)* can be satisfied if $\dfrac{\partial f_1(a^*, r^*)}{\partial a} - \delta_A$ is sufficiently larger than δ_R. This, in turn, implies that the timescale of the activator dynamics are sufficiently faster than that of the repressor dynamics. Hence, a central mechanism for the appearance of a limit cycle is a fast activator dynamics compared to the repressor dynamics. Retroactivity on a species due to downstream binding

sites has been shown to slow down the species dynamics [13, 24]. It follows that downstream binding sites can be employed to vary the relative speeds between the activator and the repressor dynamics. Hence, we will also consider the non-oscillating version of system (2.23) that does not satisfy condition *(ii)*, referred to as *Non-Functional Clock*. The non-functional clock is given by system (2.23) in which, in addition to condition *(i)*, the following condition is satisfied:

(ii)' $0 < \dfrac{\partial f_1(a^*, r^*)}{\partial a} - \delta_A < \delta_R.$

Figure 2.5 illustrates how conditions *(ii)* and *(ii)'* generate a Functional and a Non-Functional Clock, respectively, by changing the value of parameter δ_R.

2.3.1 Switching the clock off by loading the activator

In this section, we show the effect of additional DNA binding sites for the activator in a Functional Clock. Specifically, consider system (2.23) satisfying conditions *(i)* and *(ii)*. The addition of DNA binding sites q_A with affinity to the activator A, which binds as homomers, illustrated in Figure 2.4b, is modelled by the following chemical reaction

$$mA + q_A \underset{k_{b1}}{\overset{k_{a1}}{\rightleftharpoons}} D_1, \tag{2.26}$$

in which D_1 represents the complex formed by A and q. In order to model the addition of DNA binding sites that are identical copies of the ones in the operator, we assume that the affinity between the DNA site q and the activator protein A is given by the apparent dissociation constant $K_{m1} = \sqrt[m]{k_{b1}/k_{a1}}$, identical to the affinity of A to the promoters in the isolated clock. The impact in the dynamics from retroactivity can be obtained by employing binding sites with different affinities as long as the quantity of binding sites is adjusted accordingly [13] . Additionally, we assume the total concentration of binding sites $\bar{q}_A = (q_A + D_1)/K_{m1}$ to be constant.

Let the complex concentration D_1 be given in units of K_{m1} using the nondimensional variable $d_1 = D_1/K_{m1}$. The dynamics of the system after nondimensionalization are given by

$$\begin{aligned} \dot{a} &= -\delta_A a + f_1(a,r) + mG_1\delta_A d_1 - mG_1\delta_A a^m(\bar{q}_A - d_1) \\ \dot{r} &= -\delta_R r + f_2(a) \\ \dot{d}_1 &= -G_1\delta_A d_1 + G_1\delta_A a^m(\bar{q}_A - d_1), \end{aligned} \tag{2.27}$$

in which $G_1 = k_{b1}/\delta_A$ models the timescale separation between the dissociation rate and the protein degradation. Details of this derivation are presented found in the Appendix. Since binding and unbinding reactions can occur in the order of milliseconds, they are in a timescale significantly faster than expression and degradation of proteins, which occur in the order of minutes [46]. As a result, parameter G_1 is very large. This fact allows to employ a singular perturbation argument [47, 17] to facilitate the analysis of this system. To this end, define the small parameter $\epsilon := 1/G_1$ and re-write system (2.27) as

$$\begin{aligned} \dot{a} &= -\delta_A a + f_1(a,r) + \frac{m}{\epsilon}\left(\delta_A d_1 - \delta_A a^m(\bar{q}_A - d_1)\right) \\ \dot{r} &= -\delta_R r + f_2(a) \\ \dot{d}_1 &= \frac{1}{\epsilon}\left(-\delta_A d_1 + \delta_A a^m(\bar{q}_A - d_1)\right). \end{aligned} \tag{2.28}$$

In order to reduce this system to standard singular perturbation form, we perform the change of variables $y = md_1 + a$, so that system (2.28) becomes

$$\dot{y} = -\delta_A(y - md_1) + f_1(y - md_1, r) \tag{2.29}$$

$$\dot{r} = -\delta_R r + f_2(y - md_1) \tag{2.30}$$

$$\epsilon\dot{d}_1 = -\delta_A d_1 + \delta_A(y - md_1)^m(\bar{q}_A - d_1), \tag{2.31}$$

which is in standard singular perturbation form. Setting $\epsilon = 0$ one obtains from (2.31) the solution $d_1 = \frac{\bar{q}_A a^m}{a^m + 1} := \phi_1(a)$. This equation defines the slow manifold,

which can be shown to be locally exponentially stable (see Appendix). Hence, system (2.29) is well approximated by the reduced system obtained by replacing d_1 by its expression on the slow manifold $\phi_1(a)$. Specifically, we have that

$$-\delta_A a + f_1(a,r) = \dot{y} = m\dot{d}_1 + \dot{a} = m\frac{d\phi_1(a)}{da}\dot{a} + \dot{a},$$

from which we obtain that

$$\dot{a} = \frac{1}{1 + m\frac{d\phi_1(a)}{da}}(-\delta_A a + f_1(a,r)).$$

Denoting

$$\mathcal{S}_A(a,\bar{q}_A) := \frac{1}{1+\frac{d\phi_1(a)}{da}} = \frac{1}{1 + m\bar{q}_A a^{m-1}(1+a^m)^{-2}},$$

the reduced system in the original coordinates is given by

$$\begin{aligned} \dot{a} &= \mathcal{S}_A(a,\bar{q}_A)\,(-\delta_A a + f_1(a,r)) \\ \dot{r} &= -\delta_R r + f_2(a). \end{aligned} \tag{2.32}$$

Since $\mathcal{S}_A(a,\bar{q}_A) \neq 0$, the equilibria of (2.32) are the same as the ones of (2.23). Therefore, if (2.23) has a unique equilibrium (a^*, r^*), this will also be a unique equilibrium of (2.32). Also, we have that $0 < \mathcal{S}_A(a,\bar{q}_A) \leq 1$ and that $\mathcal{S}_A(a,\bar{q}_A)$ is a strictly monotonically decreasing function of the amounts of DNA binding sites $\bar{q}_A$. Hence, in system (2.32), the dynamics of the activator have been slowed down compared to the original isolated system (2.23). That is, the *effective* kinetic rate of the activator dynamics is now decreased by a factor equal to $\mathcal{S}_A(a,\bar{q}_A)$. Note additionally that

$$\lim_{\bar{q}_A\to\infty} \mathcal{S}_A(a,\bar{q}_A) = 0 \text{ and } \mathcal{S}_A(a,0) = 1. \tag{2.33}$$

The Jacobian of system (2.32) calculated at the equilibrium is given by

$$J_A(\bar{q}_A) = \begin{bmatrix} \mathcal{S}_A^*(\bar{q}_A)\left(-\delta_A + \dfrac{\partial f_1(a^*,r^*)}{\partial a}\right) & \mathcal{S}_A^*(\bar{q}_A)\dfrac{\partial f_1(a^*,r^*)}{\partial r} \\ \dfrac{\partial f_2(a^*)}{\partial a} & -\delta_R \end{bmatrix}, \tag{2.34}$$

in which we use the shorthand notation $\mathcal{S}_A^*(\bar{q}_A) := \mathcal{S}_A(\bar{q}_A, a^*)$. We have $\det(J_A(\bar{q}_A)) = \mathcal{S}_A^*(\bar{q}_A)\det(J_0) > 0$ from condition *(i)* and that

$$\operatorname{tr}(J_A(\bar{q}_A)) = \mathcal{S}_A^*(\bar{q}_A)\left(-\delta_A + \frac{\partial f_1(a^*, r^*)}{\partial a}\right) - \delta_R.$$

Hence, while the addition of load does not change the sign of the determinant of the Jacobian, it can change the sign of the trace. For large enough load, because of (2.33), the trace becomes negative and the equilibrium point becomes stable. Hence, the periodic orbit disappears as shown in the following lemma.

Proposition 2. *Consider system (2.32) satisfying conditions (i) and (ii). There exists $q^* > 0$ such that the equilibrium (a^*, r^*) is asymptotically stable if and only if $\bar{q}_A > q^*$.*

Proof. We first show that $\det(J_A(\bar{q}_A)) > 0$ for all $\bar{q}_A$. This follows from the fact that $\det(J_A(\bar{q}_A)) = \mathcal{S}_A^*(\bar{q}_A)\det(J_0) > 0$, from condition *(i)*. We now focus on

$$\operatorname{tr}(J_A(\bar{q}_A)) = \mathcal{S}_A^*(\bar{q}_A)\left[-\delta_a + \frac{\partial f_1(a^*, r^*)}{\partial a}\right] - \delta_R.$$

From (2.33) and condition *(ii)*, when $\bar{q}_A = 0$ $\operatorname{tr}(J_A(0)) > 0$. Additionally, as $\bar{q}_A \to \infty$, $\operatorname{tr}(J_A(\bar{q}_A)) \to -\delta_R < 0$. Since the trace is a monotonic smooth function of $\bar{q}_A$, one can apply the intermediate value theorem to show that there is an unique $0 < q^* < \infty$ such that $\operatorname{tr}(J_A(q^*)) = 0$. Since $\det(J_A(q^*)) > 0$, the eigenvalues of $J_A(q^*)$ are imaginary. From the monotonicity of the trace with respect to $\bar{q}_A$, it follows that the real parts of the eigenvalues of $J_A(\bar{q}_A)$ are positive for all $0 \leq \bar{q}_A < q^*$ and negative for all $\bar{q}_A > q^*$. It follows that the system goes through a Hopf bifurcation at $\bar{q}_A = q^*$, and thus presents a periodic solution for $0 \leq q_A < q^*$ while it converges to the equilibrium for $\bar{q}_A > q^*$. □

Figure 2.6 a shows the effect of load on system (2.27).

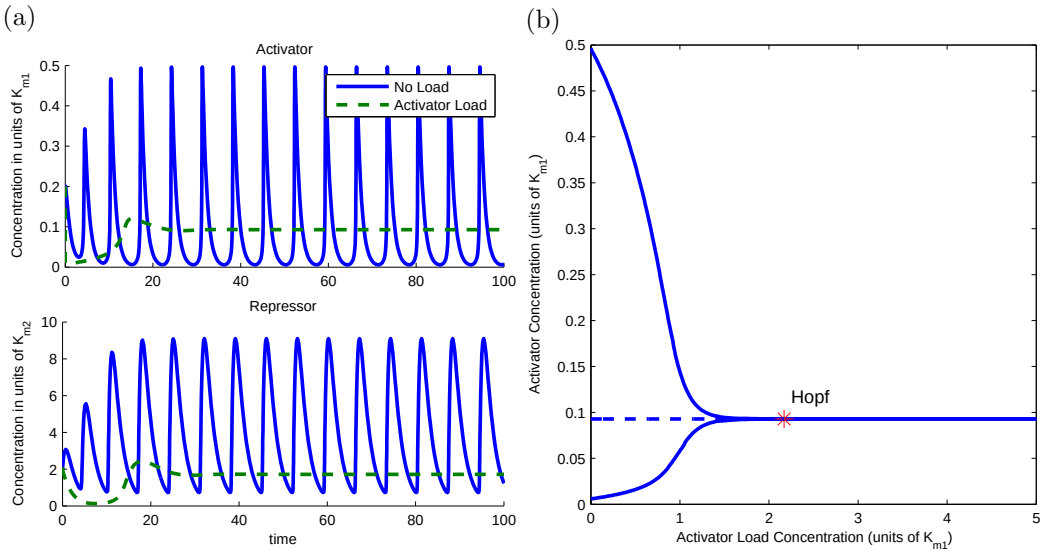

Figure 2.6: **(a) Load to the Activator can stop a Functional Clock.** The plots illustrate the trajectories of system (2.27) with two different amounts of load. The parameters in the simulation were $\beta_1 = \beta_3 = 100$, $\beta_2 = .04$, $\beta_4 = .004$, $\delta_A = 1$, $\delta_R = 0.5$, $G_1 = 100$, $m = 2$ and $n = 4$. The amount of DNA binding sites in the system with no load is $\bar{q}_A = 0$ whereas in the system with activator load is $\bar{q}_A = 20$. **(b) Bifurcation diagram with load as parameter.** A continuation of the equilibrium as a function of the load parameter $\bar{q}_A$ shows that, for this set of parameters, the amount of load to the activator required to stop the clock is on the order of the affinity coefficient K_{m1}, with the bifurcation occurring at $\bar{q}_A = 2.17$. The analysis was made on the full system (2.27) with the same parameters as before. The solid lines indicate a stable trajectory (the limit cycle to the left side of the Hopf bifurcation point and the equilibrium point to the right side of the Hopf bifurcation point). The dotted line indicates an unstable equilibrium point.

For the value of $\bar{q}_A$ for which $\mathrm{tr}(J_A(\bar{q}_A)) = 0$, the eigenvalues of the Jacobian are imaginary, hence the system goes through a Hopf bifurcation. A continuation study shows that the Hopf bifurcation is present also in the full three-state system (2.27). In particular, the amounts of load needed to switch the clock off is about four times the amplitude of the activator oscillations. For the specific choice of parameters in this example, the amount of load required to stop this clock is of the same order of the dissociation constant K_{m1}, which usually amounts to a low concentration. For example, for the NRI activator used in the oscillator in [38], $K_{m1} \approx 10pM$ [53] which amounts to approximately 10 copies of the binding site per cell in *E. coli*.

2.3.2 Switching the clock on by loading the repressor

We now consider a Non-Functional Clock and show how it can be turned into a Functional Clock by adding load to the repressor. Specifically, consider system (2.23) satisfying conditions *(i)* and *(ii)'*. Following the idea in the previous system, we model here the addition of DNA binding sites q_R with affinity to the repressor R, identical to the binding sites found in the original clock. This interaction, illustrated in Figure 2.4c, is modelled by the following chemical reaction

$$nR + q_R \underset{k_{b2}}{\overset{k_{a2}}{\rightleftharpoons}} D_2, \tag{2.35}$$

in which D_2 represents the complex formed by the R and q_R. Let the affinity between the repressor and the binding sites is given by the apparent dissociation constant $K_{m2} = \sqrt[n]{k_{b2}/k_{a2}}$. Let $d_2 := D_2/K_{m2}$ be the nondimensional concentration of complexes and $\bar{q}_R = (q_R + D_2)/K_{m2}$ be the total nondimensional concentration of binding sites. The nondimensionalized dynamics of the system are given by

$$\begin{aligned} \dot{a} &= -\delta_A a + f_1(a, r) \\ \dot{r} &= -\delta_R r + f_2(a) + n\delta_R G_2 d_2 - n\delta_R G_2 r^n(\bar{q}_R - d_2) \\ \dot{d_2} &= -\delta_R G_2 d_2 + \delta_R G_2 r^n(\bar{q}_R - d_2), \end{aligned} \tag{2.36}$$

in which $G_2 := k_{b2}/\delta_R$ models timescale separation between the dissociation rate of the complex D_2 and the repressor decay rate. It is possible to reduce the order of system (2.36) by a similar technique employed in the previous section. To this end, define $\epsilon := G_2^{-1}$. Define also the variable $y := r + nd_2$, system (2.36) can be taken to the standard singular perturbation form

$$\begin{aligned} \dot{a} &= -\delta_A a + f_1(a, y - nd_2) \\ \dot{y} &= -\delta_R(y - nd_2) + f_2(a) \\ \epsilon\dot{d_2} &= -\delta_R d_2 + \delta_R(y - nd_2)^n(\bar{q}_R - d_2). \end{aligned} \tag{2.37}$$

By setting $\epsilon = 0$, one obtains the reduced system in the original coordinates, which, since the slow manifold is locally exponentially stable (as shown in the Appendix), is a good approximation of system (2.36). This reduced system is given by

$$\begin{aligned} \dot{a} &= -\delta_A a + f_1(a, r) \\ \dot{r} &= \mathcal{S}_R(r, \bar{q}_R)(-\delta_R r + f_2(a)) \end{aligned} \tag{2.38}$$

in which

$$\mathcal{S}_R(r, \bar{q}_R) = \frac{1}{1 + n\bar{q}_R r^{n-1}(1 + r^n)^{-2}}.$$

Since $\mathcal{S}_R(r, \bar{q}_R) \neq 0$, the equilibrium points of (2.38) are the same as the ones of the isolated system (2.23). Therefore the unique equilibrium point (a^*, r^*) of (2.23) is also the unique equilibrium point of (2.38). We employ the shorthand notation $\mathcal{S}_R^*(\bar{q}_R) := \mathcal{S}_R(r, \bar{q}_R)$. It is easy to verify that $0 < \mathcal{S}_R^*(\bar{q}_R) \leq 1$ and that $\mathcal{S}_R^*(\bar{q}_R)$ is a strictly monotonically decreasing function of $\bar{q}_R$. Furthermore, we have that

$$\lim_{\bar{q}_R \to \infty} \mathcal{S}_R^*(\bar{q}_R) = 0 \text{ and } \mathcal{S}_R^*(0) = 1. \tag{2.39}$$

Hence, the addition of the load to the repressor makes the dynamics of the repressor slower compared to that of the isolated system (2.23). That is, the repressor *effective* kinetic rates are now smaller by a factor equal to $\mathcal{S}_R^*(\bar{q}_R)$, which can be arbitrarily decreased by increasing the amounts of sites $\bar{q}_R$. The Jacobian of system (2.38) calculated at the equilibrium (a^*, r^*) is given by

$$J_R(\bar{q}_R) = \begin{bmatrix} -\delta_A + \dfrac{\partial f_1(a^*, r^*)}{\partial a} & \dfrac{\partial f_1(a^*, r^*)}{\partial r} \\ \mathcal{S}_R^*(\bar{q}_R)\dfrac{\partial f_2(a^*)}{\partial a} & -\mathcal{S}_R^*(\bar{q}_R)\delta_R \end{bmatrix}. \tag{2.40}$$

Thus, the addition of load to the repressor does not change the sign of the determinant of the Jacobian as $\det(J_R(\bar{q}_R)) = \mathcal{S}_R^*(\bar{q}_R)\det(J_0) > 0$. However, it can change the sign of the trace

$$\operatorname{tr}(J_R(\bar{q}_R)) = -\delta_A + \frac{\partial f_1(a^*, r^*)}{\partial a} - \mathcal{S}_R^*(\bar{q}_R)\delta_R$$

from negative to positive as condition *(ii)'* is satisfied and condition (2.39) holds. Hence, the equilibrium point can become unstable with sufficient addition of the load and the system begins oscillating. The following Lemma shows this result.

Proposition 3. *Consider system (2.38) satisfying conditions (i) and (ii)'. There exists a* $q^* > 0$ *such that the equilibrium* (a^*, r^*) *is asymptotically stable if and only if* $\bar{q}_R < q^*$.

Proof. We first show that the $\det(J_R(\bar{q}_R)) > 0$ for all q_R. This follows from the fact that $\det(J_R(\bar{q}_R)) = \mathcal{S}_R^*(\bar{q}_R)\det(J_0) > 0$ from condition *(i)*. We now proceed to show that the trace can change its sign. Note that

$$\operatorname{tr}(J_R(\bar{q}_R)) = -\delta_A + \frac{\partial f_1(a^*, r^*)}{\partial a} - \mathcal{S}_R^*(\bar{q}_R)\delta_R.$$

From (2.39) and condition *(ii)'*, when $\bar{q}_R = 0$, $\operatorname{tr}(J_R(\bar{q}_R)) < 0$. Additionally, as $lim_{\bar{q}_R \to \infty} \operatorname{tr}(J_R(\bar{q}_R)) = -\delta_A + \dfrac{\partial f_1(a^*, r^*)}{\partial a} < 0$ from condition *(ii)'*. Since the trace is a monotonic smooth function of $\bar{q}_R$, one can apply the intermediate value theorem to show that there is an unique $0 < q^* < \infty$ such that $\operatorname{tr} J_R(q^*) = 0$. Since $\det(J_R(q^*)) > 0$, the eigenvalues of $J_R(q^*)$ are imaginary. From the monotonicity of the trace with respect to $\bar{q}_R$, it follows that the real parts of the eigenvalues of $J_R(\bar{q}_R)$ are negative for all $0 \leq \bar{q}_R < q^*$ and positive for all $q_R > q^*$. It follows thus that the system goes through a Hopf bifurcation at $\bar{q}_R = q^*$ and thus presents a periodic solution for $\bar{q}_R > q^*$ while it converges to the equilibrium for $\bar{q}_R < q^*$. □

Figure 2.7a shows the effect of load on system (2.36). Note that the parameters were chosen so that the system satisfies conditions *(i)* and *(ii)'*.

When $\operatorname{tr}(J_R(\bar{q}_R)) = 0$, a Hopf bifurcation occurs since both eigenvalues are imaginary. A continuation analysis can be used to show that this Hopf bifurcation is also present in the full system (2.36). Figure 2.7b illustrates that the amount of load

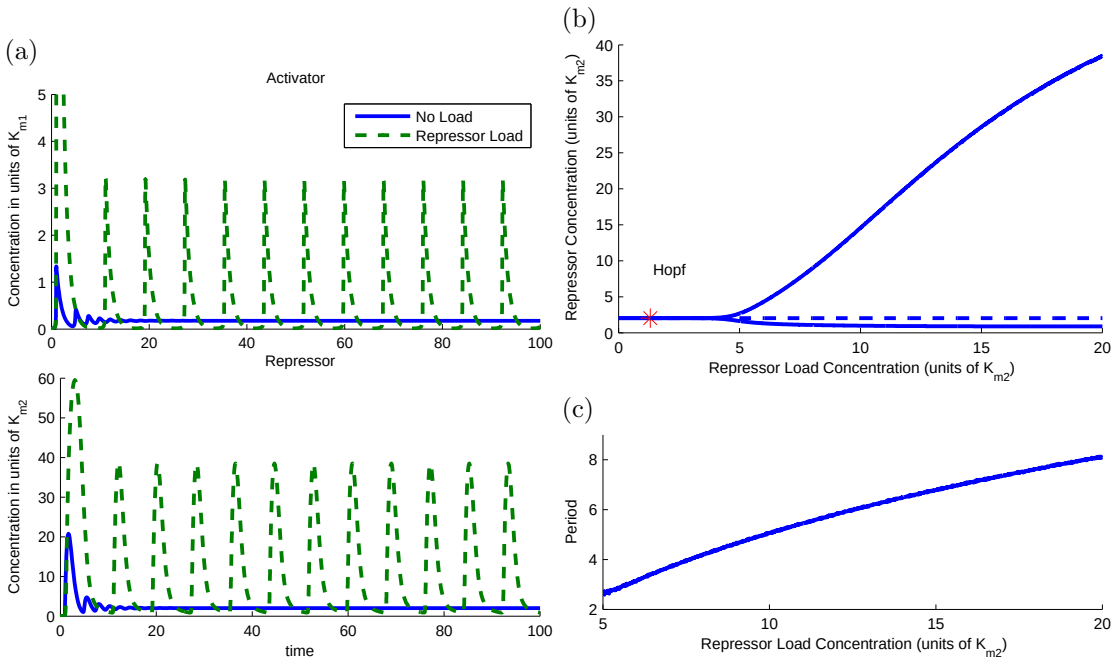

Figure 2.7: **(a) Load to the Repressor triggers a Non-functional Clock.** The plots illustrate the trajectories of system (2.36) with two different amounts of load. The parameters in the simulation were $\beta_1 = \beta_3 = 100$, $\beta_2 = .04$, $\beta_4 = .004$, $\delta_A = 1$, $\delta_R = 1.5$, $G_2 = 100$, $m = 2$ and $n = 4$. The amount of DNA binding sites in the system with no load is $\bar{q}_R = 0$ whereas in the system with repressor load is $\bar{q}_R = 20$. **(b) Hopf Bifurcation with $\bar{q}_R$ as a parameter.** A continuation of the equilibrium as a function of the load parameter $\bar{q}_R$ shows that, for this set of parameters, the amount of load required to activate the clock is in the same order of magnitude as that of the the affinity coefficient K_{m2}, with bifurcation occurring at $\bar{q}_R = 1.32$. This plot was obtained via continuation of system (2.36) with the same parameters as before. Solid lines indicate a stable trajectory (limit cycle to the right of the Hopf bifurcation and the equilibrium to its right). The dotted line indicates an unstable equilibrium point. (c) *Period increases as a function of the repressor load $\bar{q}_R$.*

required for the Hopf bifurcation is given by $\bar{q}_R = 1.32$ in units of K_{m2}. Hence, the amounts of load needed to switch the clock on is on the same order of the amounts of repressor at the equilibrium. For the LacI repressor employed in [38], $K_{m2} \approx 1pM$ [54], which amounts to few copies per cell of the load.

Figure 2.7c shows that the addition of load increases the period of oscillation. This suggests the possibility that the load can be employed not only for switching an oscillator "on" and "off" but for also tuning the period. However, the increase in period is accompanied by an increase in the amplitude of the oscillation (Figure 2.7b), which may be undesired. We discuss how the period can be changed while

maintaining the amplitude through simultaneous addition of activator and repressor loads in Section "Tuning the Clock period".

2.3.3 Stochastic simulations of the switching behavior

In order to understand how robust the switching behavior is to intrinsic noise, we employ stochastic simulations of the system. An implementation of the Gillespie algorithm [55] was employed to produce realizations of trajectories of an activator repressor clock in which both activator and repressor bind to DNA as dimers ($m = n = 2$).

In these simulations, we assumed the presence of 5 copies of each activator and repressor gene to emulate the situation in which the circuit is present in a low copy number plasmid. Expression rates and degradation rates were chosen based on the values used in the deterministic models to obtain a functional and a non-functional oscillator. The association and dissociation rates between proteins and dimers were chosen so that the apparent dissociation constants $K_{m1} = K_{m2} = 1$, which consider a bacterial transcription factor with apparent dissociation constant on the order of picomolars. A detailed description of this model is given in the Appendix.

Figure 2.8a shows that addition of binding sites with affinity to the activator can eliminate oscillations from a functional clock. Figure 2.8b shows how the addition of binding sites with affinity to the repressor can generate sustained more robust oscillations in a non-functional clock. In both situations, the amount of loads employed to switch the clock is on the order of $10^2 - 10^3$ copies of binding sites per cell, which can be achieved by inserting small arrays in high copy number plasmids.

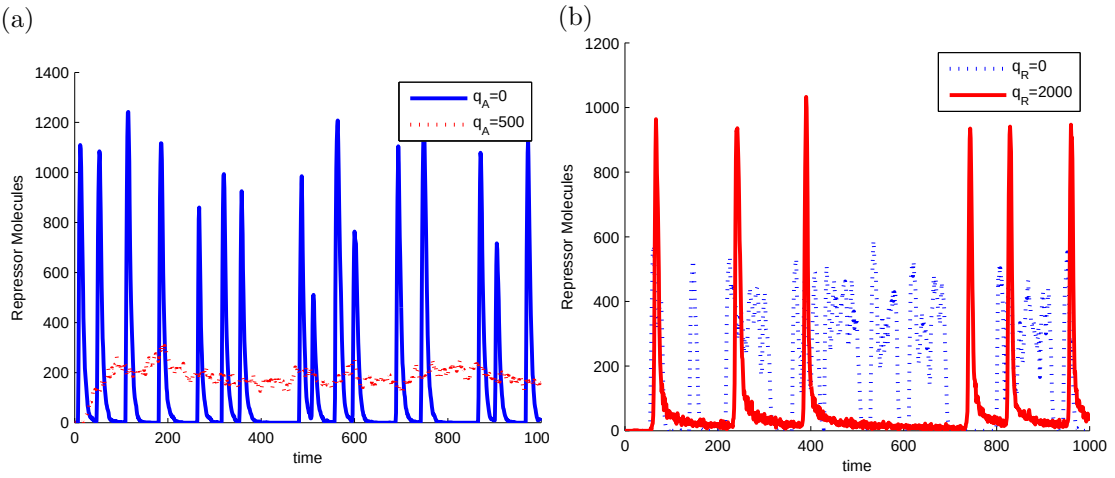

Figure 2.8: **Effect of the load on clock holds under intrinsic noise.** The plots above are stochastic realizations of an activator-repressor clock with $m = n = 2$ and containing 5 copies of activator and repressor genes. (a) *Functional clock stops with load to the activator.* We show that, with the chosen parameters, it is possible to stop the clock with an amount of load that is roughly 100 times higher than the copy number of the circuit. (b) *Load to the repressor leads to robust oscillation.* We show that, the it is possible to generate robust oscillation with roughly 400 times the number of circuit genes with the choice of parameters above.

2.3.4 Tuning the clock period

As noticed in Figure 2.7c, addition of binding sites to the repressor increases the period of the limit cycles of the system. However, this may cause an increase in the amplitude of the cycle (Figure 2.7b), which may be undesirable. In this section, we illustrate how the simultaneous addition of load to both the activator and repressor can be employed to vary the period as desired with little impact on the cycle amplitude.

Consider the nondimensional model for the system with DNA binding sites for both the activator and the repressor as shown in Figure 2.4d:

$$\begin{aligned}
\dot{A} &= -\delta_A A + g_1(A,R) + k_{u1} D_1 - k_{b1} A^m (q_{A,T} - D_1) \\
\dot{R} &= -\delta_R R + g_2(A) + k_{u2} D_2 - k_{b2} R^n (q_{R,T} - D_2) \\
\dot{D}_1 &= -k'_{u1} D_1 + k'_{b1} A^m (q_{A,T} - D_1) \\
\dot{D}_2 &= -k'_{u2} D_2 + k'_{b2} R^n (q_{R,T} - D_2).
\end{aligned} \tag{2.41}$$

Here, k_{b1}, k_{u1} model the association and dissociation rates between the activator protein and its corresponding DNA binding site q_A, k_{b2}, k_{u2} model the association and dissociation rates between the repressor protein and its corresponding DNA binding site q_R, $g_1(A,R)$, $g_2(A)$ represent the dimensional version of the Hill functions (see Appendix), and $q_{A,T}$, $q_{R,T}$ represent the total concentration of activator and repressor DNA sites.

This system can be nondimensionalized, by setting the nondimensional states $a = A/K_{m1}$, $r = R/K_{m2}$, $d_1 = D_1/K_{m1}$ and $k_2 = D_2/K_{m2}$, as shown in the Appendix, to obtain system

$$\begin{aligned}
\dot{a} &= -\delta_A a + f_1(A,R) + mG_1\delta_A d_1 - mG_1\delta_A a^m(\bar{q}_A - d_1) \\
\dot{r} &= -\delta_R r + f_2(A) + nG_2\delta_R d_2 - nG_2\delta_R r^n(\bar{q}_R - d_2) \\
\dot{d}_1 &= -G_1\delta_A d_1 + G_1\delta_A a^m(\bar{q}_A - d_1) \\
\dot{d}_2 &= -G_2\delta_R d_2 + G_2\delta_R r^n(\bar{q}_R - d_2),
\end{aligned} \tag{2.42}$$

in which $f_1(A,R)$ and $f_2(A)$ are the nondimensional Hill functions as given in expressions (2.24), $\bar{q}_A = q_{A,T}/K_{m1}$ and $\bar{q}_R = q_{R,T}/K_{m2}$, and G_1 and G_2 are as defined before. In order to employ a singular perturbation argument similar to what was done in the previous sections, define $\epsilon = 1/G_1$, $\nu = G_2/G_1$ to model the explicit timescale separation present in this system. Define also the following change of variables $y_1 := a + md_1$ and $y_2 = r + nd_2$. Substituting these in (2.42), one obtains the system in standard singular perturbation form:

$$\begin{aligned}
\dot{y}_1 &= -\delta_A(y_1 - md_1) + f_1(y_1 - md_1, y_2 - nd_2) \\
\dot{y}_2 &= -\delta_R(y_2 - nd_2) + f_2(y_1 - md_1) \\
\epsilon\dot{d}_1 &= -\delta_A d_1 + \delta_A(y_1 - md_1)^m(\bar{q}_A - d_1) \\
\epsilon\dot{d}_2 &= -\nu\delta_R d_2 + \nu\delta_R(y_2 - nd_2)^n(\bar{q}_R - d_2).
\end{aligned} \tag{2.43}$$

By setting $\epsilon = 0$, one obtains the slow manifold

$$(d_1, d_2) = \left(\bar{q}_A \frac{a^m}{a^m + 1}, \bar{q}_R \frac{r^n}{r^n + 1} \right) := (\phi_1(a), \phi_2(r)) .$$

Since the slow manifold is locally exponentially stable (see Appendix), the reduced system is a good approximation of system (2.43). Since $\dot{y}_1 = \dot{a} + m\frac{d\phi_1(a)}{da}\dot{a}$ and $\dot{y}_2 = \dot{r} + n\frac{d\phi_2(r)}{dr}\dot{r}$, this reduced system, in the original variables, takes the form

$$\begin{aligned} \dot{a} &= S_A(a, \bar{q}_A) \left(-\delta_A a + f_1(a, r) \right) \\ \dot{r} &= S_R(r, \bar{q}_R) \left(-\delta_R r + f_2(a) \right), \end{aligned} \tag{2.44}$$

in which

$$S_A(a, \bar{q}_A) = \frac{1}{1 + m\dfrac{d\phi_1(a)}{da}} = \frac{1}{1 + \bar{q}_A m^2 a^{m-1}(1 + a^m)^{-2}}$$

and

$$S_R(r, \bar{q}_R) := \frac{1}{1 + n\dfrac{d\phi_2(r)}{dr}} = \frac{1}{1 + \bar{q}_R n^2 r^{n-1}(1 + a^n)^{-2}}.$$

Let the activator and repressor loads be added at a fixed ratio $\rho = \bar{q}_A/\bar{q}_R$ and define $F(a, r, \bar{q}_R) := \dfrac{S_R(r, \bar{q}_A/\rho)}{S_A(a, \bar{q}_A)}$. System (2.44) can be re-written as

$$\begin{aligned} \dot{a} &= \left(-\delta_A a + f_1(a, r) \right) S_A(a, \bar{q}_A) \\ \dot{r} &= \left(-\delta_R r + f_2(a) \right) S_A(a, \bar{q}_A) F(a, r, \bar{q}_A). \end{aligned} \tag{2.45}$$

Since $S_A(a, \bar{q}_A) > 0$, this system is orbitally equivalent [49] to the system

$$\begin{aligned} \dot{a} &= \left(-\delta_A a + f_1(a, r) \right) \\ \dot{r} &= \left(-\delta_R r + f_2(a) \right) F(a, r, \bar{q}_A). \end{aligned} \tag{2.46}$$

Hence, if system (2.45) has a periodic orbit, system (2.46) will have a corresponding periodic orbit with identical trajectories. The corresponding periodic signals, however, will have different periods whose values depend on function $S_A(a, \bar{q}_A)$. Thus, if the value of $F(a, r, \bar{q}_A)$ does not appreciably change when $\bar{q}_A$ changes, the addition

of the load will affect the period of oscillations without impacting their amplitudes. Since

$$\frac{\partial F(a,r,\bar{q}_A)}{\partial \bar{q}_A} = \left(\frac{m^2 a^{m-1}}{(1+a^m)^2} - \rho \frac{n^2 r^{n-1}}{(1+r^n)^2} \right) \frac{(1+r^n)^4}{\left((1+r^n)^2 + \rho \bar{q}_A n^2 r^{n-1}\right)^2}, \tag{2.47}$$

we have that for large values of $\bar{q}_A$, $\frac{\partial F(a,r,\bar{q}_A)}{\partial \bar{q}_A} \approx 0$. Under these conditions, since the function $S_A(a,\bar{q}_A)$ is a monotonically decreasing function of $\bar{q}_A$, the periodic orbits of system (2.45) will display decreasing periods as $\bar{q}_A$ increases, while maintaining the same amplitude, due to orbital equivalence between system (2.46) and system (2.45). A proof of this results is given in the Appendix.

Figure 2.9a illustrates this result. The addition of repressor load to a functioning clock increases the period but also leads to a higher amplitude. This effect in the amplitude is not observed when both activator and repressor loads are added. Figure 2.9b shows this behavior for increasing amount of load. When only repressor load is added, there is an increase in the period of the limit cycles along with an increase in the amplitude, as it was seen in the previous section (Figure 2.7(b) and (c)). However, if a sufficient amount of activator load is simultaneously added along with the repressor load, the increase of the period occurs with very little impact on the amplitude of oscillations.

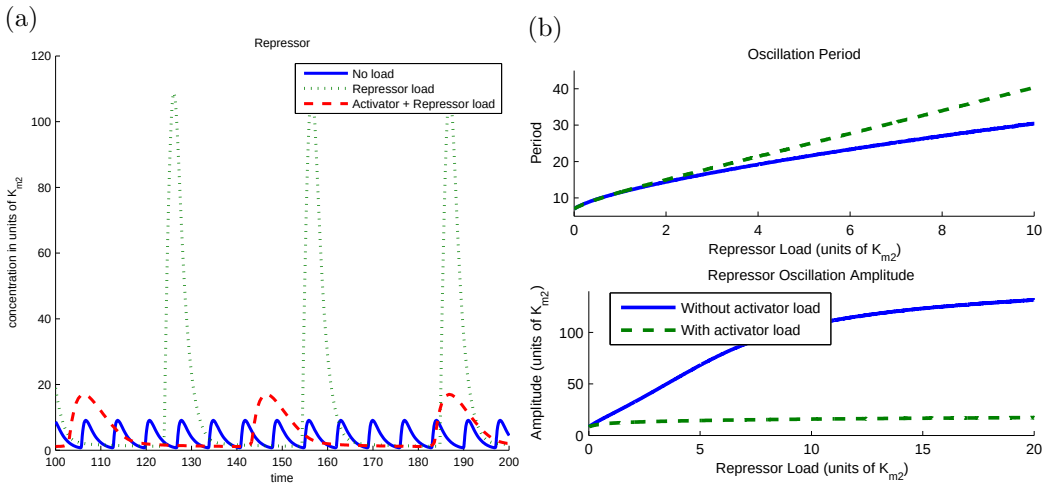

Figure 2.9: **Tuning the period without affecting the amplitude.** (a) When compared to the isolated system, the amplitude of oscillations in system (2.42) increases when we add exclusively DNA binding sites with affinity to the repressor ($\bar{q}_A = 0$, $\bar{q}_R = 10$). However, if we simultaneously add DNA binding sites with affinity to the activator, the amplitude is not affected as much ($\bar{q}_A = \bar{q}_R = 10$). (b) The period of system (2.42) can be changed with no effect on the amplitude when DNA binding sites with affinity to both the repressor and the activator are added simultaneously. The upper plot shows that a similar increase of period observed via the addition of repressor load can be obtained via the simultaneous addition of activator and repressor load. This second method has the advantage of not generating an increase in the amplitude, as shown in the lower plot. In this simulation we assumed the ratio $\rho = \bar{q}_A/\bar{q}_R = 1$. Parameters of the activator repressor system used in the simulation were $\beta_1 = \beta_3 = 100$, $\beta_2 = .04$, $\beta_3 = .004$, $\delta_A = 1$, $\delta_R = 0.5$, $G_1 = 100$, $G_2 = 100$ and $m = 2$, $n = 4$. In the traces showing only repressor load $\rho = 0$, while the traces showing simultaneous repressor and activator load, $\rho = 1$.

CHAPTER III

Insulation Devices

As discussed in Chapter II, bio-molecular systems may be susceptible to retroactivity. In this chapter, we study *insulation devices*, components capable of mitigating the retroactivity to the output of a system. Such a device can be placed between an upstream and a downstream system preventing the retroactivity from the downstream interconnection to propagate upstream as shown in Figure 1.1B.

A design principle for insulation devices presented in [13] shows that a system with a large amplification and large negative feedback has the insulation property. In Section 3.1 we generalize the design principle by showing that, given the appropriate stability and structural conditions, timescale separation is a sufficient property for insulation devices. Section 3.2 gives two candidate implementations of insulation devices based on this design principle. Finally Section 3.3 gives an analysis of tradeoffs between retroactivity attenuation and noise amplification.

3.1 Insulation Devices based on Separation of Timescale

Consider the block diagram model for a system depicted in Figure 3.1. This diagram depicts an insulation device Σ connected to an upstream system and a downstream system. In addition to the usual input signal u and output signal x, we add two additional signals travelling from downstream to upstream: a retroactivity

to the output s and a retroactivity to the input r. Retroactivity to the output s is a signal (which may depend on x and on the internal variables v of the downstream system) that appears in the dynamics of Σ whenever Σ is connected to the downstream system. Retroactivity to the input r (which may depend on u and on x) is a signal that system Σ applies to its upstream system as an input whenever Σ connects to the upstream system to receive the information u. For example, in the transcriptional component modelled in (2.1), $s = -k_{\text{on}}Z(q_T - C) + k_{\text{off}}C$ represents the retroactivity to the output generated by the addition of promoters p with affinity to protein Z. System Σ is said *isolated* when it is not connected to the downstream system. In such a case, $s = 0$. From an engineering point of view, signals s and r do not necessarily carry information but their presence are tied to signals x and u, respectively.

Figure 3.1: **Structure of an insulation device.** A system Σ with input and output signals, along with the interconnection structure with its upstream and its downstream systems. The retroactivity to the output s accounts for the change in the system Σ dynamics when it is connected to downstream systems. The retroactivity to the input r accounts for changes that Σ causes on upstream systems when it connects to receive the information u.

Let $u \in D_u \subset \mathbb{R}^q_+$, $x \in D_x \subset \mathbb{R}^n_+$, and $v \in D_v \subset \mathbb{R}^p_+$ be vectors whose components denote concentrations of chemical species, such as proteins, enzymes, DNA sites, etc. Let $r(x,u) \in \mathbb{R}^r$ and $s(x,v) \in \mathbb{R}^s$ be reaction rate vectors modelling the interaction of species in the vector u with species in the vector x and of species in the vector x with species in the vector v, respectively. Let $A \in \mathbb{R}^{r\times q}$, $B \in \mathbb{R}^{r\times n}$, $C \in \mathbb{R}^{s\times n}$, and $D \in \mathbb{R}^{s\times p}$ be constant matrices. Let $f(x,u) \in \mathbb{R}^n$, $l(v) \in \mathbb{R}^p$, and $h(v,t) \in \mathbb{R}^p$ be vector fields and G_1, G_2 be positive constants. The model that we consider for Σ in

the interconnection of Figure 3.1 is the following:

$$\begin{aligned} \dot{u} &= g(u,t) + G_1 A r(x,u) \\ \dot{x} &= G_1 B r(x,u) + G_1 f(x,u) + G_2 C s(x,v) \\ \dot{v} &= G_2 D s(x,v) + G_2 l(v) + h(v,t), \end{aligned} \tag{3.1}$$

with initial conditions $u(t_0), x(t_0), v(t_0)$. When Σ is isolated from the downstream system ($s(x,v) = 0$), the model becomes

$$\begin{aligned} \dot{u}_{\text{is}} &= g(u_{\text{is}},t) + G_1 A r(u_{\text{is}}, x_{\text{is}}) \\ \dot{x}_{\text{is}} &= G_1 B r(u_{\text{is}}, x_{\text{is}}) + G_1 f(x_{\text{is}}, u_{\text{is}}), \end{aligned} \tag{3.2}$$

with initial conditions $u_{\text{is}}(t_0) = u(t_0),\ x_{\text{is}}(t_0) = x(t_0)$.

System (3.1) is a general model for a bio-molecular system. Interconnections always occur through reactions, whose rates (r and s, in this case) appear in both the upstream and the downstream systems with different coefficients (captured by matrices A, B, C, and D). Constants G_1 and G_2 explicitly model the fact that some of the reactions may be several orders of magnitude faster than others. Constant G_1 models the timescale of system Σ while constant G_2 models the timescale of the interconnection mechanism between Σ and its downstream system.

We claim that if G_1 is large enough, Σ can be considered an insulation device. To identify the conditions that allow Σ to attenuate the retroactivity to the output and in quantifying the retroactivity to the input we define the *retroactivity to the output attenuation property* of system Σ in the interconnection structure of Figure 3.1 as follows:

Let $u(t, 1/G_1, 1/G_2),\ x(t, 1/G_1, 1/G_2),\ v(t, 1/G_1, 1/G_2)$ be the unique solution to system (3.1) and $u_{\text{is}}(t, 1/G_1)\ x_{\text{is}}(t, 1/G_1)$ be the unique solution for (3.2) for $t \in [t_0, \bar{t}_f]$ with $\bar{t}_f > t_0$. System Σ has the *retroactivity to the output attenuation*

property provided there are constants $t_b \in (t_0, \bar{t}_f]$, $G_1^* > 0$, $G_2^* > 0$, and a compact set $\Omega \subset D_x \times D_u \times D_v$ such that the following properties hold for $G_1 > G_1^*$ and $(x(t_0), u(t_0), v(t_0)) \in \Omega$:

(i) $x(t, 1/G_1, 1/G_2) - x_{\text{is}}(t, 1/G_1) = O\left(\frac{1}{G_1}\right) \forall t \in [t_b, \bar{t}_f]$ when $(G_2/G_1) \to \{O(1), 0\}$ as $G_1 \to \infty$;

(ii) $x(t, 1/G_1, 1/G_2) - x_{\text{is}}(t, 1/G_1) = O\left(\frac{G_1}{G_2}\right) \forall t \in [t_b, \bar{t}_f]$ when $(G_2/G_1) \to \infty$ as $G_1 \to \infty$ and $G_2 > G_2^*$.

If a system Σ enjoys the retroactivity to the output attenuation property, as G_1 grows, its dynamics becomes less affected by the retroactivity to the output independent of the value of G_2. The importance of this result comes from the fact that it is possible for a general bio-molecular circuit to be in the same range as, much faster than, or much slower than its downstream system [56, 57, 58, 59].

3.1.1 Retroactivity in an Insulation Device

System (3.1) displays multiple timescales. Specifically, since $G_1 \gg 1$, there are at least two timescales and when $G_2 \gg G_1$ there are three timescales. There is therefore the opportunity to employ singular perturbation to approximate the dynamics of Σ to a lower order model which can facilitate the analysis. We must therefore make the separation of timescales explicitly by bringing (3.1) to the standard singular perturbation form [47]. Fortunately, due to the nature of the interconnection in bio-molecular systems, it is often possible to separate the slow variables of a system through a linear combination of the states of the upstream and downstream systems [60, 61, 62]. This motivates an approach that employs a linear coordinate transformation to take the original system to standard singular perturbation form.

In what follows, we first determine conditions for the existence of a linear coor-

dinate transformation independent of G_1 and G_2 that transforms systems (3.1) and (3.2) to standard singular perturbation form. To this end, we restrict the class of systems (3.1) to those with the two following central properties:

P1 There is an invertible matrix $T \in \mathbb{R}^{q\times q}$ and a matrix $M \in \mathbb{R}^{n\times q}$ such that

(i) $TA + MB = 0$;

(ii) $Mf(x,u) = 0$ for all (x,u); and

(iii) $MC = 0$.

P2 There is an invertible matrix $Q \in \mathbb{R}^{n\times n}$, and a matrix $P \in \mathbb{R}^{p\times n}$ such that

(i) $QC + PD = 0$;

(ii) $Pl(v) = 0$ for all v.

Define the vector fields

$$\bar{h}(y,v) := D\ s(Q^{-1}(y-Pv),v) + l(v) \tag{3.3}$$

$$\begin{aligned}\bar{f}(z,y,v) := Q\Big[&Br\Big(Q^{-1}(y-Pv), T^{-1}\big(z - MQ^{-1}(y-Pv)\big)\Big)\\ &+ f\left((Q^{-1}(y-Pv), T^{-1}(z-MQ^{-1}(y-Pv))\right)\Big]\end{aligned} \tag{3.4}$$

$$\tilde{f}(z,x) := Br(x, T^{-1}(z-Mx)) + f(x, T^{-1}(z-Mx)), \tag{3.5}$$

and let $\epsilon_1 := 1/G_1$, $\epsilon_2 := 1/G_2$. Then, the following proposition shows that a separation of the timescales is possible.

Proposition 4. *Under properties P1 and P2, the linear change of coordinates*

$$z = Tu + Mx,\ y = Qx + Pv \tag{3.6}$$

takes systems (3.1) and (3.2) respectively to the standard singular perturbation forms

$$\begin{aligned} \dot{z} &= Tg\left(T^{-1}(z - MQ^{-1}(y - Pv)), t\right) \\ \epsilon_1 \dot{y} &= \bar{f}(z, y, v) + \epsilon_1 Ph(v, t) \\ \epsilon_2 \dot{v} &= \bar{h}(y, v) + \epsilon_2 h(v, t) \end{aligned} \tag{3.7}$$

and

$$\begin{aligned} \dot{z}_{is} &= Tg\left(T^{-1}(z_{is} - Mx_{is}), t\right) \\ \epsilon_1 \dot{x}_{is} &= \tilde{f}(z_{is}, x_{is}). \end{aligned} \tag{3.8}$$

Proof. From the linear coordinate transformation (3.6), we have that $\dot{z} = T\dot{u} + M\dot{x}$ and $\dot{y} = Q\dot{x} + P\dot{v}$. By substituting in these relations the expressions of $\dot{u}, \dot{x}$, and $\dot{v}$ from system (3.1) (from system (3.2)), writing $u = T^{-1}(z - Mx)$, and $x = Q^{-1}(y - Pv)$, one obtains system (3.7) (system (3.8)). □

Conditions $TA + MB = 0$ and $Mf(x, u) = 0$ from property P1 and the conditions from property P2 ensure the existence of a linear coordinate transformation that takes the system to standard singular perturbation form. Additionally, condition $MC = 0$ from property P1 is necessary to ensure that once $\epsilon_1 = \epsilon_2 = 0$, the dynamics of u do not depend on v, and thus that the retroactivity to the output does not directly propagate to the input.

For $(u, x, v) \in D_u \times D_x \times D_v$, define the domains D_z and D_y to be the images of D_u, D_x, D_v through transformations (3.6). We also define the map $\mathcal{F} : D_u \times D_x \to D_z \times D_x$ for all $(u, x) \in D_u \times D_x$ as $\mathcal{F}(u, x) := (Tu + Mx, x)$. Note that this map is continuous and invertible. Similarly, define the map $\mathcal{G} : D_u \times D_x \times D_v \to D_z \times D_y \times D_v$ for all $(u, x, v) \in D_u \times D_x \times D_v$ as $\mathcal{G}(u, x, v) := (Tu + Mx, Qx + Pv, v)$. Note that this map is also continuous and invertible.

3.1.2 Conditions for an Insulation Device

A nested application of Tikhonov singular perturbation theorem, as found in standard references, is employed in systems (3.7) and (3.8). To assure validity of the theorems, we impose technical assumptions which are considered valid on the domains D_u, D_x, D_v, D_z, and D_y. In what follows, we say that a square matrix $A(x)$ depending on $x \in D \subset \mathbb{R}^n$ is Hurwitz uniformly for $x \in D$ if there is a real $c > 0$ such that $\Re\{\lambda(A(x))\} < -c$ for all $x \in D$.

A1 The functions g, f, h, r, s are smooth;

A2 The functions g, f, h, r are Lipschitz continuous for all $t \in \mathbb{R}_+$;

A3 The function $v = \phi_1(y)$ is the unique solution of $\bar{h}(y, v) = 0$, it is Lipschitz continuous and smooth;

A4 The function $y = \phi_2(z)$ is the unique solution of $\bar{f}(z, y, \phi_1(y)) = 0$ and it is Lipschitz continuous;

A5 The function $x = \phi_x(z)$ is the unique solution of $\tilde{f}(z, x) = 0$ and it is Lipschitz continuous;

A6 We have that $\frac{\partial}{\partial v}\bar{h}(y, v)\big|_{v=\phi_1(y)}$ is Hurwitz uniformly for $y \in D_y$;

A7 We have that $\frac{\partial}{\partial y}\bar{f}(z, y, \phi_1(y))\Big|_{y=\phi_2(z)}$ is Hurwitz uniformly for $z \in D_z$;

A8 We have that $\frac{\partial}{\partial (y,v)} \left[\begin{array}{c} \bar{f}(z, y, v) \\ \bar{h}(y, v) \end{array} \right] \Bigg|_{y=\phi_2(z), v=\phi_1 \circ \phi_2(z)}$ is Hurwitz uniformly for $z \in D_z$;

A9 We have that $\frac{\partial}{\partial x}\tilde{f}(z, x)\Big|_{x=\phi_x(z)}$ is Hurwitz uniformly for $z \in D_z$.

Assumptions A1 and A2 guarantee existence and uniqueness of the solutions of systems (3.1) and (3.2). As a consequence, assumptions A1 and A2 also guarantee the existence and uniqueness of the solutions of systems (3.7) and (3.8). Assumptions

A3, A4, A6 and A7 guarantee the stability of the boundary layer systems obtained when employing a nested application of Tikhonov theorem to system (3.7) for the case in which $G_1 \ll G_2$. Along with assumption A8, assumptions A3 and A4 are also employed to guarantee the stability of the boundary layer system in the application of Tikhonov theorem to system (3.7) for the case in which G_1 and G_2 are of the same order of magnitude. Assumptions A5 and A9 guarantee the stability of the boundary layer system when employing Tikhonov theorem to system (3.8) and to system (3.7) when $G_1 \gg G_2$. The following proposition shows the uniqueness of the solutions given in A3 and A4 is preserved under coordinate transformations.

Proposition 5. *Let* $(y, v) = (\varphi_y(z), \varphi_v(z))$ *be a solution to* $(\bar{f}(z, y, v), \bar{h}(y, v)) = 0$. *Then, such a solution is unique. Furthermore* $\varphi_y(z) = \phi_2(z)$ *and* $\varphi_v(z) = \phi_1 \circ \phi_2(z)$.

Proof. Since $(y, v) = (\varphi_y(z), \varphi_v(z))$ is a solution to equation $(\bar{f}(z, y, v), \bar{h}(y, v)) = 0$, we have that $\bar{h}(\varphi_y(z), \varphi_v(z)) = 0$. By A3, this implies that $\varphi_v(z) = \phi_1 \circ \varphi_y(z)$. This along with $\bar{f}(z, \varphi_y(z), \varphi_v(z)) = 0$ imply that $\bar{f}(z, \varphi_y(z), \phi_1 \circ \varphi_y(z)) = 0$. This along with A4 imply that $\varphi_y(z) = \phi_2(z)$. As a consequence, we have that $\varphi_v(z) = \phi_1 \circ \varphi_y(z) = \phi_1 \circ \phi_2(z)$. □

3.1.3 Insulation from Timescale Separation

The main result of this section is based on the two following lemmas, which employ Tikhonov singular perturbation theorem in the form presented in [47]. Specifically, Lemmas 2 and 3 provide approximations of the isolated and connected system trajectories, respectively, when we consider as small parameters $\epsilon_1 := 1/G_1$ and $\epsilon_2 := 1/G_2$. These approximations are then compared with each other to obtain the retroactivity to the output attenuation property, which is the main result of the paper.

Before giving the first lemma, we define the two following sets. For any $\alpha > 0$,

define the set $R_{u,x}(\alpha) \subset D_u \times D_x$ by

$$R_{u,x}(\alpha) := \{(u,x) \in D_u \times D_x \mid \|x - \phi_x(Tu + Mx)\| < \alpha\} \tag{3.9}$$

and let $\Omega_{u,x}(\alpha)$ be any compact subset of $R_{u,x}(\alpha)$. For $\alpha > 0$, define the set $R_{u,x,v}(\alpha) \subset D_u \times D_x \times D_v$ by

$$R_{u,x,v}(\alpha) := \left\{ (u,x,v) \in D_u \times D_x \times D_v \,\middle|\, \left\| \begin{array}{c} v - \phi_1(Qx + Pv) \\ Qx + Pv - \phi_2(Tu + Mx) \end{array} \right\| < \alpha \right\}, \tag{3.10}$$

and let $\Omega_{u,x,v}(\alpha)$ be any compact subset of $R_{u,x,v}(\alpha)$. The next proposition shows the relationship between the sets $R_{u,x}$ and $R_{u,x,v}$.

Proposition 6. *Consider the sets defined in equations (3.9) and (3.10). Then, for all $\alpha > 0$ there is $\beta > 0$ such that $(u,x,v) \in R_{u,x,v}(\beta)$ implies that $(u,x) \in R_{u,x}(\alpha)$.*

Proof. Since $x = \phi_x(z)$ is the unique solution of $\tilde{f}(z,x) = 0$ and $\bar{f}(z, \phi_2(z), \phi_1 \circ \phi_2(z)) = 0$, it follows from the definition of $\bar{f}$ (equation (3.4)) that $Q^{-1}(\phi_2(z) - P\phi_1 \circ \phi_2(z)) = \phi_x(z)$. Since Q is invertible, for all $\alpha > 0$ there is $\beta_2 > 0$ such that $\|Qx - \phi_2(Tu + Mx) + P\phi_1 \circ \phi_2(Tu + Mx)\| < \beta_2$ implies $\|x - \phi_x(Tu + Mx)\| < \alpha$. By applying the triangular inequality, one can show that for all $\beta_2 > 0$ there is $\beta_1 > 0$ such that $\|v - \phi_1 \circ \phi_2(Tu + Mx)\| < \beta_1$ and $\|Qx + Pv - \phi_2(Tu + Mx)\| < \beta_1$ imply $\|Qx - \phi_2(Tu + Mx) + P\phi_1 \circ \phi_2(Tu + Mx)\| < \beta_2$. Finally, the continuity of ϕ_1 along with the triangular inequality imply that for all $\beta_1 > 0$ there is $\beta_0 > 0$ such that $\|v - \phi_1(Qx + Pv)\| < \beta_0$ and $\|Qx + Pv - \phi_2(Tu + Mx)\| < \beta_0$ imply $\|v - \phi_1 \circ \phi_2(Tu + Mx)\| < \beta_1$. Let $\beta := \min(\beta_0, \beta_1)$. □

As a consequence of this proposition, if $\Omega \subset R_{u,x,v}(\beta)$ is compact, then the set $\{(u,x) \mid (u,x,v) \in \Omega\}$ is a compact subset of $R_{u,x}(\alpha)$.

Under properties P1-P2 and assumptions A1-A9, we give the two following lemmas.

Lemma 2. *Let $u_{is}(t, 1/G_1), x_{is}(t, 1/G_1)$ be the unique solution of system (3.2) for $t \in [t_0, t_f]$ with initial condition $u_{is}(t_0) \in D_u$ and $x_{is}(t_0) \in D_x$. Let $\bar{u}(t)$ be the unique solution of system*

$$\dot{\bar{u}} = \left(T + M \frac{d\gamma_x(\bar{u})}{d\bar{u}} \right)^{-1} T g(\bar{u}, t) \tag{3.11}$$

for $t \in [t_0, \bar{t}_f]$ with initial condition $\bar{u}(t_0) = T^{-1}(z_{is}(t_0) - \phi_x(z_{is}(t_0)))$ where $z_{is}(t_0) = Tu_{is}(t_0) + Mx_{is}(t_0)$ and $x = \gamma_x(u)$ is the locally unique solution of $Br(x, u) + f(x, u) = 0$. Then, there is $\alpha > 0$ such that for all $t_b \in (t_0, \bar{t}_f]$ there exists $G_1^* > 0$ such that

$$u_{is}(t, 1/G_1) - \bar{u}(t) = O\left(\frac{1}{G_1}\right) \text{ and } x_{is}(t, 1/G_1) - \gamma_x(\bar{u}(t)) = O\left(\frac{1}{G_1}\right)$$

hold uniformly for $t \in [t_b, \bar{t}_f]$ provided $G_1 > G_1^*$ and $(u_{is}(t_0), x_{is}(t_0)) \in \Omega_{u,x}(\alpha)$.

Proof. For convenience, define $\bar{g}(z_{\text{is}}, x_{\text{is}}) := Tg\left(T^{-1}(z_{\text{is}} - Mx_{\text{is}}), t\right)$ and denote the solution of system (3.8) by $z_{\text{is}}(t, \epsilon_1)$, $x_{\text{is}}(t, \epsilon_1)$ for $t \in [t_0, t_f]$ with $z_{\text{is}}(t_0) = Tu_{\text{is}}(t_0) + Mx_{\text{is}}(t_0)$. Let $x = \phi_x(z)$ be the unique solution of the algebraic equation $\tilde{f}(z, x) = 0$ and denote by $\bar{z}_{\text{is}}(t)$ the unique solution of the reduced system

$$\dot{\bar{z}}_{\text{is}} = \bar{g}(\bar{z}_{\text{is}}, \phi_x(\bar{z}_{\text{is}})) \tag{3.12}$$

for $t \in [t_0, \bar{t}_f]$ and $\bar{z}_{\text{is}}(t_0) = z_{\text{is}}(t_0)$ (the uniqueness of the solution follows from the fact that $\bar{g}$ is Lipschitz continuous on its domain by Assumptions A2 and A5). Assumption A9 further guarantees that the boundary layer system is locally exponentially stable. The region of attraction thus contains the set of x such that $\|x - \phi_x(z(t_0))\| < \beta$ for some $\beta > 0$ sufficiently small. Define the set $R_{z,x}(\beta) = \{(z, x) \mid \|x - \phi_x(z)\| < \beta\}$. Let $\Omega_{z,x}(\beta)$ be any compact subset of $R_{z,x}(\beta)$. By

Tikhonov theorem, for all $t_b \in (t_0, \bar{t}_f]$, there exists $\epsilon_1^* > 0$ such that

$$z_{\text{is}}(t, \epsilon_1) - \bar{z}_{\text{is}}(t) = O(\epsilon_1) \text{ and } x_{\text{is}}(t, \epsilon_1) - \phi_x(\bar{z}_{\text{is}}(t)) = O(\epsilon_1) \text{ uniformly for } t \in [t_b, \bar{t}_f] \tag{3.13}$$

provided $\epsilon_1 < \epsilon_1^*$ and $(x_{\text{is}}(t_0), z_{\text{is}}(t_0)) \in \Omega_{z,x}(\beta)$.

To obtain these approximations in the original coordinate system, define

$$\bar{u}_{\text{is}} := T^{-1} \left(\bar{z}_{\text{is}} - M \phi_x(\bar{z}_{\text{is}}) \right). \tag{3.14}$$

We seek to show that $\bar{u}_{\text{is}}(t)$ satisfies the differential equation (3.11). Since $x = \phi_x(z)$ is the locally unique solution of $\tilde{f}(z, x) = 0$, we must have that

$$\tilde{f}(z, \phi_x(z)) = 0. \tag{3.15}$$

Since $\tilde{f}(z, x) = Br\left(x, T^{-1}(z - Mx)\right) + f\left(x, T^{-1}(z - Mx)\right)$, equation (3.15) implies that

$$Br\left(\phi_x(\bar{z}_{\text{is}}), T^{-1}\left(\bar{z}_{\text{is}} - M\phi_x(\bar{z}_{\text{is}})\right)\right) + f\left(\phi_x(\bar{z}_{\text{is}}), T^{-1}\left(\bar{z}_{\text{is}} - M\phi_x(\bar{z}_{\text{is}})\right)\right) = 0. \tag{3.16}$$

From the assumptions of the lemma, we have that $x = \gamma_x(u)$ is the locally unique solution of $Br(x, u) + f(x, u) = 0$. This along with equation (3.16) imply that $\phi_x(\bar{z}_{\text{is}}) = \gamma_x(T^{-1}\left(\bar{z}_{\text{is}} - M\phi_x(\bar{z}_{\text{is}})\right)) = \gamma_x(\bar{u}_{\text{is}})$. As a consequence, we can re-write equation (3.14) as $\bar{z}_{\text{is}} = T\bar{u}_{\text{is}} + M\gamma_x(\bar{u}_{\text{is}})$. Taking the time derivative of both sides of this expression, we obtain $\dot{\bar{z}}_{\text{is}} = T\dot{\bar{u}}_{\text{is}} + M\frac{d\gamma_x(\bar{u}_{\text{is}})}{d\bar{u}_{\text{is}}}\dot{\bar{u}}_{\text{is}}$. Employing equation (3.12) on the left-hand side and re-arranging the terms, we obtain that

$$\dot{\bar{u}}_{\text{is}} = \left(T + M\frac{d\gamma_x(\bar{u}_{\text{is}})}{d\bar{u}_{\text{is}}} \right)^{-1} \bar{g}(\bar{z}_{\text{is}}, \phi_x(\bar{z}_{\text{is}})),$$

in which (by equations (3.8)) we have that

$$\bar{g}(\bar{z}_{\text{is}}, \phi_x(\bar{z}_{\text{is}})) = Tg\left(T^{-1}(\bar{z}_{\text{is}} - M\phi_x(\bar{z}_{\text{is}})), t\right) = Tg(\bar{u}_{\text{is}}, t)$$

, leading to $\bar{u}_{\rm is}(t)$ satisfying the differential equation (3.11) for $t \in [t_0, \bar{t}_f]$ with $\bar{u}_{\rm is}(t_0) = T^{-1}(\bar{z}_{\rm is}(t_0) - M\phi_x(\bar{z}_{\rm is}(t_0)))$. Since

$$u_{\rm is}(t, \epsilon_1) = T^{-1}[z_{\rm is}(t, \epsilon_1) - Mx_{\rm is}(t, \epsilon_1)]$$

and equations (3.13) hold, we have that

$$u_{\rm is}(t, \epsilon_1) = T^{-1}[\bar{z}_{\rm is}(t) + O(\epsilon_1) - M(\phi_x(\bar{z}_{\rm is}(t)) + O(\epsilon_1))]$$

, which, by employing equation (3.14) and the fact that

$$\phi_x(\bar{z}_{\rm is}) = \gamma_x(T^{-1}\left(\bar{z}_{\rm is} - M\phi_x(\bar{z}_{\rm is})\right)) = \gamma_x(\bar{u}_{\rm is})$$

, leads to

$$\begin{gathered} u_{\rm is}(t, \epsilon_1) - \bar{u}_{\rm is}(t) = O(\epsilon_1) \text{ and} \\ x_{\rm is}(t, \epsilon_1) - \gamma_x(\bar{u}_{\rm is}(t)) = O(\epsilon_1) \text{ uniformly for } t \in [t_b, \bar{t}_f] \end{gathered} \tag{3.17}$$

provided that $\epsilon_1 < \epsilon_1^*$ and $(z_{\rm is}(t_0), u_{\rm is}(t_0)) \in \Omega_{z,x}(\beta)$. Since $R_{z,x}(\beta)$ is the image of $R_{u,x}(\beta)$ under the continuous map $\mathcal{F}$, we have that for any compact set $\Omega_{z,x}(\beta) \subset R_{z,x}(\beta)$, there is a compact subset $\Omega_{u,x}(\beta) \subset R_{u,x}(\beta)$ such that $\Omega_{z,x}(\beta) = \mathcal{F}(\Omega_{u,x}(\beta))$. As a consequence, equations (3.17) hold provided $\epsilon_1 < \epsilon_1^*$ and $(u_{\rm is}(t_0), x_{\rm is}(t_0)) \in \Omega_{u,x}(\beta)$ with $\Omega_{u,x}(\beta) := \mathcal{F}^{-1}(\Omega_{z,x}(\beta))$. Set $\alpha = \beta$ and $G_1^* := 1/\epsilon_1^*$. □

Lemma 3. *Let $x(t, 1/G_1, 1/G_2)$, $u(t, 1/G_1, 1/G_2)$, $v(t, 1/G_1, 1/G_2)$ be the unique solution of system (3.1) for $t \in [t_0, t_f]$ with initial conditions $(x(t_0), u(t_0), v(t_0)) \in D_x \times D_u \times D_v$. Let $\bar{u}(t)$ be the unique solution of system*

$$\dot{\bar{u}} = \left(T + M\frac{d\gamma_x(\bar{u})}{d\bar{u}}\right)^{-1} Tg(\bar{u}, t), \tag{3.18}$$

for $t \in [t_0, \bar{t}_f]$ with initial condition $\bar{u}(t_0) = T^{-1}(z(t_0) - \phi_x(z(t_0)))$ with $z(t_0) = Tu(t_0) + Mx(t_0)$ and $x = \gamma_x(u)$ the locally unique solution of $f(x, u) + Br(x, u) = 0$. Then, there is $\alpha > 0$ such that for all $t_b \in (t_0, \bar{t}_f]$ there are $G_1^* > 0$ and $G_2^* > 0$ such that the following properties hold for $(u(t_0), x(t_0), v(t_0)) \in \Omega_{u,x,v}(\alpha)$ and $G_1 > G_1^*$:

(i) $x(t, 1/G_1, 1/G_2) - \gamma_x(\bar{u}(t)) = O\left(\frac{1}{G_1}\right)$ *and* $u(t, 1/G_1, 1/G_2) - \bar{u}(t) = O\left(\frac{1}{G_1}\right)$ *uniformly for* $t \in [t_b, \bar{t}_f]$ *when* $G_2/G_1 \to \{O(1), 0\}$ *as* $G_1 \to \infty$*;*

(ii) $x(t, 1/G_1, 1/G_2) - \gamma_x(\bar{u}(t)) = O\left(\frac{G_1}{G_2}\right)$ *and* $u(t, 1/G_1, 1/G_2) - \bar{u}(t) = O\left(\frac{G_1}{G_2}\right)$ *uniformly for* $t \in [t_b, \bar{t}_f]$ *when* $G_2/G_1 \to \infty$ *as* $G_1 \to \infty$ *and* $G_2 > G_2^*$.

Proof. Define for convenience the function $\bar{g}(z, y, v, t) := Tg\big(T^{-1}(z - MQ^{-1}(y - Pv)), t\big)$. Let $z(t, \epsilon_1, \epsilon_2)$, $y(t, \epsilon_1, \epsilon_2)$, $v(t, \epsilon_1, \epsilon_2)$ be the unique solution of system (3.7) for $t \in [t_0, t_f]$ with initial conditions $z(t_0) = Tu(t_0) + Mx(t_0)$, $y(t_0) = Qx(t_0) + Pv(t_0)$, and $v(t_0)$. There are three cases: $\epsilon_2/\epsilon_1 \to 0$ as $\epsilon_1 \to 0$, $\epsilon_2/\epsilon_2 \to O(1)$ as $\epsilon_1 \to 0$, and $\epsilon_2/\epsilon_1 \to \infty$ as $\epsilon_1 \to 0$.

Case 1: $\epsilon_2/\epsilon_1 \to 0$ as $\epsilon_1 \to 0$. We perform a nested application of Tikhonov singular perturbation theorem. Define the new small parameters $\mu_1 := \epsilon_1$ and $\mu_2 := \epsilon_2/\epsilon_1$ and re-write system (3.7) as

$$\begin{aligned} \dot{z} &= \bar{g}(z, y, v, t) \\ \mu_1 \dot{y} &= \bar{f}(z, y, v) + \mu_1 P h(v, t) \\ \mu_2 \mu_1 \dot{v} &= \bar{h}(y, v) + \mu_2 \mu_1 h(v, t). \end{aligned} \tag{3.19}$$

Set $\mu_2 = 0$ and let $v = \phi_1(y)$ be the locally unique solution of $\bar{h}(y, v) = 0$. Let also $\bar{z}(t, \epsilon_1)$ and $\bar{y}(t, \epsilon_1)$ be the unique solution of the reduced system obtained once $\mu_2 = 0$

$$\begin{aligned} \dot{z} &= \bar{g}(z, y, \phi_1(y), t) \\ \mu_1 \dot{y} &= \bar{f}(z, y, \phi_1(y)) + \mu_1 P h(\phi_1(y), t) \end{aligned} \tag{3.20}$$

for $t \in [t_0, T_a]$, $\bar{z}(t_0) = z(t_0)$, and $\bar{y}(t_0) = y(t_0)$ (uniqueness of the solution follows from Assumptions A2 and A3). Assumption A6 further guarantees that the boundary layer system is locally exponentially stable. For some $\beta > 0$ sufficiently small, the region of attraction contains the set of v such that $\|v - \phi_1(y(t_0))\|$ is sufficiently

small. Define the set $R_{y,v}(\beta) := \{(y, v) \in D_y \times D_v \mid \|v - \phi_1(y)\| < \beta\}$ and let $\Omega_{y,v}(\beta) \subset R_{y,v}(\beta)$ be compact. Then, by Tikhonov theorem, for all $t_b > 0$ there is $\mu_2^* > 0$ such that

$$\begin{aligned} z(t, \mu_1, \mu_1\mu_2) - \bar{z}(t, \mu_1) &= O(\mu_2) \text{ and} \\ y(t, \mu_1, \mu_1\mu_2) - \bar{y}(t, \mu_1) &= O(\mu_2) \text{ uniformly for } t \in [t_0, T_a] \\ v(t, \mu_1, \mu_1\mu_2) - \phi_1(\bar{y}(t, \mu_1)) &= O(\mu_2) \text{ uniformly for } t \in [t_b, T_a] \end{aligned} \tag{3.21}$$

hold provided $\mu_2 < \mu_2^*$ and $(\bar{y}(t_0), v(t_0)) \in \Omega_{y,v}(\beta)$.

System (3.20) is also in standard singular perturbation form with small parameter μ_1. Set $\mu_1 = 0$ and let $y = \phi_2(z)$ be the locally unique solution of $\bar{f}(z, y, \phi_1(y)) = 0$. Let $\tilde{z}(t)$ be the unique solution of the resulting reduced system when $\mu_1 = 0$

$$\dot{\tilde{z}} = \bar{g}(\tilde{z}, \phi_2(\tilde{z}), \phi_1 \circ \phi_2(\tilde{z}), t) \tag{3.22}$$

for $t \in [t_0, \bar{t}_f]$ with $\tilde{z}(t_0) = \bar{z}(t_0)$ (uniqueness of the solution follows from Assumptions A2, A3, and A4). Furthermore, Assumption A7 guarantees that the boundary layer system is locally exponentially stable. For some $\delta > 0$ sufficiently small, the region of attraction contains the set of y such that $\|y - \phi_2(z(t_0))\| < \delta$. Define the set $R_{z,y}(\delta) := \{(z, y) \in D_z \times D_y \mid \|y - \phi_2(z)\| < \delta\}$ and let $\Omega_{z,y}(\delta) \subset R_{z,y}(\delta)$ be compact. Then, from Tikhonov theorem, for all $t_b > 0$, there is $\mu_1^* > 0$ such that

$$\begin{aligned} \bar{z}(t, \mu_1) - \tilde{z}(t) &= O(\mu_1) \text{ uniformly for } t \in [t_0, \bar{t}_f] \\ \bar{y}(t, \mu_1) - \phi_2(\tilde{z}(t)) &= O(\mu_1) \text{ uniformly for } t \in [t_b, \bar{t}_f] \end{aligned} \tag{3.23}$$

hold provided $\mu_1 < \mu_1^*$ and $(\tilde{z}(t_0), \bar{y}(t_0)) \in \Omega_{z,y}(\delta)$. As a consequence of relations (3.23), for $\mu_1 < \mu_1^*$ the solution of system (3.20) is uniquely defined for $t \in [t_0, \bar{t}_f]$. We can thus let $T_a = \bar{t}_f$ so that for $\mu_2 < \mu_2^*$, with μ_2^* sufficiently small, also the solution of system (3.19) is uniquely defined for $t \in [t_0, \bar{t}_f]$. Let $\eta := \min(\beta, \delta)$ and

define

$$R_{z,y,v}(\eta) := \left\{ (z,y,v) \in D_z \times D_y \times D_v \mid \left\| \begin{array}{c} v - \phi_1(y) \\ y - \phi_2(z) \end{array} \right\| < \eta \right\}.$$

Let $\Omega_{z,y,v}(\eta) \subset R_{z,y,v}(\eta)$ be any compact set. Combining expression (3.21) with $T_a = \bar{t}_f$ and expression (3.23), the solution of system (3.1) satisfies

$$\begin{aligned} v(t,\mu_1,\mu_1\mu_2) - \phi_1 \circ \phi_2(\tilde{z}(t)) &= O(\mu_1) + O(\mu_2) y(t,\mu_1,\mu_1\mu_2) - \phi_2(\tilde{z}(t)) \\ &= O(\mu_1) + O(\mu_2) \\ z(t,\mu_1,\mu_1\mu_2) - \tilde{z}(t) &= O(\mu_1) + O(\mu_2) \text{ uniformly for } t \in [t_b, \bar{t}_f], \end{aligned} \tag{3.24}$$

in which we have used that $\phi_1(\phi_2(z)+O(\mu_1)) = \phi_1 \circ \phi_2(z) + O(\mu_1)$ since ϕ_1 is smooth. In order to return to the original coordinate system, define

$$\bar{u} = T^{-1}\left(\tilde{z} - MQ^{-1}(\phi_2(\tilde{z}) - P\phi_1 \circ \phi_2(\tilde{z}))\right). \tag{3.25}$$

We seek to show that $\bar{u}(t)$ satisfies equation (3.11). Since $y = \phi_2(z)$ is the locally unique solution of $\bar{f}(z,y,\phi_1(y)) = 0$, by the definition of $\bar{f}$ (equation (3.4)), we have that $Br(Q^{-1}(\phi_2(\tilde{z}) - P\phi_1 \circ \phi_2(\tilde{z})), \bar{u}) + f(Q^{-1}(\phi_2(\tilde{z}) - P\phi_1 \circ \phi_2(\tilde{z})), \bar{u}) = 0$. This equation along with the fact that $x = \gamma_x(u)$ is the locally unique solution of $Br(x,u) + f(x,u) = 0$ lead to

$$\begin{aligned} Q^{-1}\big(\phi_2(\tilde{z}) - P\phi_1 \circ \phi_2(\tilde{z})\big) &= \gamma_x\big(T^{-1}(\tilde{z} - MQ^{-1}(\phi_2(\tilde{z}) - P\phi_1 \circ \phi_2(\tilde{z})))\big) \\ &= \gamma_x(\bar{u}). \end{aligned} \tag{3.26}$$

Substituting this into equation (3.25) and re-arranging the terms, we obtain the equation $\tilde{z} = T\bar{u} + M\gamma_x(\bar{u})$. Taking the time derivative both sides, we obtain that $\dot{\tilde{z}} = T\dot{\bar{u}} + M\frac{d\gamma_x(\bar{u})}{d\bar{u}}\dot{\bar{u}}$. Employing equation (3.22) on the left-hand side and re-arranging the terms, we obtain $\dot{\bar{u}} = \left(T + M\frac{d\gamma_x(\bar{u})}{d\bar{u}}\right)^{-1} \bar{g}(\tilde{z}, \phi_2(\tilde{z}), \phi_1 \circ \phi_2(\tilde{z}), t)$, in which we have that

$$\bar{g}(\tilde{z}, \phi_2(\tilde{z}), \phi_1 \circ \phi_2(\tilde{z}), t) = Tg\left(T^{-1}(\tilde{z} - MQ^{-1}(\phi_2(\tilde{z}) - P\phi_1 \circ \phi_2(\tilde{z}))), t\right)$$

with $T^{-1}(\tilde{z} - MQ^{-1}(\phi_2(\tilde{z}) - P\phi_1 \circ \phi_2(\tilde{z}))) = \bar{u}$ from equation (3.25). Therefore, $\bar{u}(t)$ is the unique solution of (3.18) for $t \in [t_0, \bar{t}_f]$ and

$$\bar{u}(t_0) = T^{-1}\left(\tilde{z}(t_0) - MQ^{-1}[\phi_2(\tilde{z}(t_0)) - P\phi_1 \circ \phi_2(\tilde{z}(t_0))]\right),$$

in which $\tilde{z}(t_0) = z(t_0)$. Since $x = \phi_x(z)$ is the unique solution of $\tilde{f}(z, x) = 0$ and $\bar{f}(z, \phi_2(z), \phi_1 \circ \phi_2(z)) = 0$, it follows from the definition of $\bar{f}$ (equation (3.4)) that $Q^{-1}[\phi_2(z) - P\phi_1 \circ \phi_2(z)] = \phi_x(z)$. Thus, $\bar{u}(t_0) = T^{-1}[z(t_0) - M\phi_x(z(t_0))]$.

From coordinate transformation (3.6), we have

$$x(t, \mu_1, \mu_1\mu_2) = Q^{-1}(y(t, \mu_1, \mu_1\mu_2) - Pv(t, \mu_1, \mu_1\mu_2)).$$

Employing the relations for y and v from (3.24), we obtain

$$x(t, \mu_1, \mu_1\mu_2) = Q^{-1}[\phi_2(\tilde{z}(t)) + O(\mu_1) + O(\mu_2) - P\left(\phi_1 \circ \phi_2(\tilde{z}(t)) + O(\mu_1) + O(\mu_2)\right)].$$

By employing equations (3.25) and (3.26), one obtains that $x(t, \mu_1, \mu_1\mu_2) = \gamma_x(\bar{u}(t)) + O(\mu_1) + O(\mu_2)$. Similarly, from the change of variable

$$u(t, \mu_1, \mu_1\mu_2) = T^{-1}\big(z(t, \mu_1, \mu_1\mu_2) - MQ^{-1}\big[y(t, \mu_1, \mu_1\mu_2) - Pv(t, \mu_1, \mu_1\mu_2)\big]\big),$$

and expressions (3.24) and (3.25), we obtain that $u(t, \mu_1, \mu_1\mu_2) = \bar{u}(t) + O(\mu_1) + O(\mu_2)$. Hence, we have that

$$\begin{aligned} u(t, \mu_1, \mu_1\mu_2) - \bar{u}(t) &= O(\mu_1) + O(\mu_2) \text{ and} \\ x(t, \mu_1, \mu_1\mu_2) - \gamma_x(\bar{u}(t)) &= O(\mu_1) + O(\mu_2) \end{aligned} \tag{3.27}$$

uniformly for $t \in [t_b, \bar{t}_f]$ provided $\mu_1 < \mu_1^*$, $\mu_2 < \mu_2^*$, and $(\tilde{z}(t_0), \bar{y}(t_0), v(t_0)) \in \Omega_{z,y,v}(\eta)$. Since $R_{z,y,v}(\eta)$ is the image of $R_{u,x,v}(\eta)$ under the continuous map $\mathcal{G}$, we have that for any compact set $\Omega_{z,x,v}(\eta) \subset R_{z,x,v}(\eta)$, there is a compact set $\Omega_{u,x,v}(\eta) \subset R_{u,x,v}(\eta)$ such that $\Omega_{z,x,v}(\eta) = \mathcal{G}(\Omega_{u,x,v}(\eta))$. As a consequence, equations (3.27) hold

provided $\mu_1 < \mu_1^*$, $\mu_2 < \mu_2^*$, and $(u(t_0), x(t_0), v(t_0)) \in \Omega_{u,x,v}(\eta)$ with $\Omega_{u,x,v}(\eta) = \mathcal{G}^{-1}(\Omega_{z,x,v}(\eta))$. Define $\epsilon_1^{\text{case 1}} := \mu_1^*$ and $\alpha^{\text{Case 1}} := \eta$.

Case 2: $\epsilon_2/\epsilon_1 = O(1)$ as $\epsilon_1 \to 0$. Letting $a := \epsilon_1/\epsilon_2$, system (3.7) becomes

$$\begin{aligned} \dot{z} &= \bar{g}(z, y, v, t) \\ \epsilon_1 \dot{y} &= \bar{f}(z, y, v) + \epsilon_1 P h(v, t) \\ \epsilon_1 \dot{v} &= a\bar{h}(y, v) + \epsilon_1 h(v, t). \end{aligned} \tag{3.28}$$

Denote the solution of system (3.28) by $z(t, \epsilon_1)$, $y(t, \epsilon_1)$, and $v(t, \epsilon_1)$ for $t \in [t_0, t_f]$. By Proposition 5, $(y, v) = (\phi_2(z), \phi_1 \circ \phi_2(z))$ is the locally unique solution of

$$(\bar{f}(z, y, v), \bar{h}(y, v)) = 0.$$

Define $\phi_3(z) := \phi_1 \circ \phi_2(z)$ to simplify notation. Let $\bar{z}(t)$ be the unique solution of the reduced system

$$\dot{z} = \bar{g}(z, \phi_2(z), \phi_3(z), t) \tag{3.29}$$

for $t \in [t_0, \bar{t}_f]$ and $\bar{z}(t_0) = z(t_0)$ (uniqueness of the solution follows from Assumptions A2, A3, and A4). Furthermore, Assumption A8 guarantees that the boundary layer system is locally exponentially stable. For some $\beta > 0$ sufficiently small, the region of attraction contains the set of all (y, v) such that $\|(y, v) - (\phi_2(z(t_0)), \phi_3(z(t_0)))\| < \beta$. Define the set $R_{z,y,v}(\beta) := \{(z, y, v) \in D_z \times D_y \times D_v \mid \|(y, v) - (\phi_2(z), \phi_3(z))\| < \beta\}$ and let $\Omega_{z,y,v}(\beta) \subset R_{z,y,v}(\beta)$ be compact. Then, by Tikhonov theorem, for all $t \in (t_0, \bar{t}_f]$ there is $\epsilon_1^{\text{Case 2}} > 0$ such that

$$\begin{aligned} &z(t, \epsilon) - \bar{z}(t) = O(\epsilon_1) \text{ uniformly for } t \in [0, \bar{t}_f] \\ &y(t, \epsilon) - \phi_2(\bar{z}(t)) = O(\epsilon_1) \text{ and } v(t, \epsilon) - \phi_3(\bar{z}(t)) = O(\epsilon_1) \text{ uniformly for } t \in [t_b, \bar{t}_f], \end{aligned} \tag{3.30}$$

provided $\epsilon_1 < \epsilon_1^{\text{Case 2}}$ and $(z(t_0), y(t_0), v(t_0)) \in \Omega_{z,y,v}(\beta)$.

Define

$$\bar{u} := T^{-1}(\bar{z} - MQ^{-1}(\phi_2(\bar{z}) - P\phi_3(\bar{z}))). \tag{3.31}$$

We seek to determine the differential equation that $\bar{u}(t)$ obeys. Due to the fact that $\bar{f}(z, \phi_2(z), \phi_3(z)) = 0$, we have by the definition of $\bar{f}$ (equation (3.4)) that

$$\begin{aligned} &Br\Big(Q^{-1}(\phi_2(z) - P\phi_3(z)), T^{-1}(z - MQ^{-1}(\phi_2(z) - P\phi_3(z)))\Big) \\ &+ f\Big(Q^{-1}(\phi_2(z) - P\phi_3(z)), T^{-1}(z - MQ^{-1}(\phi_2(z) - P\phi_3(z)))\Big) = 0. \end{aligned}$$

Given that by assumption $x = \gamma_x(u)$ is the locally unique solution of $Br(x, u) + f(x, u) = 0$, we must have that

$$Q^{-1}(\phi_2(\bar{z}) - P\phi_3(\bar{z}))) = \gamma_x\left(T^{-1}[\bar{z} - MQ^{-1}(\phi_2(\bar{z}) - P\phi_3(\bar{z}))]\right) = \gamma_x(\bar{u}).$$

Substituting this in equation (3.31), we obtain that $\bar{z} = T\bar{u} + M\gamma_x(\bar{u})$. Computing the time derivative both sides of this equation, employing equation (3.29) and equation (3.31), one obtains that $\bar{u}(t)$ is the solution of (3.18) for $t \in [t_0, \bar{t}_f]$ with

$$\bar{u}(t_0) = T^{-1}\Big(\bar{z}(t_0) - MQ^{-1}[\phi_2(\bar{z}(t_0)) - P\phi_3(\bar{z}(t_0))]\Big)$$

and $\bar{z}(t_0) = z(t_0)$. Since, as for Case 1, we have that $Q^{-1}[\phi_2(\bar{z}(t_0)) - P\phi_3(\bar{z}(t_0))] = \phi_x(\bar{z}(t_0))$, then $\bar{u}(t_0) = T^{-1}[\bar{z}(t_0) - M\phi_x(\bar{z}(t_0))]$.

Finally, employing the change of coordinates (3.6) and approximations (3.30), we obtain that

$$u(t, \epsilon_1) - \bar{u}(t) = O(\epsilon_1) \text{ and } x(t, \epsilon_1) - \gamma_x(\bar{u}(t)) = O(\epsilon_1) \tag{3.32}$$

hold uniformly for $t \in [t_b, \bar{t}_f]$ provided $(z(t_0), y(t_0), v(t_0)) \in \Omega_{z,y,v}(\beta)$ and $\epsilon_1 < \epsilon_1^{\text{Case 2}}$. Define the new region $\bar{R}_{z,y,v}(\eta) := \{(z, y, v) \mid \|(y, v) - (\phi_2(z), \phi_1(y))\| < \eta\}$. By the

continuity of ϕ_1 and the triangular inequality, it follows that for all $\beta > 0$ there is $\eta > 0$ such that $\bar{R}_{z,y,v}(\eta) \subset R_{z,y,v}(\beta)$. Since $\Omega_{z,y,v}(\beta)$ is an arbitrary compact subset of $R_{z,y,v}(\beta)$, it can be chosen such that $\Omega_{z,y,v}(\beta) = \bar{\Omega}_{z,y,v}(\eta)$ for $\bar{\Omega}_{z,y,v}(\eta)$ a suitable compact subset of $\bar{R}_{z,y,v}(\eta)$. Since $\bar{R}_{z,y,v}(\eta) = \mathcal{G}(R_{u,x,v}(\eta))$ and $\mathcal{G}$ is a continuous mapping, we have that for all compact sets $\bar{\Omega}_{z,y,v}(\eta) \subset \bar{R}_{z,y,v}(\eta)$ there is a compact set $\Omega_{u,x,v}(\eta) \subset R_{u,x,v}(\eta)$ such that $\bar{\Omega}_{z,y,v}(\eta) = \mathcal{G}(\Omega_{u,x,v}(\eta))$. As a consequence, equations (3.32) hold provided $\epsilon_1 < \epsilon_1^{\text{Case 2}}$ and $(u(t_0), x(t_0), v(t_0)) \in \Omega_{u,x,v}(\eta)$ with $\Omega_{u,x,v}(\eta) = \mathcal{G}^{-1}(\bar{\Omega}_{z,y,v}(\eta))$. Define $\alpha^{\text{Case 2}} := \eta$.

Case 3: $\epsilon_2/\epsilon_1 \to \infty$ as $\epsilon_1 \to 0$. In this case, only the change of coordinates $z = Tu + Mx$ is applied to system (3.1), leading to the system in the new coordinates

$$\begin{aligned} \dot{z} &= g(T^{-1}(z - Mx), t), \\ \epsilon_1 \dot{x} &= \tilde{f}(z, x) + \frac{\epsilon_1}{\epsilon_2} Cs(x, v), \\ \epsilon_2 \dot{v} &= Ds(x, v) + l(v) + \epsilon_2 h(v, t). \end{aligned} \tag{3.33}$$

Let $x = \phi_x(z)$ be the locally unique solution to the equation $\tilde{f}(z, x) = 0$ (in which we have that $\phi_x(z) = Q^{-1}[\phi_2(z) - P\phi_1 \circ \phi_2(z)]$) and let $\bar{z}(t), \bar{v}(t, \epsilon_2)$ be the unique solution of the reduced system

$$\begin{aligned} \dot{z} &= g(T^{-1}(z - M\phi_x(z)), t) \\ \epsilon_2 \dot{v} &= Ds(\phi_x(z), v) + l(v) + \epsilon_2 h(v, t) \end{aligned} \tag{3.34}$$

for $t \in [t_0, \bar{t}_f]$ with $\bar{z}(t_0) = z(t_0)$ and $\bar{v}(t_0) = v(t_0)$ (uniqueness of the solution follows from Assumptions A2 and A5). Assumption A9 further guarantees that the boundary layer system is locally exponentially stable. For some $\beta > 0$ sufficiently small, the region of attraction contains the set of x such that $\|x - \phi_x(z(t_0))\| < \beta$. Define the set $R_{z,x}(\beta) := \{(z, x) \in D_z \times D_x \mid \|x - \phi_x(z)\| < \beta\}$. Let $\Omega_{z,x}(\beta)$ be any compact set contained in $R_{z,x}(\beta)$. From Tikhonov theorem, there is $\beta > 0$ such that

for all $t_b \in (0, \bar{t}_f]$, there exist $\epsilon_1^{\text{Case 3}} > 0$ such that

$$\begin{aligned} &z(t, \epsilon_1, \epsilon_2) - \bar{z}(t) = O(\epsilon_1) \text{ and } v(t, \epsilon_1, \epsilon_2) - \bar{v}(t, \epsilon_2) = O(\epsilon_1) \text{ uniformly for } t \in [0, \bar{t}_f] \\ &x(t, \epsilon_1, \epsilon_2) - \phi_x(\bar{z}(t)) = O(\epsilon_1) \text{ uniformly for } t \in [t_b, \bar{t}_f] \end{aligned} \tag{3.35}$$

provided $\epsilon_1 < \epsilon_1^{\text{Case 3}}$ and $(z(t_0), x(t_0)) \in \Omega_{z,x}(\beta)$. In order to obtain the approximations in the original coordinate system, define $\bar{u} = T^{-1}(\bar{z} - M\phi_x(\bar{z}))$. Since $x = \gamma_x(u)$ is the locally unique solution of $Br(x, u) + f(x, u) = 0$ and $x = \phi_x(z)$ is the locally unique solution of $Br(x, T^{-1}(z - Mx)) + f(x, T^{-1}(z - Mx)) = 0$, we have that $\phi_x(\bar{z}) = \gamma_x(T^{-1}(\bar{z} - M\phi_x(\bar{z}))) = \gamma_x(\bar{u})$. Then, we can write $\bar{z} = T\bar{u} + M\gamma_x(\bar{u})$ and conclude that $\bar{u}(t)$ is the unique solution to system (3.11) for $t \in [t_0, \bar{t}_f]$ with $\bar{u}(t_0) = T^{-1}[\bar{z}(t_0) - M\phi_x(\bar{z}(t_0))]$. By employing the coordinate change $z = Tu + Mx$ as performed in Case 1, we finally obtain that

$$u(t, \epsilon_1, \epsilon_2) - \bar{u}(t) = O(\epsilon_1) \text{ and } x(t, \epsilon_1, \epsilon_2) - \gamma_x(\bar{u}(t)) = O(\epsilon_1), \tag{3.36}$$

uniformly for $t \in [t_b, \bar{t}_f]$ provided $\epsilon_1 < \epsilon_1^{\text{Case 3}}$ and $(z(t_0), x(t_0)) \in \Omega_{z,x}(\beta)$. Since $R_{z,x}(\beta)$ is the image of $R_{u,x}(\beta)$ under the continuous map $\mathcal{F}$, for any compact set $\Omega_{z,x}(\beta) \subset R_{z,x}(\beta)$, there is a compact set $\Omega_{u,x}(\beta) \subset R_{u,x}(\beta)$ such that $\Omega_{z,x}(\beta) = \mathcal{F}(\Omega_{u,x}(\beta))$. As a consequence, equations (3.36) hold provided $\epsilon_1 < \epsilon_1^{\text{Case 3}}$ and $(u(t_0), x(t_0)) \in \Omega_{u,x}(\beta)$. By Proposition 6, for all $\beta > 0$ there is $\eta > 0$ such that $(u, x, v) \in R_{u,x,v}(\eta)$ implies $(u, x) \in R_{u,x}(\beta)$. Let $\Omega_{u,x,v}(\eta) \subset R_{u,x,v}(\eta)$ be any compact set. Then, $(u, x, v) \in \Omega_{u,x,v}(\eta)$ implies $(u, x) \in \Omega_{u,x}(\beta)$ for some compact set $\Omega_{u,x}(\beta) \subset R_{u,x}(\beta)$. As a consequence, equations (3.36) hold provided $(u(t_0), x(t_0), v(t_0)) \in \Omega_{u,x,v}(\eta)$. Let $\alpha^{\text{Case 3}} := \eta$.

By combining Case 1, Case 2, and Case 3, the result of the theorem follows with $\alpha = \min(\alpha^{\text{Case 1}}, \alpha^{\text{Case 2}}, \alpha^{\text{Case 3}})$, $G_1^* = 1/\epsilon_1^*$ with $\epsilon_1^* = \min(\epsilon_1^{\text{Case 1}}, \epsilon_1^{\text{Case 2}}, \epsilon_1^{\text{Case 3}})$, and

$G_2^* := 1/(\epsilon_1^*\mu_2^*)$. □

By combining the results of the lemmas, we can obtain the main result of the section.

Theorem 1. *Under Properties P1-P2 and Assumptions A1-A9, system* Σ *has the retroactivity to the output attenuation property.*

Proof. By virtue of Lemma 2, we have that there is $\alpha_1 > 0$ such that for all $t_b \in (t_0, \bar{t}_f]$ there exists $G_1^a > 0$ such that $x_{\text{is}}(t, 1/G_1) - \gamma_x(\bar{u}(t)) = O(\frac{1}{G_1})$ hold uniformly for $t \in [t_b, \bar{t}_f]$ whenever $G_1 > G_1^a$ and $(u_{\text{is}}(t_0), x_{\text{is}}(t_0)) \in \Omega_{u,x}(\alpha_1)$. Similarly, Lemma 3 shows that there is $\alpha_2 > 0$ such that for all $t_b \in (t_0, \bar{t}_f]$ there are $G_1^b > 0$ and $G_2^* > 0$ such that *(i)* and *(ii)* hold uniformly for in $t \in [t_b, \bar{t}_f]$ whenever $G_1 > G_1^b$ and $(u(t_0), x(t_0), v(t_0)) \in \Omega_{u,x,v}(\alpha_2)$. By Proposition 6, for all $\alpha_1 > 0$ there is $\eta > 0$ such that $(u, x, v) \in R_{u,x,v}(\eta)$ implies $(u, x) \in R_{u,x}(\alpha_1)$. Let $\Omega_{u,x,v}(\eta) \subset R_{u,x,v}(\eta)$ be any compact set. Then, $(u, x, v) \in \Omega_{u,x,v}(\eta)$ implies $(u, x) \in \Omega_{u,x}(\alpha_1)$ for some compact set $\Omega_{u,x}(\alpha_1) \subset R_{u,x}(\alpha_1)$. Letting $G_1^* := \max(G_1^a, G_1^b)$ and $\alpha := \min(\eta, \alpha_2)$, we obtain the desired result. □

3.2 Proposed Realizations of an insulation device

In this section, we show how the interconnection structure of system (3.1) is found in bio-molecular systems extracted from natural signal transduction pathways and how it can be used to build insulation devices. In particular, we consider as system Σ two post-translational modification systems which are recurrent motifs in signal transduction: phosphorylation cycles and phosphotransfer systems. In both examples, the system output is connected to the downstream system through the binding of transcription factors to DNA. We show that the retroactivity to the output

attenuation property holds when the downstream interconnection dynamics are of the same order as, much faster or much slower than the dynamics of system Σ.

3.2.1 Example 1: Phosphorylation

Phosphorylation cycles are among the most common intracellular signal transduction mechanisms. They have been observed in virtually every organism, carrying signals that regulate processes such as cell motility, nutrition, interaction with environment and cell death [63].

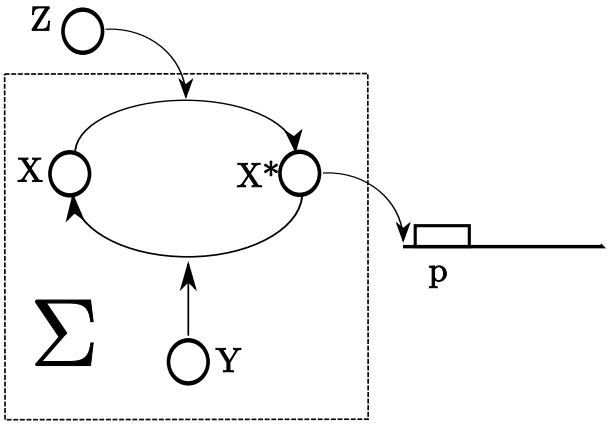

Figure 3.2: **Phosphorylation-device based insulation device.** System Σ is a phosphorylation cycle. Its product X* activates transcription through the reversible binding of X* to downstream DNA promoter sites p.

Consider system Σ modelling the phosphorylation cycle as shown in Figure 3.2. This system takes as input a kinase Z that phosphorylates a protein X. The phosphorylated form of X, denoted X^*, is a transcription factor, which binds to downstream DNA promoter binding sites p. The phosphorylated protein X^* is converted to the original dephosphorylated form by phosphatase Y. A standard two-step reaction model for the phosphorylation and dephosphorylation reactions is given by

$$Z + X \underset{\beta_2}{\overset{\beta_1}{\rightleftharpoons}} C_1 \xrightarrow{k_1} X^* + Z \text{ and } Y + X^* \underset{\alpha_2}{\overset{\alpha_1}{\rightleftharpoons}} C_2 \xrightarrow{k_2} X + Y,$$

respectively, in which C_1 and C_2 are the complexes of protein Z with substrate X and

of protein Y with protein X*, respectively [64]. The binding reactions of transcription factor X* with downstream binding sites p are given by $\mathrm{X}^* + \mathrm{p} \underset{k_{\mathrm{off}}}{\overset{k_{\mathrm{on}}}{\rightleftharpoons}} \mathrm{C}$, in which C is the complex of X* bound to site p. In this system, the total amounts of proteins X and Y and the total amount of promoter p are conserved. Their total amounts are denoted X_T, Y_T, and p_T, respectively, so that the conservation laws are given by $X_T = X + X^* + C_1 + C_2 + C$, $Y_T = Y + C_2$, and $p_T = X^* + p$. Assuming Z is expressed at time-varying rate $k(t)$ and decays at rate δ, the differential equations for the concentrations of the various species of system Σ when connected to the downstream system are given by

$$\begin{aligned}
\dot{Z} &= k(t) - \delta Z - \beta_1 Z(X_T - X^* - C_1 - C_2 - C) + (\beta_2 + k_1)C_1 \\
\dot{C}_1 &= \beta_1 Z(X_T - X^* - C_1 - C_2 - C) - (\beta_2 + k_1)C_1 \\
\dot{C}_2 &= -(k_2 + \alpha_2)C_2 + \alpha_1 X^*(Y_T - C_2) \\
\dot{X}^* &= k_1 C_1 + \alpha_2 C_2 - \alpha_1 X^*(Y_T - C_2) + k_{off} C - k_{on} X^*(p_T - C) \\
\dot{C} &= -k_{off} C + k_{on} X^*(p_T - C).
\end{aligned} \tag{3.37}$$

A common approach to take a system to the standard singular perturbation form is to rewrite it in terms of non-dimensional variables [47, 65]. To this end, let $\bar{k} := \max_t k(t)/\delta$ and define the non-dimensional input $\tilde{k}(t) := k(t)/(\delta\bar{k})$. Define also the new variables $u := \dfrac{Z}{\bar{k}}$, $x_1 := \dfrac{C_1}{X_T}$, $x_2 := \dfrac{C_2}{X_T}$, $x_3 := \dfrac{X^*}{X_T}$, $v := \dfrac{C}{p_T}$ and $\tau = \delta t$. For a variable x, denote $\dot{x} := dx/d\tau$. The system (3.37) in these new variables

becomes

$$\begin{aligned}
\dot{u} &= \tilde{k}(t) - u - \frac{\beta_1 X_T}{\delta} u \left(1 - x_1 - x_2 - x_3 - \frac{p_T}{X_T} v\right) + \frac{(\beta_2 + k_1) X_T}{\delta \bar{k}} x_1 \\
\dot{x}_1 &= \frac{\beta_1 \bar{k}}{\delta} u \left(1 - x_1 - x_2 - x_3 - \frac{p_T}{X_T} v\right) - \frac{\beta_2 + k_1}{\delta} x_1 \\
\dot{x}_2 &= -\frac{k_2 + \alpha_2}{\delta} x_2 + \frac{\alpha_1 Y_T}{\delta} x_3 \left(1 - \frac{X_T}{Y_T} x_2\right) \\
\dot{x}_3 &= \frac{k_1}{\delta} x_1 + \frac{\alpha_2}{\delta} x_2 - \frac{\alpha_1 Y_T}{\delta} x_3 \left(1 - \frac{X_T}{Y_T} x_2\right) + \frac{p_T k_{off}}{X_T \delta} v - \frac{k_{on} p_T}{\delta} x_3 (1 - v) \\
\dot{v} &= -\frac{k_{off}}{\delta} v + \frac{k_{on} X_T}{\delta} x_3 (1 - v).
\end{aligned} \tag{3.38}$$

In this example, we assume the parameter k_{off} to be much larger than k_1, k_2, $\alpha_1 Y_T$, α_2, $\beta_1 X_T$, β_2, which are in turn much larger than δ [66, 46, 56, 59]. This timescale differences can be made explicit by defining the large parameters $G_1 := \dfrac{k_1}{\delta}$ and $G_2 := \dfrac{k_{\text{off}}}{\delta}$, in which $G_2 \gg G_1 \gg 1$. Define also the non-dimensional constants $a_1 := \dfrac{\alpha_1 Y_T}{k_1}$, $a_2 := \frac{\alpha_2}{k_1}$, $b_1 := \dfrac{\beta_1 X_T}{k_1}$, $b_2 := \dfrac{\beta_2}{k_1}$, $\rho := \dfrac{X_T}{Y_T}$ and $c_2 := \dfrac{k_2}{k_1}$. Define also the dissociation constant $k_d := k_{\text{off}}/k_{\text{on}}$. By employing these constants, system (3.38) can be re-written as

$$\begin{aligned}
\dot{u} &= \tilde{k}(t) - u - G_1 b_1 u \left(1 - x_1 - x_2 - x_3 - \frac{p_T}{X_T} v\right) + G_1 \frac{X_T (b_2 + 1)}{\bar{k}} x_1 \\
\dot{x}_1 &= G_1 \frac{b_1 \bar{k}}{X_T} u \left(1 - x_1 - x_2 - x_3 - \frac{p_T}{X_T} v\right) - G_1 (b_2 + 1) x_1 \\
\dot{x}_2 &= -G_1 (c_2 + a_2) x_2 + G_1 a_1 x_3 \left(1 - \rho x_2\right) \\
\dot{x}_3 &= G_1 x_1 + G_1 a_2 x_2 - G_1 a_1 x_3 \left(1 - \rho x_2\right) + G_2 \frac{p_T}{X_T} v - G_2 \frac{p_T}{k_d} x_3 (1 - v) \\
\dot{v} &= -G_2 v + G_2 \frac{X_T}{k_d} x_3 (1 - v).
\end{aligned} \tag{3.39}$$

The domains for the variables of this system are given by $D_u := \mathbb{R}_+$, $D_x := [0,1] \times [0,1] \times [0,1]$, and $D_v := [0,1]$. Compare system (3.39) with the structure of model (3.1). The retroactivity to the input term $r = -b_1 u \left(1 - x_1 - x_2 - x_3 - (p_T/X_T) v\right) + (X_T (b_2 + 1)/\bar{k}) x_1$ is a function of the downstream system state v. This implies that the retroactivity to the output of impacts directly the retroactivity to the in-

put. In order to remove this effect, and therefore, match the structure of system (3.1), in which r does not depend on v, we require the ratio p_T/X_T to be small enough so that the term $(p_T/X_T)v$ becomes negligible with respect to one, since $v \in [0,1]$. This assumption gives a limit to the amount of load that can be added to the system for any fixed value of X_T. Under this assumption, the system fits the structure (3.1) with $g(u,t) = \tilde{k}(t) - u$, $r(x,u) = b_1 u\,(1 - x_1 - x_2 - x_3) - \frac{(b_2+1)X_T}{k} x_1$, $[f(x,u) = \begin{bmatrix} 0 \\ -(c_2+a_2)x_2 + a_1 x_3\,(1-\rho x_2) \\ x_1 + a_2 x_2 - a_1 x_3\,(1-\rho x_2) \end{bmatrix}$, $s(x,v) = -\frac{p_T}{X_T}v + \frac{p_T}{k_d} x_3\,(1-v)$, $l(v) = 0$, $h(v,t) = 0$, $A = -1$, $B = \begin{bmatrix} \bar{k}/X_T & 0 & 0 \end{bmatrix}^T$, $C = \begin{bmatrix} 0 & 0 & -1 \end{bmatrix}^T$ and $D = \frac{X_T}{p_T}$. By inspection of the matrices A, B, C and D, we can choose matrices $T = 1$, $M = [\frac{X_T}{k}\ 0\ 0]$, $Q = \mathbb{I}_3$ (3 by 3 identity matrix) and $P = \begin{bmatrix} 0 & 0 & \frac{p_T}{X_T} \end{bmatrix}^T$ that satisfy properties P1 and P2. This can be verified by checking that indeed $TA + MB = 0$, $Mf(x,u) = 0$, $MC = 0$, $QC + PD = 0$ and, trivially, $Pl(v)$=0. The linear coordinate transformation that takes this system to the standard singular perturbation form is, thus, given by $z := Tu + Mx = u + \frac{X_T}{k} x_1$ and $y = (y_1, y_2, y_3) := Qx + Pv = \left(x_1, x_2, x_3 + \frac{p_T}{X_T} v\right)$.

Figure 3.3 shows that, for low values of G_1, the system does not attenuate the retroactivity to the output s as the permanent behavior of the isolated and connected systems are different. By contrast, and in accordance to the theory, large values of G_1 lead to retroactivity to the output attenuation. Note also that this property is achieved even if the gain G_2 multiplying the state-dependent disturbance $s(x,v)$ is much larger than G_1.

In practice, while reactions rates k_1, k_2, α_2 and β_2 are often much larger than δ, constants α_1 and β_1 may not achieve such high values [56]. It is, however, possible

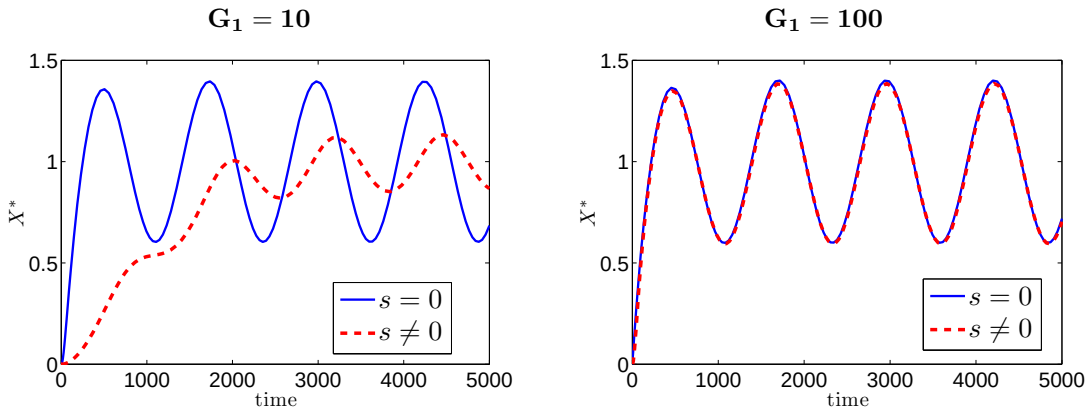

Figure 3.3: **Response of an insulation device based on a phosphorylation cycle.** Output response to a sinusoidal signal $k(t) = \delta(1 + 0.5 \sin \omega t)$ of the phosphorylation system Σ. The parameter values are given by $\omega = 0.005$, $\delta = 0.01$, $X_T = 5000$, $Y_T = 5000$, $\alpha_1 = \beta_1 = 2 \times 10^{-6} G_1$, and $\alpha_2 = \beta_2 = k_1 = k_2 = 0.01 G_1$, in which $G_1 = 10$ (left-side panel), and $G_1 = 1000$ (right-side panel). The downstream system parameters are $k_{\text{on}} = 100$, $k_{\text{off}} = 100$ and, thus, $G_2 = 10000$. Simulations for the connected system ($s \neq 0$) correspond to $p_{TOT} = 100$ while simulations for the isolated system ($s = 0$) correspond to $p_T = 0$.

to compensate for this and obtain the desired timescale separation by having larger amounts of X_T and Y_T. Large values of X_T and Y_T are also instrumental in removing the direct effect of retroactivity to the output on the retroactivity to the input. Finally, large values of X_T and Y_T are also necessary to guarantee the stability of the boundary layer system, as concluded when showing that property A7 holds. In a synthetic bio-molecular system, expression level of proteins X and Y can be tuned by having their respective genes under the control of inducible promoters. It is therefore possible to tune this system so that the retroactivity to the output attenuation property holds.

Since we are considering the case in which $G_1 \ll G_2$, it is necessary to show that technical assumptions A1-A7 and A9 are satisfied. Properties A1 and A2 can be verified by inspection of (3.39). Expression $\bar{h}(y, v) = 0$ leads to $p_T v^2 - v(X_T y_3 + p_T + k_d) + X_T y_3 = 0$ which leads to the unique isolated solution

$$v = \phi_1(y) = \frac{X_T y_3 + p_T + k_d - \sqrt{(X_T y_3 + p_T + k_d)^2 - 4 p_T X_T y_3}}{2 p_T}$$

in the domain $D_v = [0, 1]$. This function is Lipschitz continuous as the argument of the square root is bounded away from zero and thus A3 is satisfied. To calculate the function $\phi_2(z)$, we first set $\bar{f}(z, y, \phi_1(y)) = 0$ obtaining the system of equations

$$\begin{aligned}
&-(b_2+1)C_1 + (z - C_1)\left(1 - \frac{y_3 - \phi_1(y)}{X_T} - \frac{C_1}{X_T} - \frac{C_2}{X_T}\right) = 0 \\
&-(c+a_2)C_2 + a_1(y_3 - \phi_1(y_3))\left(1 - \frac{C_2}{Y_T}\right) = 0 \\
&C_1 + a_2 C_2 - a_1(y_3 - \phi_1(y_3))\left(1 - \frac{C_2}{Y_T}\right) = 0.
\end{aligned}$$

Solving for y, one can find the identities $C_1 = cC_2$ and

$$C_2 = \frac{\dfrac{a_1}{a_2 + c}(y_3 - \phi_1(y_3))}{1 + \dfrac{a_1}{Y_T(a_2 + c)}(y - \phi_1(y_3))}.$$

Since we want to obtain an insulation with zero gain, we expect that $X_p \approx Z \ll Y_T$. Also, by design, X_T and *ytot* are of the same order of magnitude. Since $y_3 = X^* + C$, $C \ll X_T$ and $X^* \ll Y_T$, then $y - \phi_1(y) \ll Y_T$. Also, recall that $a_1/(a_2 + c) = O(1)$. Then $\dfrac{a_1}{Y_T(a_2 + c)}(y - \phi_1(y)) \ll 1$ and the above expression can be approximated by $C_2 = \dfrac{a_1}{a_2 + c}(y - \phi_1(y))$. Finally, we can then obtain from the expression

$$(z - C_1) = \frac{c(b_2 + 1)C_2}{1 - \left(\frac{a_2 + c}{a_1} + c + 1\right)\dfrac{C_2}{X_T}}.$$

It was already established that C_2 is of the same order of X_p and thus $C_2 \ll X_T$. Also, since $\frac{a_2+c}{a_1} + c + 1 = O(1)$, the denominator of the above expression approaches 1 and thus, $z = (b_2 + 2)C_1$. With the above expressions, the isolated solution of $\bar{f}(z, y, \phi_1(y)) = 0$ is given by

$$\begin{bmatrix} C_1 \\ C_2 \\ y \end{bmatrix} = \phi_2(z) = \begin{bmatrix} z(b_2 + 2)^{-1} \\ z(cb_2 + 2c)^{-1} \\ \phi_1(y) + \frac{(a_2+c)z}{a_1 c(b_2+2)} \end{bmatrix}. \tag{3.40}$$

Assumption A4 is therefore satisfied. Assumption A5 can be shown to be satisfied in a similar way.

$$\frac{\partial \bar{h}(y,v)}{\partial v} = \delta \frac{\partial}{\partial C}\left[-k_d C + \left(y p_T - C(p_T + y) + C^2\right)\right] = \delta(-k_d - p_T - y + 2C).$$

The Jacobian matrix $\dfrac{\partial \bar{h}(y,v)}{\partial v}$ evaluated at $v = \phi_1(y)$ is given by

$$\left.\frac{\partial \bar{h}(y,v)}{\partial v}\right|_{v=\phi_1(y)} = -\sqrt{(X_T y_3 + p_T + k_d)^2 - 4 p_T X_T y_3},$$

in which the argument of the square root is always bounded away from zero. Therefore, A6 is satisfied. The Jacobian $\dfrac{\partial \bar{f}}{\partial y}$ gives $\dfrac{\partial \bar{f}}{\partial y} = \begin{bmatrix} -\tilde{A} & -\tilde{B} & -\eta\tilde{B} \\ 0 & -\tilde{C} & \tilde{D} \\ 1 & -c_2 + \tilde{C} & -\tilde{D} \end{bmatrix}$, in which $\eta = 1 - \dfrac{p_T}{X_T}\dfrac{d\phi_1(y)}{dy_3}$,

$$\tilde{A} = b_2 + 1 + (1 - y_1 - y_2 - y_3 + (p_T/X_T)\phi_1(y)) + (\bar{k}/X_T)z - y_1,$$

$\tilde{B} = (\bar{k}/X_T)z - y_1$, $\tilde{C} = c_2 + a_2 + a_1\rho(y_3 - (p_T/X_T)\phi_1(y))$, $\tilde{D} = a_1\eta\,(1 - \rho y_2)$. We show that this Jacobian matrix is Hurwitz by employing the Routh-Hurwitz criterion. Note first that $\tilde{A}$, $\tilde{B}$, $\tilde{C}$ and $\tilde{D}$ are all positive terms. The characteristic equation of the Jacobian is given by

$$\Delta(\lambda) = \lambda^3 + \lambda^2(\tilde{A} + \tilde{C} + \tilde{D}) + \lambda(\tilde{A}\tilde{C} + \tilde{A}\tilde{D} + c\tilde{D} + \eta\tilde{B}) + c\tilde{A}\tilde{D} + \tilde{B}(\eta\tilde{C} + \tilde{D}).$$

Employing Routh-Hurwitz method, the terms in the first column of the Routh-Hurwitz table are given by $\mu_0 = 1$, $\mu_1 = \tilde{A} + \tilde{C} + \tilde{D}$, $\mu_2 = (\tilde{A} + \tilde{C} + \tilde{D})(\tilde{A}\tilde{C} + \tilde{A}\tilde{D}) + c\tilde{D}(\tilde{C} + \tilde{D}) + \eta\tilde{B}(\tilde{A} + \tilde{D}) - \tilde{B}\tilde{D}$, and $\mu_3 = (c\tilde{A}\tilde{D} + \eta\tilde{B}\tilde{C} + \tilde{B}\tilde{D})$. Provided that X_T is large enough, all the coefficients are positive and, therefore, the real part of all eigenvalues of $\dfrac{\partial \bar{h}(y,v)}{\partial v}$ is negative and property A7 is satisfied. Similarly, it is possible to show that assumptions A4, A5 and A9 are satisfied.

3.2.2 Example 2: Phosphotransfer

Phosphotransfer systems are also a common motif in cellular signal transduction [67, 68]. These structures are composed of proteins that can phosphorylate each other. By contrast to kinase-mediated phosphorylation, in which the phosphate donor is usually ATP, in phosphotransfer the phosphate group comes from the donor protein itself. Each protein carrying a phosphate group can donate it to the next protein in the system through a reversible reaction. In this section, we describe a module extracted from the phosphotransferase system [69]. In this example, we consider all the three possible relationships between the timescale of the downstream interconnection and that of the phosphotranfer device.

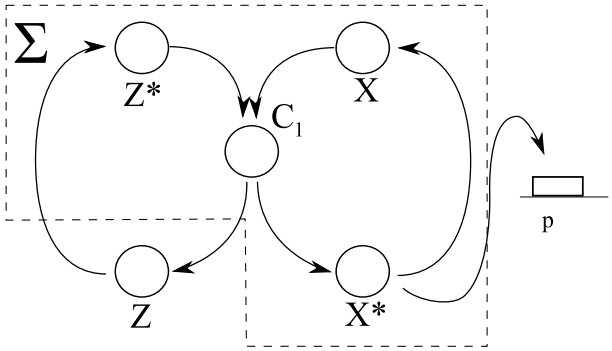

Figure 3.4: **Insulation device based on a two-component system phosphotransfer system.** System Σ is a phosphotransfer system. The output X* activates transcription through the reversible binding of X* to downstream DNA promoter sites p.

In this section, we model the phosphotransfer module shown in Figure 3.4. Let X be a transcription factor in its inactive form and let X^* be the same transcription factor once it has been activated by the addition of a phosphate group. Let Z^* be a phosphate donor, that is, a protein that can transfer its phosphate group to the acceptor X. The standard phosphotransfer reactions [57] can be modelled according to the two-step reaction model $Z^* + X \underset{k_2}{\overset{k_1}{\rightleftharpoons}} C_1 \underset{k_4}{\overset{k_3}{\rightleftharpoons}} X^* + Z$, in which C_1 is the complex of Z bound to X bound to the phosphate group. Additionally, protein Z

can be phosphorylated and protein X^* dephosphorylated by other phosphotransfer interactions. These reactions are modelled as one step reactions depending only on the concentrations of Z and X^*, that is, $Z \xrightarrow{\pi_1} Z^*$, $X^* \xrightarrow{\pi_2} X$. Protein X is assumed to be conserved in the system, that is, $X_{TOT} = X + C_1 + X^* + C$. We assume that protein Z is produced with time-varying production rate $k(t)$ and decays with rate δ. The active transcription factor X^* binds to downstream DNA binding sites p with total concentration p_{TOT} to activate transcription through the reversible reaction $p + X^* \underset{k_{off}}{\overset{k_{on}}{\rightleftharpoons}} C$. Since the total amount of p is conserved, we also have that $C + p = p_{TOT}$. The ODE model corresponding to this system is thus given by the equations

$$\begin{aligned}
\dot{Z} &= k(t) - \delta Z + k_3 C_1 - k_4 X^* Z - \pi_1 Z \\
\dot{C}_1 &= k_1 X_T \left(1 - \frac{X^*}{X_T} - \frac{C_1}{X_T} - \frac{C}{X_T}\right) Z^* - k_3 C_1 - k_2 C_1 + k_4 X^* Z \\
\dot{Z}^* &= \pi_1 Z + k_2 C_1 - k_1 X_T \left(1 - \frac{X^*}{X_T} - \frac{C_1}{X_T} - \frac{C}{X_T}\right) Z^* \\
\dot{X}^* &= k_3 C_1 - k_4 X^* Z - k_{on} X^* (p_T - C) + k_{off} C - \pi_2 X^* \\
\dot{C} &= k_{on} X^* (p_T - C) - k_{off} C.
\end{aligned} \tag{3.41}$$

As performed in Example 1, we introduce non-dimensional variables for this system. Let $\bar{k} := \max_t k(t)/\delta$ and define the non-dimensional input $\tilde{k} := k(t)/(\delta \bar{k})$. Define also the non-dimensional variables $u := \frac{Z}{\bar{k}}$, $x_1 = \frac{C_1}{X_T}$, $x_2 = \frac{Z^*}{\bar{k}}$, $x_3 = \frac{X^*}{X_T}$, $v = \frac{C}{p_T}$ and $\tau := \delta t$. For a variable x, denote $\dot{x} := dx/d\tau$. System (3.41) in these new

variables becomes

$$\begin{aligned}
\dot{u} &= \tilde{k}(t) - u + \frac{k_3 X_T}{\delta \bar{k}} x_1 - \frac{k_4 X_T}{\delta} x_3 u - \frac{\pi_1}{\delta} u \\
\dot{x}_1 &= \frac{k_1 \bar{k}}{\delta} \left(1 - x_1 - x_3 - \frac{p_T}{X_T} v\right) x_2 - \frac{k_3}{\delta} x_1 - \frac{k_2}{\delta} x_1 + \frac{k_4 \bar{k}}{\delta} x_3 u \\
\dot{x}_2 &= \frac{\pi_1}{\delta} u + \frac{k_2 X_T}{\delta \bar{k}} x_1 - \frac{k_1 X_T}{\delta} \left(1 - x_1 - x_3 - \frac{p_T}{X_T} v\right) x_2 \\
\dot{x}_3 &= \frac{k_3}{\delta} x_1 - \frac{k_4 \bar{k}}{\delta} x_3 u - \frac{k_{on} p_T}{\delta} x_3 (1 - v) + \frac{k_{off} p_T}{\delta X_T} v - \frac{\pi_2}{\delta} x_3 \\
\dot{v} &= \frac{X_T k_{on}}{\delta} x_3 (1 - v) - \frac{k_{off}}{\delta} v.
\end{aligned} \tag{3.42}$$

Phosphotranferase reactions are much faster than gene expression and protein decay rates [57]. To make this timescale separation explicit, we define the large parameter $G_1 := \frac{k_2}{\delta} \gg 1$ and define the non-dimensional constants $\bar{k}_1 := \frac{k_1 X_T}{k_2}$, $\bar{k}_3 := \frac{k_3}{k_2}$, $\bar{k}_4 := \frac{k_4 X_T}{k_2}$, $\bar{\pi}_1 := \frac{\pi_1}{k_2}$ and $\bar{\pi}_2 := \frac{\pi_2}{k_2}$. The fact that the process of protein binding and unbinding to promoter sites is much faster than protein production and decay [66, 46] is made explicit by the ratio $G_2 := \frac{k_{off}}{\delta} \gg 1$. In this example we do not make any assumption on the relationship between G_1 and G_2. Let also the dissociation constant be $k_d := k_{off}/k_{on}$. By using these constants, system (3.42) can be written as

$$\begin{aligned}
\dot{u} &= \tilde{k}(t) - u + G_1 \frac{\bar{k}_3 X_T}{\bar{k}} x_1 - G_1 \bar{k}_4 x_3 u - G_1 \bar{\pi}_1 u \\
\dot{x}_1 &= G_1 \frac{\bar{k}_1 \bar{k}}{X_T} \left(1 - x_1 - x_3 - \frac{p_T}{X_T} v\right) x_2 - G_1 \bar{k}_3 x_1 - G_1 x_1 + G_1 \frac{\bar{k}_4 \bar{k}}{X_T} x_3 u \\
\dot{x}_2 &= G_1 \bar{\pi}_1 u + G_1 \frac{X_T}{\bar{k}} x_1 - G_1 \bar{k}_1 \left(1 - x_1 - x_3 - \frac{p_T}{X_T} v\right) x_2 \\
\dot{x}_3 &= G_1 \bar{k}_3 x_1 - G_1 \frac{\bar{k}_4 \bar{k}}{X_T} x_3 u - G_1 \bar{\pi}_2 x_3 - G_2 \frac{p_T}{k_d} x_3 (1 - v) + G_2 \frac{p_T}{X_T} v \\
\dot{v} &= G_2 \frac{X_T}{k_d} x_3 (1 - v) - G_2 v.
\end{aligned} \tag{3.43}$$

The domain for the states of this system are given by $D_z = \mathbb{R}_+$, $D_x = [0, 1] \times \mathbb{R}_+ \times [0, 1]$ and $D_v = [0, 1]$. Compare system (3.43) with system (3.1). In system (3.43), the

internal dynamics term is given by $f = \begin{bmatrix} \frac{\bar{k}_1\bar{k}}{X_T}\left(1 - x_1 - x_3 - \frac{p_T}{X_T}v\right)x_2 - x_1 \\ \frac{X_T}{\bar{k}}x_1 - \bar{k}_1\left(1 - x_1 - x_3 - \frac{p_T}{X_T}v\right)x_2 \\ \bar{k}_3 x_1 - \frac{\bar{k}_4\bar{k}}{X_T}ux_3 - \bar{\pi}_2 x_3 \end{bmatrix}$ and it depends on output term v. Therefore, in order for system (3.43) to fit the structure of system (3.1), we require that the ratio p_T/X_T to be small enough so that $(p_T/X_T)v$ becomes negligible with respect to 1 in the term $(1-x_1-x_3-(p_T/X_T)v)$, as $v \in [0,1]$. This assumption, in practice, limits the amount of load this insulation device can accommodate for a given amount of X_T. Under this assumption, system (3.43) fits the structure of model (3.1) with $g(u,t) = \tilde{k}(t) - u$, $r(x,u) = \begin{bmatrix} \frac{\bar{k}_3 X_T}{\bar{k}}x_1 - \bar{k}_4 x_3 u \\ -\bar{\pi}_1 u \end{bmatrix}$, $f(x,u)\begin{bmatrix} \frac{\bar{k}_1\bar{k}}{X_T}(1 - x_1 - x_3)x_2 - x_1 \\ \frac{X_T}{\bar{k}}x_1 - \bar{k}_1(1 - x_1 - x_3)x_2 \\ \bar{k}_3 x_1 - \frac{\bar{k}_4\bar{k}}{X_T}ux_3 - \bar{\pi}_2 x_3 \end{bmatrix}$, $s(x,v) = -\frac{p_T}{k_d}x_3(1-v) + \frac{p_T}{X_T}v$, $l(v) = 0$, $h(v,t) = 0$, $A := [1\ 1]$, $B = \begin{bmatrix} -\frac{\bar{k}}{X_T} & 0 \\ 0 & -1 \\ 0 & 0 \end{bmatrix}$, $C = \begin{bmatrix} 0 \\ 0 \\ 1 \end{bmatrix}$, $D = -\frac{X_T}{p_T}$. By inspecting matrices A, B, C and D it is possible to choose matrices $T = 1$, $M = \begin{bmatrix} \frac{X_T}{\bar{k}} & 1 & 0 \end{bmatrix}$, $Q = \mathbb{I}_{3\times 3}$ and $P = \begin{bmatrix} 0 & 0 & \frac{p_T}{X_T} \end{bmatrix}^T$, which satisfy properties P1 and P2. This can be verified by checking that indeed $TA+MB = 0$, $Mf(x,u) = 0$, $MC = 0$, $QC+PD = 0$ and, trivially, $Pl(v) = 0$. By applying the linear coordinate transformation given

by $z = Tu + Mx$ and $y = Qx + Pv$, we obtain the system

$$\begin{aligned}
\dot{z} &= k(t) - \left(z - \frac{X_T}{\bar{k}}y_1 - y_2\right) \\
\epsilon_1\dot{y}_1 &= \frac{\bar{k}_1\bar{k}}{X_T}\left(1 - y_1 - y_3 + \frac{p_T}{X_T}v\right)y_2 - \bar{k}_3 y_1 - y_1 \\
&\quad + \frac{\bar{k}_4\bar{k}}{X_T}\left(y_3 - \frac{p_T}{X_T}v\right)\left(z - \frac{X_T}{\bar{k}}y_1 - y_2\right) \\
\epsilon_1\dot{y}_2 &= \bar{\pi}_1\left(z - \frac{p_T}{X_T}y_1 - y_2\right) + y_1 - \bar{k}_1\left(1 - y_1 - y_3 + \frac{p_T}{X_T}v\right)y_2 \\
\epsilon_1\dot{y}_3 &= \bar{k}_3 y_1 - \frac{\bar{k}_4\bar{k}}{X_T}\left(y_3 - \frac{p_T}{X_T}v\right)\left(z - \frac{X_T}{\bar{k}}y_1 - y_2\right) - \bar{\pi}_2\left(y_3 - \frac{p_T}{X_T}v\right) \\
\epsilon_2\dot{v} &= \frac{X_T}{k_d}\left(y_3 - \frac{p_T}{X_T}v\right)(1 - v) - v.
\end{aligned} \tag{3.44}$$

In this example, we do not claim any relationship between G_1 and G_2. In this the situation it is necessary to show that all assumptions A1-A9 are satisfied to prove that the retroactivity to the output property holds.

Assumptions A1 and A2 can be readily verified by inspection of (3.41). As in the phosphorylation system, we have that $\bar{h}(y, v) = \frac{1}{k_d}(X_T y_3 - p_T v) - v$. Therefore, A3 and A6 are satisfied as it was for the phosphorylation system.

Here, we verify the slow manifold is indeed stable. Since the function

$$\phi_1(y) = \frac{y_3 + p_T + k_d - \sqrt{(y_3 + p_T + k_d)^2 - 4p_T y_3}}{2}$$

is sufficiently smooth (the argument of the square root is bounded away from zero) we define the diffeomorphism $w := \Psi(y) = \begin{bmatrix} y_1 & y_2 & y_3 - \phi_1(y) \end{bmatrix}^T$. Define $\hat{f}(z, w) := \bar{f}(z, y, \phi_1(y))\big|_{y=\Psi^{-1}(w)}$. Since under a diffeomorphism the linearization of a non-linear system is invariant [70], it is sufficient to show that $\frac{\partial \hat{f}(z,w)}{\partial w}\big|_{w=\Psi(\phi_2(z))}$ is Hurwitz. We have that $\frac{\partial \hat{f}(z,w)}{\partial w} = \begin{bmatrix} -\tilde{E} - \rho\tilde{F} & \rho\tilde{B} - \tilde{A} & \tilde{D} - \tilde{C} \\ -\frac{\bar{\pi}_1}{\rho} + \tilde{F} & -\bar{\pi}_1 - \tilde{B} & \frac{\tilde{C}}{\rho} \\ \tilde{E} & \tilde{A} & -\tilde{D} - \bar{\pi}_2 \end{bmatrix}$, in which $\rho = \frac{\bar{k}}{X_T}$, $\tilde{A} =$

$\bar{k}_4\bar{k}w_3$, $\tilde{B} = X_T(1-w_1-w_3)$, $\tilde{C} = \bar{k}w_2$, $\tilde{D} = \bar{k}_4\bar{k}(z - \frac{w_1}{\rho} - w_2)$, $\tilde{E} = \bar{k}_3 + \frac{\tilde{A}}{\rho}$ and $\tilde{F} = \frac{\bar{k}_2}{\rho} + \frac{\tilde{C}}{\rho}$. The characteristic equation of this Jacobian is given by

$$\begin{aligned}
\Delta(\lambda) &= \lambda^3 + \lambda^2(\tilde{E} + \rho\tilde{F} + \bar{\pi}_1 + \bar{\pi}_2 + \tilde{B} + \tilde{D}) \\
&+\lambda(\bar{\pi}_1\bar{\pi}_2 + \tilde{A}\bar{k}_2/\rho + \bar{\pi}_1\bar{k}_3 + \bar{\pi}_1\tilde{D} + \bar{\pi}_2\tilde{B} + \tilde{B}\tilde{D} \\
&\quad + \rho\bar{\pi}_1\tilde{F} + \tilde{B}\tilde{E} + \rho\tilde{D}\tilde{F} + \bar{\pi}_1\tilde{B} + \tilde{E}\tilde{C} + \bar{\pi}_2\tilde{E} + \rho\bar{\pi}_2\tilde{F}) \\
&+\bar{\pi}_1\bar{\pi}_2\bar{k}_3 + \bar{\pi}_1\tilde{C}\bar{k}_3 + \rho\bar{\pi}_1\bar{\pi}_2\tilde{F} + \rho\bar{\pi}_1\tilde{D}\tilde{F} + \bar{\pi}_2\tilde{B}\tilde{E} + \bar{\pi}_1\bar{\pi}_2\tilde{B} + \bar{\pi}_1\tilde{B}\tilde{D} + \bar{\pi}_2\tilde{A}\tilde{F}.
\end{aligned}$$

Write the characteristic equation as $\Delta(\lambda) = \lambda^3 + \alpha_2\lambda^2 + \alpha_1\lambda + \alpha_0$ where α_i are implicitly defined. The terms on the first column of the Routh-Hurwitz table are given by 1, α_2, $(\alpha_1\alpha_2 - \alpha_0)/\alpha_2$ and α_0. Since all α_i are positive, we are guaranteed to have only positive terms on the first column of the Routh-Hurwitz table if $\alpha_2\alpha_1 - \alpha_0 > 0$. In particular, the term $\alpha_2\alpha_1 - \alpha_0$ can be reduced to $\alpha_2\alpha_1 - \alpha_0 = \mu + \bar{\pi}_1\bar{k}_2\bar{k}_4\bar{k}\left(z - \frac{w_1}{\rho} - w_2\right) - \frac{\bar{\pi}_2\bar{k}_2\bar{k}_4w_3}{\rho}$, in which the term $\mu > 0$. It remains to show that $\bar{k}_2\bar{k}_4[\bar{\pi}_1(z - w_1/\rho - w_2) - \bar{\pi}_2w_3/\rho] \geq 0$ on the manifold $w = \Psi(\phi_2(z))$. From the system of equations $\bar{f}(x, y, \phi_1(y)) = 0$, one can obtain the identity $\bar{\pi}_2(y_3 - p_T\phi_1(y)/X_T) = \rho\bar{\pi}_1(z - y_1/\rho - y_2)$. The function $y = \phi_2(z)$ is obtained by solving the system of equations $\bar{f}(z, y, \phi_1(y)) = 0$.

$$\begin{aligned}
&\bar{k}\left(1 - y_1 - y_3 + \frac{p_T}{X_T}\phi_1(y)\right)y_2 - \bar{k}_2y_1 - \bar{k}_3y_1 \\
&+ \bar{k}_4\bar{k}\left(z - \frac{y_1}{\rho} - y_2\right)\left(y_3 - \frac{X_T}{p_T}\phi_1(y)\right) = 0 \\
&\bar{\pi}_1\left(z - \frac{y_1}{\rho} - y_2\right) + \frac{\bar{k}_2}{\rho}y_1 - X_T\left(1 - y_1 - y_3 + \frac{p_T}{X_T}\phi_1(y)\right)y_2 = 0 \\
&\bar{k}_3y_1 - \bar{k}_4\bar{k}\left(z - \frac{y_1}{\rho} - y_2\right)\left(y_3 - \frac{p_T}{X_T}\phi_1(y)\right) - \bar{\pi}_2\left(y_3 - \frac{p_T}{X_T}\phi_1(y)\right) = 0.
\end{aligned}$$

Multiplying the second equation by ρ and adding it with the first and the third equations, this system leads to $\bar{\pi}_2(y_3 - p_T\phi_1(y)/X_T) = \rho\bar{\pi}_1(z - y_1/\rho - y_2)$. Substituting

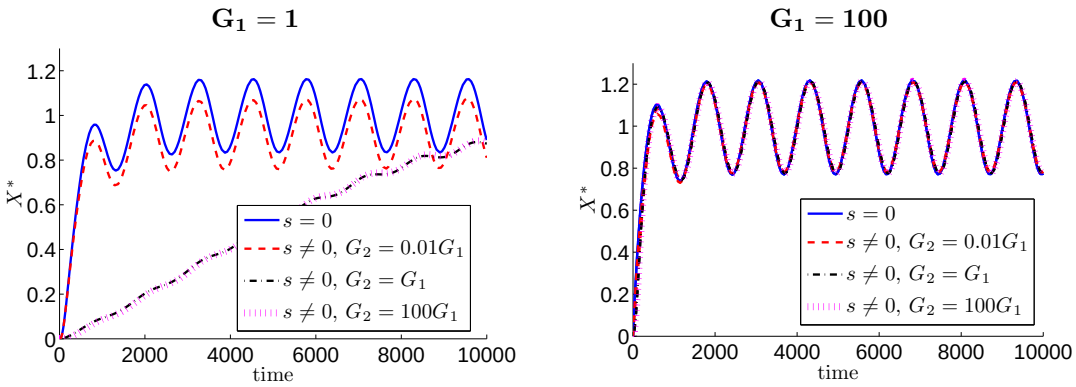

Figure 3.5: **Response of an insulation device based on a phosphotransferase system.** Output response of the phosphotransfer system with a periodic signal $k(t) = \delta(1 + 0.5sin\omega t)$. The parameters are given by $\delta = 0.01$, $X_T = 5000$, $k_1 = k_2 = k_3 = k_4 = \pi_1 = \pi_2 = 0.01G_1$ in which $G_1 = 1$ (left-side panel), and $G_1 = 100$ (right-side panel). The downstream system parameters are given by $k_d = 1$ and $k_{off} = 0.01G_2$, in which G_2 assumes the values indicated on the legend. The isolated system ($s = 0$) corresponds to $p_{TOT} = 0$ while the connected system ($s \neq 0$) corresponds to $p_{TOT} = 100$.

$y = \Psi^{-1}(w)$ in this identity, we obtain that $\bar{\pi}_2 w_3 - \bar{\pi}_1(z - w_1/\rho - w_2) = 0$. As a result, $\alpha_2\alpha_1 - \alpha_0 = \mu > 0$ and thus, the Jacobian matrix $\frac{\partial \hat{f}(z,w)}{\partial w}\Big|_{w=\Psi(\phi_2(z))}$ is Hurwitz satisfying condition A7.

We illustrate the retroactivity to the output attenuation property of this system using simulations for the cases in which $G_1 \gg G_2$, $G_1 = G_2$, and $G_1 \ll G_2$. Figure 3.5 shows that, for a periodic input $k(t)$, the system with low value for G_1 suffers the impact of retroactivity to the output. However, for a large value of G_1, the permanent behavior of the connected system becomes similar to that of the isolated system, whether $G_1 \gg G_2$, $G_1 = G_2$ or $G_1 \ll G_2$. Notice that, in the bottom panel of Figure 3.5, when $G_1 \gg G_2$, the impact of the retroactivity to the output is not as dramatic as it is when $G_1 = G_2$ or $G_1 \ll G_2$. This is due to the fact that s is scaled by G_2 and it is not related to the retroactivity to the output attenuation property. This confirms the theoretical result that, independently of the order of magnitude of G_2, the system can arbitrarily attenuate retroactivity for large enough G_1.

3.3 Tradeoff between insulation property and noise

To understand how noise can be affected by the use of an insulation device, we investigate how the large gains associated with the timescale separation affect a stochastic model a simple model of an insulation device. To that end consider a transcription component similar to the one shown in Chapter II, in which the DNA confers full protection to the transcription factor.

The transcription rate of the gene z, which expresses the protein Z, is given by a time varying function $Gk(t)$ that depends on the transcription factor U. Parameter G models the input amplification gain. The degradation rate of protein Z is also assumed to be tunable and thus identified by $G\delta$. We first show that the variable gain parameter G can be adjusted to improve the insulation properties, as shown in [13].

The transcription factor Z is also an input to the downstream load through the reversible binding of Z to promoter sites p. Neglecting the Z messenger RNA dynamics, which are typically much faster than transcription and decay dynamics, the system can be modelled by the chemical equations

$$\varnothing \underset{G\delta}{\overset{Gk(t)}{\rightleftharpoons}} \mathrm{Z},\ \mathrm{Z} + \mathrm{p} \underset{k_{\mathrm{off}}}{\overset{k_{\mathrm{on}}}{\rightleftharpoons}} \mathrm{C}. \tag{3.45}$$

We assume that $k(t)$ and δ are of the same order and denote $k_d = k_{\mathrm{off}}/k_{\mathrm{on}}$. We also assume that the production and decay processes are slower than binding and unbinding reactions, that is, $k_{\mathrm{off}} \gg G\delta$, $k_{\mathrm{on}} \gg G\delta$ [46]. Let the total concentration of promoter be p_T. The deterministic ordinary differential equation model of system (3.45) is given by

$$\begin{aligned} [\dot{Z}] &= Gk(t) - G\delta[Z] + k_{\mathrm{off}}[C] - k_{\mathrm{on}}(p_T - [C])[Z] \\ [\dot{C}] &= -k_{\mathrm{off}}[C] + k_{\mathrm{on}}(p_T - [C])Z, \end{aligned} \tag{3.46}$$

in which $[Z]$ and $[C]$ denote the concentrations of Z and C respectively. In this section, the bracket notation is used to contrast concentrations from Z and C, the random variables denoting the number of molecules. Figure 3.6 shows that adding load to the system decreases the amplitude of the concentration signal $[Z]$. This effect is due retroactivity to the output of the transcriptional component. The figure shows also how the retroactivity effect can be compensated by increasing the gains G.

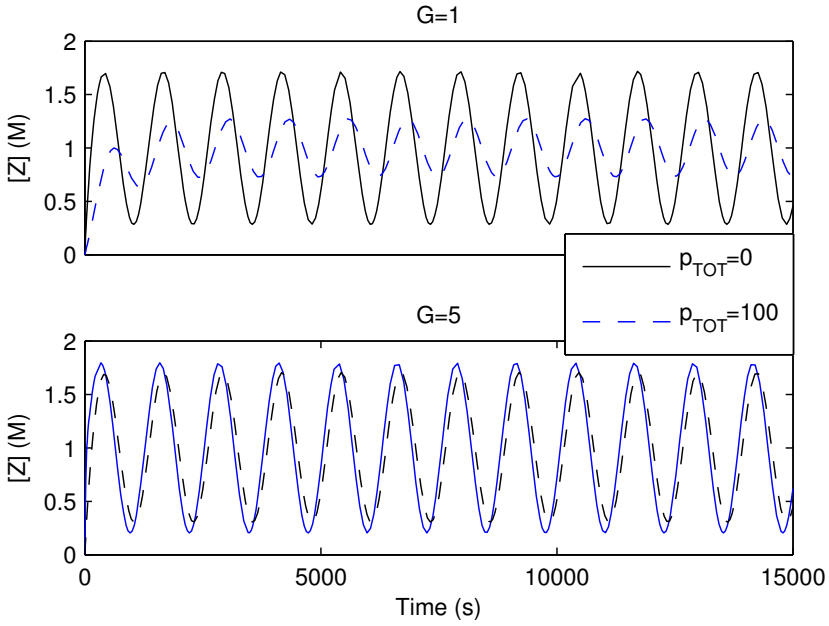

Figure 3.6: **Retroactivity attenuation on an amplification/feedback insulation device.** Effect of retroactivity from the load on system (3.46). Here, $\omega = 0.005\text{rad/s}$, $\delta = 0.01\text{M}^{-1}\text{s}^{-1}$, $k_{\text{off}} = 50\text{M}^{-2}$ and $k_d = 20\text{Ms}^{-1}$. The input signal is $k(t) = \delta(1 + 0.8\sin(\omega t))\text{s}^{-1}$. The top plot shows how adding the load impacts $[Z]$. The bottom plot shows how increasing G can reduce the impact of the retroactivity from the load. For this plot we chose $G = 1 + R_l$ (see text).

To identify by what amounts G should be increased to compensate the retroactivity effect, we perform a linearized analysis of (3.46) about $k(t) = \bar{k}$, and the corresponding equilibrium $[\bar{Z}] = \bar{k}/\delta$ and $[\bar{C}] = [\bar{Z}]p_T/([\bar{Z}] + k_d)$. The dynamics of small perturbations about the equilibrium $(\bar{k}, [\bar{Z}], [\bar{C}])$ are, with abuse of notation,

given by

$$\begin{aligned}[\dot{Z}] &= Gk(t) - (G\delta + k_{\text{on}}(p_T - [\bar{C}]))[Z] + (k_{\text{off}} + k_{\text{on}}[\bar{Z}])[C] \\ [\dot{C}] &= k_{\text{on}}(p_T - [\bar{C}])[Z] - (k_{\text{off}} + k_{\text{on}}[\bar{Z}])[C].\end{aligned} \tag{3.47}$$

Since $k_{\text{on}} \gg \delta$ and $k_{\text{off}} = k_{\text{on}}k_d$, write

$$k_{\text{on}} = \delta/\epsilon \text{ and } k_{\text{off}} = \delta k_d/\epsilon, \tag{3.48}$$

in which $\epsilon \ll 1$. Let $y = [Z] + [C]$. Substituting (3.48) into (3.47) and writing the system in terms of y and $[C]$, one obtains the system in the standard singular perturbation form

$$\dot{y} = Gk(t) - (G\delta(y - [C]) \tag{3.49}$$

$$\epsilon[\dot{C}] = \delta(p_T - [\bar{C}])y - \delta(p_T - [\bar{C}] + k_d + [\bar{Z}])[C] \tag{3.50}$$

Setting $\epsilon = 0$, one obtains the expression of the slow manifold as $[C] = k_d p_T[Z]/([\bar{Z}] + k_d)^2 = :\gamma([Z])$. It can be shown that this manifold is exponentially stable. Defining the constant

$$R_l = \frac{k_d p_T}{(\bar{k}/\delta + k_d)^2}, \tag{3.51}$$

the expression of the slow manifold can be rewritten as $\gamma([Z]) = R_l[Z]$. Letting $[Z] = y - \gamma([Z])$, we obtain that $[\dot{Z}] = \dot{y} - R_l[\dot{Z}]$, in which $\dot{y} = Gk(t) - G\delta[Z]$. The approximated dynamics of $[Z]$ on the slow manifold then becomes

$$[\dot{Z}] = \frac{G}{1 + R_l}(k(t) - \delta[Z]). \tag{3.52}$$

Thus, for small perturbations about the equilibrium, we should choose $G \approx 1 + R_l$ to compensate for retroactivity from the load. In real systems, however, there are practical limitations on how much the gain can be increased so that retroactivity may not be completely rejected.

3.3.1 Master Equation

Let $\mathbf{P}\left(Z, C, p; t | Z_0, C_0, p_0; t_0 = 0\right)$ denote the conditional probability that at time t, the number of molecules of the species Z, C and p are Z, C and p respectively, given that the number of molecules were Z_0, C_0 and p_0 at the initial time $t_0 = 0$. Throughout this chapter we omit the dependency on initial conditions and write $\mathbf{P}(Z, C, p; t)$ for convenience. Let Ω denote the volume of the system. Then the relation between concentrations and number of molecules is given by $Z = \Omega[Z]$ and $C = \Omega[C]$. Define the step operator as $\mathbb{E}_X^a f(X) = f(X + a)$. The Master Equation [71] for the system described in (3.45) is given by

$$\begin{aligned}\dot{\mathbf{P}}(Z, C, p; t) = \big(&Gk(t)\Omega(\mathbb{E}_Z^{-1} - 1) + G\delta(\mathbb{E}_Z^{+1} - 1)Z \\ &+ k_{\text{on}}\Omega^{-1}(\mathbb{E}_Z^{+1}\mathbb{E}_p^{+1}\mathbb{E}_C^{-1} - 1)Zp + k_{\text{off}}(\mathbb{E}_Z^{-1}\mathbb{E}_p^{-1}\mathbb{E}_C^{+1} - 1)C\big)\,\mathbf{P}(Z, C, p; t).\end{aligned}$$

Since $p + C = \Omega p_T$ with probability one, the equation can be reduced to the two-state Master Equation

$$\begin{aligned}\dot{\mathbf{P}}(Z, C; t) = \big(&Gk(t)\Omega(\mathbb{E}_Z^{-1} - 1) + G\delta(\mathbb{E}_Z^{+1} - 1)Z \\ &+ k_{\text{on}}(\Omega^{-1}(\mathbb{E}_Z^{+1}\mathbb{E}_C^{-1} - 1)Z(\Omega p_T - C) + k_{\text{off}}(\mathbb{E}_Z^{-1}\mathbb{E}_C^{+1} - 1)C\big)\,\mathbf{P}(Z, C; t).\end{aligned} \tag{3.53}$$

3.3.2 Linear Noise Approximation

Since the coefficients of $\mathbf{P}(Z, C; t)$ in equation (3.53) are not linear functions of the states, we cannot obtain a closed set of exact equations for the moments [72]. To proceed with the analysis, we thus employ the Ω-expansion [71].

Define the change of variables

$$Z = \Omega\phi_Z + \Omega^{1/2}\zeta \text{ and } C = \Omega\phi_C + \Omega^{1/2}\xi, \tag{3.54}$$

in which ζ and ξ are random variables and ϕ_Z, ϕ_C are deterministic quantities. Let also $\Pi(\zeta, \xi; t) := \mathbf{P}(\Omega\phi_Z + \Omega^{1/2}\zeta, \Omega\phi_C + \Omega^{1/2}\xi; t)$. Then, the left hand side of equation

(3.53) becomes

$$\dot{P}(Z,C;t) = \partial_t \Pi(\zeta,\xi;t) - \Omega^{1/2}\dot{\phi_Z}\partial_\zeta \Pi(\zeta,\xi;t) - \Omega^{1/2}\dot{\phi_C}\partial_\xi \Pi(\zeta,\xi;t), \tag{3.55}$$

in which $\partial_x := \partial/\partial_x$. By performing Taylor expansion of the step operator in the new variables ζ and ξ, we obtain the identities

$$\mathbb{E}_Z^a = \sum_{k=0}^{\infty} \frac{(a\Omega^{-1/2})^k}{k!}\partial_\zeta^k,\ \mathbb{E}_C^a = \sum_{k=0}^{\infty} \frac{(a\Omega^{-1/2})^k}{k!}\partial_\xi^k. \tag{3.56}$$

Substituting (3.53) and (3.56) in equation (3.55), solving for $\partial_t \Pi(\zeta,\xi;t)$ and collecting the terms in powers of Ω up to order Ω^0, we obtain

$$\begin{aligned}
\partial_t \Pi(\zeta,\xi;t) = \Omega^{1/2}\Big[&\big(\dot{\phi_Z} - Gk(t) + G\delta\phi_Z + k_{\text{on}}\phi_Z(p_T-\phi_C) - k_{\text{off}}\phi_C\big)\partial_\zeta \\
&+ \big(\dot{\phi_C} - k_{\text{on}}\phi_Z(p_T-\phi_C) + k_{\text{off}}\phi_C\big)\partial_\xi\Big]\Pi(\zeta,\xi;t) \\
&+ \Omega^0\Big[\partial_\zeta\big((G\delta + k_{\text{on}}(p_T-\phi_C))\zeta + (-k_{\text{on}}\phi_Z - k_{\text{off}})\xi\big) \\
&+ \partial_\xi\big(-k_{\text{on}}(p_T-\phi_C)\zeta + (k_{\text{on}}\phi_Z + k_{\text{off}})\xi\big) \\
&+ \frac{1}{2}\partial_\zeta^2\big(Gk(t) + G\delta\phi_Z + k_{\text{on}}\phi_Z(p_T-\phi_C) + k_{\text{off}}\phi_C\big) \\
&+ \frac{1}{2}\partial_\xi^2\big(k_{\text{on}}\phi_Z(p_T-\phi_C) + k_{\text{off}}\phi_C\big) \\
&+ \partial_\zeta\partial_\xi\big(-k_{\text{on}}\phi_Z(p_T-\phi_C) - k_{\text{off}}\phi_C\big)\Big]\Pi(\zeta,\xi;t) + O(\Omega^{-1/2}).
\end{aligned} \tag{3.57}$$

Setting the coefficient of $\Omega^{1/2}$ in equation (3.57) to zero, one obtains the macroscopic laws for the deterministic variables ϕ_Z and ϕ_C:

$$\begin{aligned}
\dot{\phi_Z} &= Gk(t) - \delta\phi_Z - k_{\text{on}}\phi_Z(p_T-\phi_C) + k_{\text{off}}\phi_C \\
\dot{\phi_C} &= k_{\text{on}}\phi_Z(p_T-\phi_C) - k_{\text{off}}\phi_C.
\end{aligned} \tag{3.58}$$

By taking the volume to be large enough to make $O(\Omega^{-1/2})$ negligible in equation

(3.57), we obtain the Fokker-Planck equation[1]

$$\begin{aligned}\partial_t \Pi(\zeta,\xi;t) = \Big[&\partial_\zeta\big((G\delta + k_{\text{on}}(p_T-\phi_C))\zeta + (-k_{\text{on}}\phi_Z \\ &- k_{\text{off}})\xi\big) + \partial_\xi\big(-k_{\text{on}}(p_T-\phi_C)\zeta + (k_{\text{on}}\phi_Z + k_{\text{off}})\xi\big) \\ &+ \frac{1}{2}\partial_\zeta^2\big(Gk(t) + G\delta\phi_Z + k_{\text{on}}\phi_Z(p_T-\phi_C) + k_{\text{off}}\phi_C\big) \\ &+ \frac{1}{2}\partial_\xi^2\big(k_{\text{on}}\phi_Z(p_T-\phi_C) + k_{\text{off}}\phi_C\big) \\ &+ \partial_\zeta\partial_\xi\big(-k_{\text{on}}\phi_Z(p_T-\phi_C) - k_{\text{off}}\phi_C\big)\Big]\Pi(\zeta,\xi;t).\end{aligned} \tag{3.59}$$

The above procedure, often referred to as Linear Noise Approximation, takes the jump Markov process defined by equation (3.53) and approximates it by the continuous Markov process that solves equation (3.59) [73]. This approximation is valid for large volumes and when the jumps on the original process are small compared to the total number of molecules [73]. Since all reactions have stoichiometry 1, this second condition is satisfied by guaranteeing $\Omega\phi_Z(t) \gg 1$ and $\Omega\phi_C(t) \gg 1$ for all time. Since we already take Ω large to satisfy the first condition, we just need to guarantee $\phi_C(t) > 0$ and $\phi_Z(t) > 0$.

Given a general Fokker-Planck equation of the form

$$\partial P_t(\mathbf{x};t) = -\sum_i \partial_i A_i(\mathbf{x},t)P(\mathbf{x},t) + \frac{1}{2}\sum_i\sum_j \partial_i\partial_j B_{ij}(\mathbf{x},t)P(\mathbf{x},t), \tag{3.60}$$

it is possible to derive differential equations for the expectancy of any polynomial function $f(\mathbf{x})$. Multiplying both sides of equation (3.60) by $f(\mathbf{x})$ and integrating both sides over the state space one obtains the differential equation [73]

$$\langle \dot{f(\mathbf{x})} \rangle = \sum_i \langle A_i \partial_i f(\mathbf{x}) \rangle + \frac{1}{2}\sum_i\sum_j \langle B_{ij}\partial_i\partial_j f(\mathbf{x}) \rangle . \tag{3.61}$$

Repeating this process with the Fokker-Planck equation (3.59), we obtain the differ-

[1] The function $\Pi(\zeta,\xi;t)$ was scaled so that it integrates to 1 [71].

ential equations for the first order moments as

$$\begin{aligned}\langle\dot{\zeta}\rangle &= -\delta\langle\zeta\rangle - k_{\text{on}}(p_T-\phi_C)\langle\zeta\rangle + k_{\text{on}}\phi_Z\langle\xi\rangle + k_{\text{off}}\langle\xi\rangle \\ \langle\dot{\xi}\rangle &= k_{\text{on}}(p_T-\phi_C)\langle\zeta\rangle - k_{\text{on}}\phi_Z\langle\xi\rangle - k_{\text{off}}\langle\xi\rangle .\end{aligned} \tag{3.62}$$

Setting the initial conditions of the macroscopic equations (3.58) to correspond to the initial values of the number of species, that is, setting $\phi_Z(0) = \Omega^{-1}Z_0$ and $\phi_C(0) = \Omega^{-1}C_0$, then $\langle\zeta(0)\rangle = 0$ and $\langle\xi(0)\rangle = 0$. In doing so, $\langle\zeta(t)\rangle = 0$ and $\langle\xi(t)\rangle = 0$ for all time. Therefore, $\zeta(t)$ and $\xi(t)$ are zero-mean random processes.

Similarly, the dynamics of the second order moments are given by

$$\begin{aligned}\langle\dot{\zeta^2}\rangle &= -2G\delta\left\langle\zeta^2\right\rangle - 2k_{\text{on}}(p_T-\phi_C)\left\langle\zeta^2\right\rangle + 2k_{\text{on}}\phi_Z\langle\zeta\xi\rangle \\ &\quad + 2k_{\text{off}}\langle\zeta\xi\rangle + k_{\text{on}}\phi_Z(p_T-\phi_C) + k_{\text{off}}\phi_C + Gk(t) + G\delta\phi_Z \\ \langle\dot{\zeta\xi}\rangle &= -G\delta\langle\zeta\xi\rangle + k_{\text{on}}\phi_Z\left\langle\xi^2\right\rangle + k_{\text{off}}\left\langle\xi^2\right\rangle + k_{\text{on}}(p_T-\phi_C)\left\langle\zeta^2\right\rangle \\ &\quad - k_{\text{on}}\phi_Z\langle\zeta\xi\rangle - k_{\text{off}}\zeta\xi - k_{\text{on}}\phi_Z(p_T-\phi_C) - k_{\text{off}}\phi_C \\ \langle\dot{\xi^2}\rangle &= 2k_{\text{on}}(p_T-\phi_C)\langle\zeta\xi\rangle - 2k_{\text{on}}\phi_Z\left\langle\xi^2\right\rangle - 2k_{\text{off}}\left\langle\xi^2\right\rangle \\ &\quad + k_{\text{on}}\phi_Z(p_T-\phi_C) + k_{\text{off}}\phi_C.\end{aligned} \tag{3.63}$$

To validate the Fokker-Planck approximation (3.59), we compare the time dependent mean and standard deviation of the concentrations predicted by numerical integrations of equations (3.58) and (3.63) with the mean and standard-deviation from sample realizations given by a Stochastic Simulation Algorithm (SSA) implementation [55]. Let the means be denoted by $\mu_{[Z]} = \langle[Z]\rangle$ and $\mu_{[C]} = \langle[C]\rangle$ and the standard deviations denoted by $\sigma_{[Z]} = \sqrt{\left\langle(\Omega^{-1}Z)^2 - \mu_{[Z]}^2\right\rangle}$ and $\sigma_{[C]} = \sqrt{\left\langle(\Omega^{-1}C)^2 - \mu_{[C]}^2\right\rangle}$. To obtain these quantities from the Fokker-Plank approximation, recall that ζ and ξ are zero-mean random variables and that ϕ_Z and ϕ_C are deterministic. Then, from the substitution of variables (3.54) the mean concentration of Z and C are given by $\mu_{[Z]} = \phi_Z$, $\mu_{[C]} = \phi_C$. The standard deviation of $[Z]$ is given by $\sigma_{[Z]} = \sqrt{\Omega^{-1}\langle\zeta^2\rangle}$

and $\sigma_{[C]} = \sqrt{\Omega^{-1}\langle\xi^2\rangle}$. To obtain these quantities from N realizations Z_i and C_i of the SSA we used the sample mean and the biased sample variance estimator, that is, $\mu_{[Z]} = \sum_i^N Z_i/(N\Omega)$, $\mu_{[C]} = \sum_i^N C_i/(N\Omega)$, $\sigma^2_{[Z]} = \sum_{i=1}^N((\Omega^{-1}Z_i)^2 - \mu^2_{[Z]})/N$ and $\sigma^2_{[C]} = \sum_i^N((\Omega^{-1}C_i)^2 - \mu^2_{[C]})/N$.

Figure 3.7 shows that the means and standard deviations of Z and C predicted by the Fokker-Planck equation are very close to the values obtained from the samples of the SSA. This comparison was made using different values of G, p_T and k_d, all showing that the Fokker-Planck equation is a satisfactory approximation for the Master Equation.

3.3.3 Signal to Noise Ratio Analysis

One of the traditional metrics used to assess noise in many electrical engineering applications is the signal-to-noise ratio. This quantity is usually defined by taking the ratio between the power of the signal and the power of the noise and gives a measure of how much the noise corrupts the signal.

For this study, we consider periodic input signals and characterize the signal-to-noise ratio as a function of the input frequency. Since concentrations are always positive, we consider inputs of the form $k(t) = \bar{k} + \tilde{k}(t)$, in which $\bar{k}$ is a constant bias and $\tilde{k}(t) = A_0 sin(\omega t)$ is a periodic signal with amplitude $A_0 < \bar{k}$ and frequency ω. We assume that all the information transmitted is contained in the signal $\tilde{k}(t)$. Therefore, to obtain a signal-to-noise figure of merit, the power of a signal is taken to be the square of its amplitude. The power of the noise is quantified by the steady-state variance calculated when the input is constant equal to the bias, that is, $k(t) = \bar{k}$. Denoting A the amplitude of a signal and $\bar{\sigma}^2$ the steady-state variance,

the figure of merit for the noise is given by

$$SNR := \frac{A^2}{\bar{\sigma}^2}. \tag{3.64}$$

To calculate the values of $\bar{\sigma}^2$, set $k(t) = \bar{k}$ in equations (3.58) and (3.63). The corresponding equilibrium values of the deterministic variables ϕ_Z and ϕ_C are obtained from equations (3.58) as

$$\bar{\phi_Z} = \frac{\bar{k}}{\delta} \text{ and } \bar{\phi_C} = \frac{p_T \bar{\phi_Z}}{1 + \delta k_d/\bar{k}} = \frac{p_T/k_d}{1 + \bar{\phi_Z}/k_d}. \tag{3.65}$$

Substituting (3.65) in equations (3.63) and setting the time derivatives to zero, the equilibrium values for the second-order moments become

$$\langle \bar{\zeta^2} \rangle = \frac{\bar{k}}{\delta},\ \langle \bar{\zeta\xi} \rangle = 0 \text{ and } \langle \bar{\xi^2} \rangle = \frac{\bar{\phi_Z} p_T k_d}{(\bar{k}/\delta + k_d)^2} = \bar{\phi_Z} R_l,$$

in which R_l is the same constant defined in expression (3.51).

From the change of variables (3.54), and since ζ and ξ are zero-mean, we have that $\bar{\sigma}^2_{[Z]} = \Omega^{-1}\langle \bar{\zeta^2} \rangle$ and $\bar{\sigma}^2_{[C]} = \Omega^{-1}\langle \bar{\xi^2} \rangle$ leading to expressions

$$\bar{\sigma}^2_{[Z]} = \frac{\bar{\phi_Z}}{\Omega} \text{ and } \bar{\sigma}^2_{[C]} = \frac{\bar{\phi_Z} R_l}{\Omega}. \tag{3.66}$$

For small amplitudes of the signal $\tilde{k}(t)$, $\bar{\sigma}^2$ approximates the time-average value of the time-dependent variance $\sigma(t)$ when the system is subject to the input $k(t) = \bar{k} + \tilde{k}(t)$.

Due to the fact that ζ and ξ are zero-mean random variables, $\langle Z \rangle = \Omega\phi_Z$ and $\langle C \rangle = \Omega\phi_C$. Therefore, the amplitude of the mean concentration signals $[Z]$ and $[C]$ are equal to the amplitude of ϕ_Z and ϕ_C, respectively. To calculate this amplitude, we proceed by linearizing equation (3.58) about the equilibrium corresponding to the fixed input $k(t) = \bar{k}$. With abuse of notation, the linear system becomes

$$\begin{aligned} \dot{\phi_Z} &= G\tilde{k}(t) - (G\delta - k_{\text{on}}(p_T - \bar{\phi_C}))\phi_Z + (k_{\text{on}}\bar{\phi_Z} + k_{\text{off}})\phi_C, \\ \dot{\phi_C} &= k_{\text{on}}(p_T - \bar{\phi_C})\phi_Z - (k_{\text{on}}\bar{\phi_Z} + k_{\text{off}})\phi_C. \end{aligned} \tag{3.67}$$

In order to obtain the amplitude of the signals ϕ_Z and ϕ_C, we compute the transfer functions from $\tilde{k}$ to ϕ_Z and ϕ_C. Let $\Phi_Z(s)$, $\Phi_C(s)$ and $\tilde{K}(s)$ denote the Laplace transform of $\phi_Z(t)$, $\phi_C(t)$ and $\tilde{k}(t)$ respectively, from (3.67) we obtain

$$\begin{aligned}\Phi_Z(s) &= \frac{G(s + k_{\text{on}}\bar{\phi_Z} + k_{\text{off}})\tilde{K}(s)}{(s + G\delta)(s + k_{\text{on}}\bar{\phi_Z} + k_{\text{off}}) + sk_{\text{on}}(p_T - \bar{\phi_C})} \\ \Phi_C(s) &= \frac{k_{\text{on}}(p_T - \bar{\phi_C})\Phi_Z(s)}{s + k_{\text{on}}\bar{\phi_Z} + k_{\text{off}}}.\end{aligned} \tag{3.68}$$

By using the substitution (3.48) and setting $\epsilon = 0$, we obtain the simplified transfer functions

$$\begin{aligned}G_1(s) &= \frac{\Phi_Z(s)}{\tilde{K}(s)} = \frac{G}{s(1 + R_l) + G\delta} \\ G_2(s) &= \frac{\Phi_C(s)}{\tilde{K}(s)} = \frac{GR_l}{s(1 + R_l) + G\delta}.\end{aligned}$$

Therefore, for a input signal $\tilde{k}(t)$ with frequency ω and amplitude A_0, the amplitude of the concentrations are

$$\begin{aligned}A_{[Z]} &= |G_1(j\omega)|A_0 = \sqrt{\frac{G^2}{G^2\delta^2 + \omega^2(1 + R_l)^2}}A_0, \\ A_{[C]} &= |G_2(j\omega)|A_0 = \sqrt{\frac{G^2R_l^2}{G^2\delta^2 + \omega^2(1 + R_l)^2}}A_0.\end{aligned} \tag{3.69}$$

Substituting expressions (3.66) and (3.69) in the definition (3.64), the signal-to-noise ratios obtained for an input $\tilde{k}(t)$ with amplitude A_0 and frequency ω are

$$SNR_Z(\omega) = \frac{\Omega}{k\delta}\frac{G^2}{G^2 + \frac{\omega^2}{\delta^2}(1 + R_l)^2}A_0^2, \tag{3.70}$$

$$SNR_C(\omega) = \frac{\Omega}{k\delta}\frac{G^2R_l}{G^2 + \frac{\omega^2}{\delta^2}(1 + R_l)^2}A_0^2. \tag{3.71}$$

Recalling from (3.51) that R_l is monotonically increasing with p_T, expression (3.70) shows that for a signal with non-zero frequency addition of load p_T leads to a lower value of SNR_Z. Notice that the higher the frequency, the more sensitive SNR_Z is to the load. Increasing the gain G improves the SNR_Z and in the limit when $G \to \infty$, $SNR_Z \to \Omega A_0^2/(\bar{k}\delta)$ giving a theoretical upper bound on the SNR_Z.

Equation (3.71) shows that the effect of increasing G on SNR_C is similar to the effect on SNR_Z: as the gain increases, the signal-to-noise ratio increases, and in the limit when $G \to \infty$, $SNR_C \to \Omega R_l A_0^2/\bar{k}\delta$. The effect of increasing the load, however is not trivial. If we are able to increase the gain to $G \approx 1 + R_l$ to compensate for the retroactivity, then SNR_C decreases with a higher load. If, instead, the value of G cannot be large enough to reach $1 + R_l$, then increasing p_T will reduce SNR_C. This is a consequence of the fact that when G cannot compensate for the retroactivity the amplitude $A_{[Z]}$ decreases and consequently so does $A_{[C]}$.

3.3.4 Frequency analysis of disturbances and the Langevin approach

In Section 3.3.3, we have shown that increasing the gain G is beneficial for both rejecting retroactivity to the upstream component and decreasing the noise-to-signal ratio. However, as shown in Figure 3.8, increasing the gain G impacts the frequency content of the noise in a single realization. For low values of G, the error signal between a realization and the mean is of lower frequency when compared to a higher gain. This effect is not captured by the signal-to-noise metric because the averaging process used to calculate the standard deviation smooths out the noise.

To study this problem, we employ the Langevin equation derived from the Master Equation (3.53). As shown in [74], a Master Equation of the form

$$\frac{dP(\mathbf{X};t)}{dt} = \sum_{j=1}^{M} (\prod_{i=1}^{N} \mathbb{E}_{x_i}^{v_{ij}} - 1) a_j(\mathbf{X}) P(\mathbf{X};t),$$

can be approximated by a Langevin system of equations of the form

$$\frac{dX_i}{dt} = \sum_{j=1}^{M} v_{ij} a_j(\mathbf{X}(t)) + \sum_{j=1}^{M} v_{ij} a_j^{1/2}(\mathbf{X}(t)) \Gamma_j(t),$$

in which $\Gamma_j(t)$ are independent Gaussian white noise processes. Applying the above approximation to the Master Equation (3.53), one obtains the system of Langevin

equations

$$\begin{aligned}\dot{Z} &= Gk(t) - G\delta Z - k_{\text{on}}(p_T - C)Z + k_{\text{off}}C + \sqrt{Gk(t)}\,\Gamma_1(t) \\ &\quad - \sqrt{G\delta Z}\,\Gamma_2(t) - \sqrt{k_{\text{on}}(p_T - C)Z}\,\Gamma_3(t) + \sqrt{k_{\text{off}}C}\,\Gamma_4(t), \\ \dot{C} &= k_{\text{on}}(p_T - C)Z - k_{\text{off}}C + \sqrt{k_{\text{on}}(p_T - C)Z}\,\Gamma_3(t) - \sqrt{k_{\text{off}}C}\,\Gamma_4(t).\end{aligned} \tag{3.72}$$

The above system can be viewed as a non-linear system with five inputs, $k(t)$ and $\Gamma_i(t)$ for $i = 1, 2, 3, 4$. Let $k(t) = \bar{k}$, $\Gamma_1(t) = \Gamma_2(t) = \Gamma_3(t) = \Gamma_4(t) = 0$ be constant inputs and let $\bar{Z}$ and $\bar{C}$ be the corresponding equilibrium points. Then for small amplitude signals $\tilde{k}(t)$ the linearization of the system (3.72) leads, with abuse of notation, to

$$\begin{aligned}\dot{Z} &= G\tilde{k}(t) - G\delta Z - k_{\text{on}}(p_T - \bar{C})Z + k_{\text{on}}\bar{Z}C + k_{\text{off}}C \\ &\quad + \sqrt{G\bar{k}}\,\Gamma_1(t) - \sqrt{\delta\bar{Z}}\,\Gamma_2(t) - \sqrt{k_{\text{off}}\bar{C}}\,\Gamma_3(t) + \sqrt{k_{\text{on}}(p_T - \bar{C})\bar{Z}}\,\Gamma_4(t) \\ \dot{C} &= k_{\text{on}}(p_T - \bar{C})Z - k_{\text{on}}\bar{Z}C - k_{\text{off}}C + \sqrt{k_{\text{off}}\bar{C}}\,\Gamma_3(t) - \sqrt{k_{\text{on}}(p_T - \bar{C})\bar{Z}}\,\Gamma_4(t).\end{aligned}$$

We can further simplify the above expressions by noting that $\delta\bar{Z} = G\bar{k}$ and $k_{\text{on}}(p_T - \bar{C})\bar{Z} = k_{\text{off}}\bar{C}$. Also, since Γ_j are independent identical Gaussian white noises, we can write $\Gamma_1(t) - \Gamma_2(t) = \sqrt{2}N_1(t)$ and $\Gamma_3(t) - \Gamma_4(t) = \sqrt{2}N_2(t)$, in which $N_1(t)$ and $N_2(t)$ are independent Gaussian white noises identical to $\Gamma_j(t)$. This simplification leads to the system

$$\begin{aligned}\dot{Z} &= G\tilde{k}(t) - G\delta Z - k_{\text{on}}(p_T - \bar{C})Z + k_{\text{on}}\bar{Z}C + k_{\text{off}}C \\ &\quad + \sqrt{2G\bar{k}}N_1(t) - \sqrt{2k_{\text{off}}\bar{C}}N_2(t), \\ \dot{C} &= k_{\text{on}}(p_T - \bar{C})Z - k_{\text{on}}\bar{Z}C - k_{\text{off}}C + \sqrt{2k_{\text{off}}\bar{C}}N_2(t).\end{aligned} \tag{3.73}$$

This is a system with three inputs: the deterministic input $\tilde{k}(t)$ and two independent white noise sources $N_1(t)$ and $N_2(t)$. One can interpret N_1 as the source of the fluctuations caused by the production and degradation reactions while N_2 is the

source of fluctuations caused by binding and unbinding reactions. Since the system is linear, we can analyse the different contributions of each noise source separately and independent from the signal $\tilde{k}(t)$.

The transfer function from N_1 to Z is

$$T_1(s) = \frac{\sqrt{G\bar{k}}}{(s+G\delta)(s+k_{\text{on}}\bar{Z}+k_{\text{off}})+sk_{\text{on}}(p_T-\bar{C})}.$$

Employing substitutions (3.48) and setting $\epsilon = 0$, we simplify the transfer function to

$$T_1(s) = \frac{Z(s)}{N_1(s)} = \frac{\sqrt{2G\bar{k}}}{s(1+R_l)+G\delta}. \tag{3.74}$$

The DC gain of this transfer function is equal to $T_1(0) = \sqrt{2\bar{k}}/\sqrt{G}\delta$. Thus, as G increases, the DC gain decreases. But for large enough frequencies ω, $j\omega(1+R_l)+G\delta \approx j\omega(1+R_l)$, and the amplitude $|T_1(j\omega)| \approx \sqrt{2\bar{k}G}/\omega(1+R_l)$ becomes a monotone function of G. This effect is illustrated in the upper plot of Figure 3.9. The frequency at which the amplitude of $|T_1(j\omega)|$ computed with $G=1$ intersects the amplitude $|T_2(j\omega)|$ computed with $G>1$ is given by the expression

$$\omega_e = \frac{\delta\sqrt{G}}{(1+R_l)}.$$

Thus, when increasing the gain from 1 to $G>1$, we reduce the noise at frequencies lower than ω_e but we increase it at frequencies larger than ω_e.

The transfer function from the second white noise source N_2 to Z is given by

$$T_2(s) = \frac{\sqrt{2k_{\text{off}}\bar{C}}s}{s^2+(G\delta+k_{\text{on}}(p_T-\bar{C})+k_{\text{on}}\bar{Z}+k_{\text{off}})s+G\delta(k_{\text{on}}\bar{Z}+k_{\text{off}})}.$$

Using substitutions (3.48) and multiplying numerator and denominator by ϵ, we obtain the transfer function

$$T_2(s) = \frac{\sqrt{\epsilon}\sqrt{2\delta\bar{C}}s}{\epsilon s^2+(\epsilon G\delta+\delta(p_T-\bar{C})+\delta\bar{Z}+\delta k_d)s+G\delta(\delta\bar{Z}+\delta k_d)}. \tag{3.75}$$

This transfer function has one zero at $s = 0$ and two poles at

$$s_{\pm} = \frac{\delta}{2\epsilon}\Bigg[- \epsilon G - p_T + \bar{C}) - \bar{Z} + k_d \pm \sqrt{(\epsilon G + p_T - \bar{C} + \bar{Z} + k_d)^2 - 4\epsilon G(\bar{Z} + k_d)}\Bigg].$$

When $\epsilon \to 0$, $s_- \to -\infty$ and $s_+ \to -G\delta/(1 + R_l)$. Thus, the contribution of $N_2(t)$ to Z is relevant only on the high frequency range due to the high-pass nature of the transfer function. Furthermore, increasing the gain G increases the cutoff frequency given by the pole s_+. It is also important to note that $N_2(s)$ is scaled by $\sqrt{\epsilon}$, making the noise on the low-frequency caused by $N_2(t)$ negligible when compared to that caused by $N_1(t)$. The Bode plot of the transfer function $T_2(s)$ is shown in the lower plot of Figure 3.9.

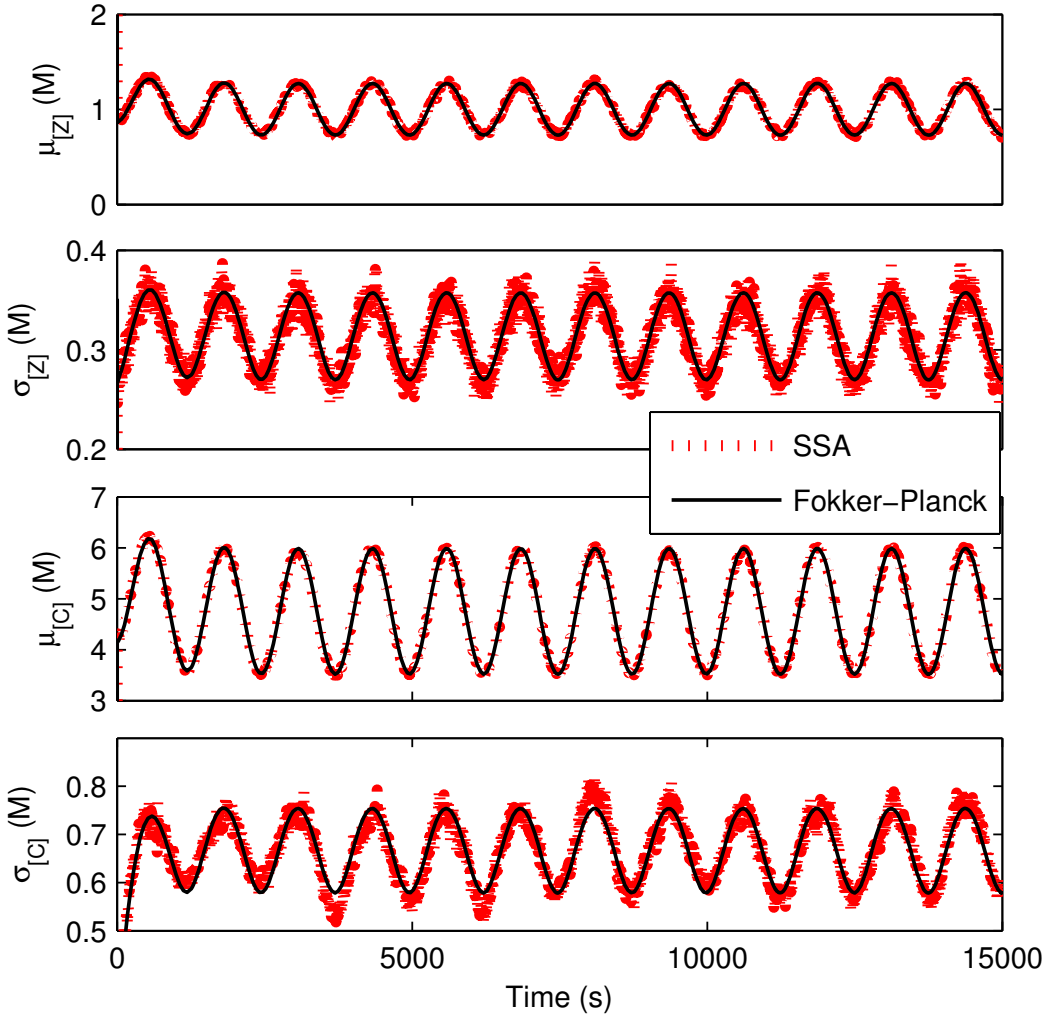

Figure 3.7: **The sample means and variances from SSA and from Fokker-Planck equation are shown to be very close to each other.** For these plots, $\delta = 0.01\text{M}^{-1}\text{s}^{-1}$, $k_d = 20\text{M}$, $k_{\text{off}} = 50\text{M}^{-1}\text{s}^{-1}$ with input signal $k(t) = \delta(1 + 0.8\sin\omega t)\text{s}^{-1}$ and volume $\Omega = 10\text{M}^{-1}$. To simulate the time varying input in the SSA, we imposed a deterministic time-varying concentration of a Z protein messenger with concentration $k(t) = \delta(1 + 0.8\sin(\omega t))$. Means from SSA were calculated using 500 realizations.

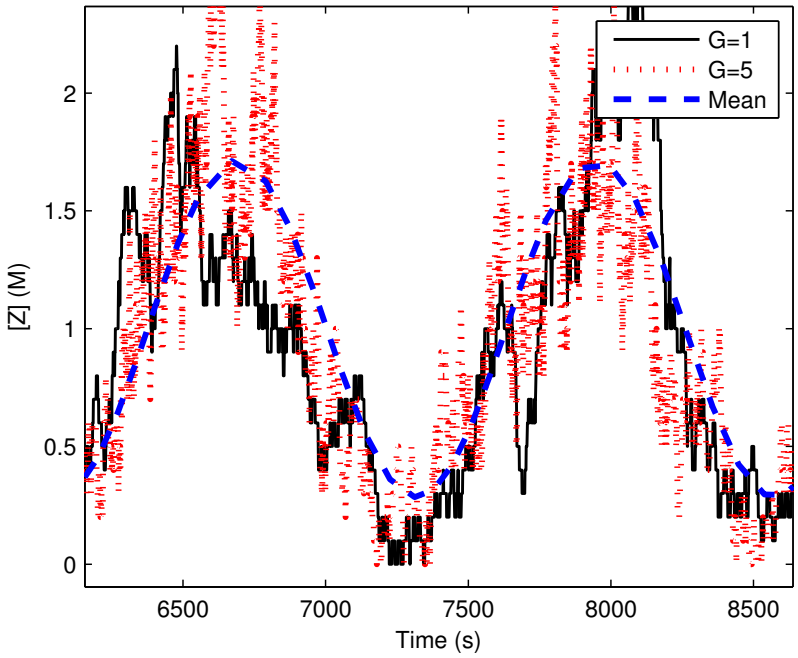

Figure 3.8: **Increasing the value of G produces a disturbance signal of higher frequency.** Two realizations are shown with different values for G without load. The parameters used in the simulations are $\delta = 0.01\mathrm{M}^{-1}\mathrm{s}^{-1}$, $k_d = 20\mathrm{M}$, $k_{\mathrm{off}} = 50\mathrm{M}^{-1}\mathrm{s}^{-1}$, $\omega = 0.005\mathrm{rad/s}$ and $\Omega = 10\mathrm{M}^{-1}$. The input signal used is $k(t) = \delta(1 + 0.8\sin\omega t)\mathrm{s}^{-1}$. The mean of the signal is given as reference.

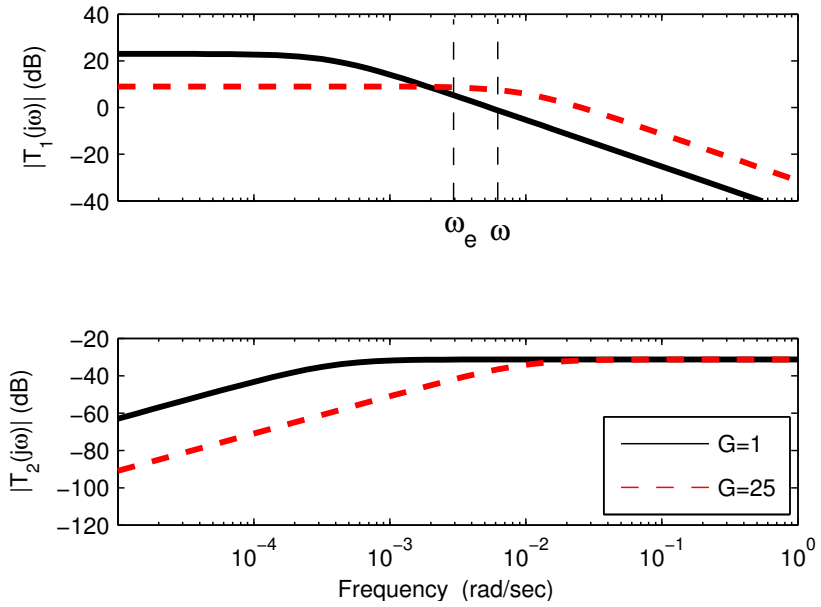

Figure 3.9: **Magnitude of the transfer functions $T_1(s)$ and $T_2(s)$.** The parameters used in this plot are $\delta = 0.01\text{M}^{-1}\text{s}^{-1}$, $k_d = 1\text{M}$, $k_{\text{off}} = 50\text{M}^{-1}\text{s}^{-1}$, $\omega = 0.005\text{rad/s}$, $p_T = 100\text{M}$. When G increases from 1 to $1 + R_l = 25$, contribution from N_1 decreases but it now spreads to a higher range of the spectrum. Note that there was an increase on the noise at the frequency of interest ω. Increasing G reduces the contribution from N_2 in the low frequency range, leaving the high frequency range unaffected. Note also that the amplitude of T_2 is significantly smaller than that of T_1.

CHAPTER IV

Measuring Retroactivity *in vivo*

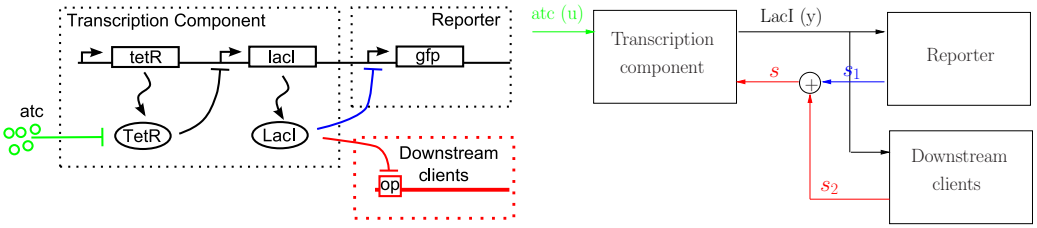

Figure 4.1: **Layout of gene circuit employed to study retroactivity.** (a) Genetic diagram. The circuit plasmid contains both the transcription component and the reporter system. The downstream clients to which the transcription component connects are realized by a plasmid containing one operator site with affinity to LacI. The *connected system* refers to cells co-transformed with both the circuit plasmid and the plasmid with operator sites. The *isolated system* refers to cells co-transformed with the circuit plasmid and a plasmid that does not contain the operator site but is of the same type as the one with operator site. (b) Block diagram illustration of the different parts of the gene circuit. The transcription component takes as input u anhydrotetracycline (atc) and gives as output y the repressor LacI. This output is used as an input by both the reporter system and the downstream clients. Upon interconnection with either the reporter or the downstream clients, retroactivities s_1 from the reporter and s_2 from the downstream clients, respectively, arise.

Figure 4.1(a) shows the details of the gene circuit employed to characterize retroactivity effects. The upstream transcription component takes as input atc (u) and provides as an output LacI-LVA (y). LacI is in turn taken as an input by a reporter system assembled on the same plasmid as the transcription component. The reporter system produces GFP-LVA as an indirect measurement of LacI. Since LacI is a repressor, we should expect that GFP decreases as atc increases. The downstream clients contain LacI operators and are assembled on a different plasmid. Both the reporter and the downstream clients apply retroactivity to the upstream transcription

component (see Figure 4.1(b)). Here, we are interested in characterizing the effects of retroactivity s_2 from the downstream clients on the response of the transcription component to atc. Hence, we consider as the *isolated system* the circuit of Figure 4.1(a), in which the operator sites in the downstream clients are absent, resulting into $s_2 = 0$. We consider as the *connected system* the circuit of Figure 4.1(a), in which the operator sites in the downstream clients are present.

Experimentally, we realize the isolated system through cells in which we co-transformed the pACYC184-based plasmid (with the transcription component and reporter), which we refer to as circuit plasmid, with pUC18-based plasmid that do not have LacI operator sites, which we refer to as blank plasmid. We realize the connected system through cells in which we co-transformed the circuit plasmid with pUC18-based plasmid including the operator site for LacI, which we refer to as client plasmid. The difference between the responses of GFP to atc in the isolated and connected system configurations characterize the effects of retroactivity s_2 from the downstream clients on the transcription component.

We modelled the circuit of Figure 4.1(a) by a set of ordinary differential equations (ODE) describing the rate of change of LacI and GFP. Let p_T be the concentration of the circuit plasmid (proportional to the circuit plasmid copy number) and q_T be the concentration of the clients plasmid (proportional to the clients plasmid copy number). Let $\lambda = q_T/p_T$, $l = [LacI]/p_T$, $g = [GFP]/p_T$, let c_1 denote the concentration of LacI bound to downstream clients promoter sites divided by p_T, and let c_2 denote the concentration of LacI bound to the promoter of the reporter divided by

p_T. Then, we have the following ODE model for the connected system:

$$\dot{l} = \alpha_1 \frac{u^n}{1+u^n} - \delta l \overbrace{\underbrace{-(p_T k'_{\text{on}})l(1-c_1) + k'_{\text{off}}c_1}_{s_1} \underbrace{-(p_T k_{\text{on}})l(\lambda - c_2) + k_{\text{off}}c_2}_{s_2}}^{s} \tag{4.1}$$

$$\dot{c}_1 = (p_T k'_{\text{on}})l(1-c_1) - k'_{\text{off}}c_1 - \delta c_1 \tag{4.2}$$

$$\dot{c}_2 = (p_T k_{\text{on}})l(\lambda - c_2) - k_{\text{off}}c_2 - \delta c_2 \tag{4.3}$$

$$\dot{g} = \alpha_2(1-c_1) - \delta g, \tag{4.4}$$

in which u is the concentration of atc in units of its dissociation constant from TetR, n is the cooperativity of atc binding TetR, $k_{\text{on}}, k'_{\text{on}}, k_{\text{off}}, k'_{\text{off}}$ are the association and dissociation rate constants, respectively, of LacI with the promoter and operator sites, and δ is the decay rate constant (including dilution and degradation). Here, α_1 and α_2 are the maximal expression rates per promoter. Since the complexes also decay, we are assuming the non-asylum model according to which proteins are not protected by decay when bound to DNA [30]. The reader is referred to the Appendix for the detailed derivation of the model and for the parameter values.

Note that the retroactivity term s_2 depends only on λ and not on the absolute value of the downstream clients amount q_T. This indicates that the effects of retroactivity depend on the ratio between the circuit plasmid copy number and the clients plasmid copy number, but not on the absolute value of the latter. We remark that the binding/unbinding reactions are much faster than the production and decay of LacI. Furthermore, the dissociation constant $k_d = k_{\text{off}}/(p_T k_{\text{on}})$ of LacI with the operator sites is very small, implying that once LacI binds, it unbinds very rarely. These features are relevant for understanding the experimental results illustrated in the following section.

The retroactivity to the output of the transcription component s appears as a rate in the equation for LacI and has two components: s_1 is the retroactivity due to the

reporter and s_2 is the retroactivity due to the downstream clients. Here, we study the effect that s_2 has on the response of LacI to atc, indirectly measured through GFP. Hence, the isolated system is represented by the above equations, in which we have set $s_2 = 0$, but $s_1 \neq 0$. It follows that the isolated system configuration still has an intrinsic retroactivity due to the reporter. Given that the expressions of s_1 and s_2 are similar, the qualitative effects that s_1 has on the transcription component are the same as those that s_2 has. Therefore, to characterize the qualitative effect of retroactivity s on the transcription component, it is enough to characterize the effect of s_2 on the response of GFP to atc.

4.1 Metrics to measure retroactivity on the response of the gene circuit

We characterize the effects of retroactivity on the dynamic response of GFP to sudden changes of atc. For completeness, we also show the effects on the steady state transfer curve from atc to GFP. For the dynamic response, we consider two experiments: an induction experiment and a de-induction experiment. In the induction experiment, LacI starts from zero (GFP starts from its maximal unrepressed value) at time zero and a high constant non-zero value of atc is applied, so that LacI rises and GFP decreases reaching zero. In the de-induction experiment, LacI starts from a non-zero steady state reached through pre-induction with a non-zero high value of atc (so that GFP starts from zero). Then, atc is suddenly removed ($atc = 0$) so that LacI decreases toward zero and GFP rises toward its maximal unrepressed value. In order to quantify the effect of retroactivity on dynamics, we measure the response time of GFP, which mirrors the one of LacI. There are several standard metrics to determine the response time of a system. In this chapter, we consider the t_{50} (t_{20}), which, in our experiments, is given by the time GFP takes to change by 50% (20%)

of its maximal unrepressed value from when atc is applied or removed.

4.2 Mechanistic Model

In this section, we describe the mechanistic model employed when analyzing the implemented circuit. The first subsection shows a simplification of the output stage that maps the amounts of atc into the number of free operator sites with affinity to TetR and regulate the expression of LacI. In the following section, we model the remainder of the circuit along with a nondimensionalization that allows a clear understanding of the qualitative impact of retroactivity. The reaction rates employed in the simulation as well as constants employed in calculating the results in this section can be found in Table 4.1.

4.2.1 Simplification of the model for the input

Since we are interested in modelling the retroactivity to the output of the transcription component, we can simplify the input stage to an input/output static model without compromising the analysis. This model maps the concentration of atc to the amount of free tetO genes (O) in the cell, able to express LacI.

The set of reactions that model the input stage are given in Table 4.2. In order to obtain these equations, the following assumptions are made. Due to a high affinity rate, TetR is almost always in the form of a dimer [82]. This is modelled by assuming that the amount of free monomer (M) is insignificant compared to that of the total amount of dimer (D). Additionally, the TetR dimer has two atc binding sites that bind independently due to the distance between the sites and the activity [83]. We further assume the concentration of free inducer to be constant and not affected by its binding to TetR. This comes from a "trapping" effect: while the free atc can freely diffuse through the membrane, the atc bound to TetR cannot diffuse out,

Table 4.1: Rates and constants employed in the simulations. The sources in parenthesis indicate values calculated from other values from this table. Dilution rate (line 3) was calculated based on the observed doubling time between 100-120 mins. LacI tetramer expression per gene (line 17) was based on experimental data provided by the Registry of Biological Parts [75].

	Description		Value	Source
	Common Constants			
(1)	Cell Volume	V_{cell}	10^{-15}L	[76]
(2)	Concentration of 1 molecule per cell	C_0	1.8nM	(1)
(3)	Dilution rate	δ_ℓ	10^{-4}s^{-1}	experimental
(4)	LVA Degradation	δ_g	$3 \times 10^{-4}\text{s}^{-1}$	[77, 78]
(5)	Total Decay	δ	$4 \times 10^{-4}\text{s}^{-1}$	(3) and (4)
(6)	Circuit plasmids per cell	p_T	20 copies per cell	Table 4.4
	Constants related to Input			
(7)	TetR(B) and atc association rate	k_{a1}	$10^6\text{M}^{-1}\text{s}^{-1}$	[79]
(8)	TetR(B) and atc dissociation rate	k_{d1}	$5 \times 10^{-6}\text{s}^{-1}$	[79]
(9)	TetR and operator association rate	k_{a2}	$2.7 \times 10^8\text{M}^{-1}\text{s}^{-1}$	[80]
(10)	TetR and operator dissociation rate	k_{d2}	$1.5 \times 10^{-3}\text{s}{-1}$	[80]
	Constants related to Circuit			
(11)	Dissociation constant between LacI tetramer and reporter operator	K_{d3}	1×10^{-11}M	[81]
(12)	Dissociation rate between LacI tetramer and reporter operator	k_{off}	$7.4 \times 10^{-3}\text{s}^{-1}$	[80]
(13)	Association rate between LacI tetramer and reporter operator	k_{on}	$7.4 \times 10^8\text{M}^{-1}\text{s}^{-1}$	(11) and (12)
(14)	Dissociation constant between LacI tetramer and client operator	K_{d3}	1.8×10^{-12}M	[81]
(15)	Dissociation rate between LacI tetramer and client operator	k'_{off}	$9 \times 10^{-4}\text{s}^{-1}$	[81]
(16)	Association rate between LacI tetramer and client operator	k'_{on}	$5 \times 10^8\text{M}^{-1}\text{s}^{-1}$	(14) and (15)
	Constants in simulation			
(17)	LacI tetramer expression per gene	κ_t	20	[75]
(18)	Association rate ratio between client and reporter sites	ζ_3	0.67	(13) and (16)
(19)	Dissociation rate ratio between client and reporter sites	η_3	0.12	(12) and (15)
(20)	Time-scale separation between decay and dissociation rates	Γ	18	(5) and (12)
(21)	Non-dimensionalized dissociation constant	κ_{D3}	7×10^{-5}	(2), (6) and (13)
(22)	Client to circuit plasmids ratio	λ	2.5 clients per circuit	Table 4.4

and therefore the intracellular concentration of free atc quickly equilibrates with the extracellular concentration of atc [84].

Table 4.2: Reactions for input model (Section 4.2.1).

Description	Reaction
Expression of TetR monomer (M)	$\emptyset \xrightarrow{k_+} \mathrm{M}$
Dimerization of TetR monomers to obtain a dimer (D)	$2\ \mathrm{M} \underset{b_2}{\overset{b_1}{\rightleftharpoons}} D$
TetR monomer degradation	$\mathrm{M} \xrightarrow{\delta} \emptyset$
Degradation of one monomer of TetR dimer	$\mathrm{D} \xrightarrow{2\delta} \mathrm{M}$
First atc (i) binding to TetR dimer (complex D_1 formation)	$\mathrm{D} + \mathrm{i} \xrightarrow{k_{a1}} \mathrm{D}_1$
Degradation of one monomer of TetR dimer	$\mathrm{D}_1 \xrightarrow{2\delta} \mathrm{M}$
Second atc binding to TetR dimer (complex D_2 formation)	$\mathrm{D}_1 + \mathrm{i} \xrightarrow{k_{a1}} \mathrm{D}_2$
Degradation of one monomer of TetR dimer	$\mathrm{D}_2 \xrightarrow{2\delta} \mathrm{M}$
Operator tetO (O) binding to first TetR dimer (complex C_4 formation)	$\mathrm{O} + \mathrm{D} \underset{k_{d2}}{\overset{k_{a2}}{\rightleftharpoons}} \mathrm{C}_4$
Degradation of one monomer of TetR dimer	$\mathrm{C}_4 \xrightarrow{2\delta} \mathrm{O} + \mathrm{M}$
Operator tetO binding to second TetR dimer (complex C_5 formation)	$\mathrm{C}_4 + \mathrm{D} \underset{k_{d2}}{\overset{k_{a2}}{\rightleftharpoons}} \mathrm{C}_5$
Degradation of one monomer of TetR dimer	$\mathrm{C}_5 \xrightarrow{2\delta} \mathrm{C}_4 + \mathrm{M}$

We assume further that the total amount of operator sites is constant via the conservation law $O_T := O + C_4 + C_5$. From these, one can obtain the following ODE system

$$\dot{M} = k_+ - \delta M - 2b_1 M^2 + 2b_2 D + 2\delta D + 2\delta D_1 + 2\delta D_2 + 2\delta(C_4 + C_5) \tag{4.5}$$

$$\dot{D} = b_1 M^2 - b_2 D - 2\delta D - k_{a1} D i - 2\delta(C_4 + C_5) \tag{4.6}$$

$$\dot{D_1} = k_{a1} D i - 2\delta D_1 - k_{a1} D_1 i \tag{4.7}$$

$$\dot{D_2} = k_{a1} D_1 i - 2\delta D_2 \tag{4.8}$$

$$\dot{C_4} = k_{a2}(O_T - C_4 - C_5)D - k_{d2} C_4 - k_{a2} C_4 D + k_{d2} C_5 - 2\delta C_4 + 2\delta C_5 \tag{4.9}$$

$$\dot{C_5} = k_{a2} C_4 D - k_{d2} C_5 - 2\delta C_5. \tag{4.10}$$

Define the concentration of total amount of monomers of TetR to be $R_T = M +$

$2D + 2D_1 + 2D_2 + 2C_4 + 2C_5$. Note that the dynamics of R_T are given by $\dot{R}_T = \dot{M} + 2\dot{D} + 2\dot{D}_1 + 2\dot{D}_2 + 2\dot{C}_4 + 2\dot{C}_5 = k_+ - \delta R_T$ and therefore the total amount of TetR repressor at the steady state is $R_T^* = k_+/\delta$, independent of the total amount of operator sites O_T or the inducer concentration i. To obtain the steady state solution for the variables in the system, we set the left hand side of the equations (4.7-4.8) to zero, to find the following expressions:

$$D_1 = \frac{k_{a1} i}{2\delta + k_{a1} i} D \tag{4.11}$$

$$D_2 = \frac{k_{a1} i}{2\delta} D_1 = \frac{(k_{a1} i)^2}{2\delta\,(2\delta + k_{a1} i)} D. \tag{4.12}$$

By setting the left hand side of equations (4.5-4.6) to zero and adding them with weights 1 and 2, respectively, we obtain the equation

$$k_+ - \delta M - 2\delta D + 2\delta D_1 + 2\delta D_2 - 2\delta(C_4 + C_5) - 2k_{a1} D i = 0. \tag{4.13}$$

Recall our assumption that $M \ll D$ which leads to $M + 2D \approx 2D$. Also, recall that $k_+ = R_T^* \delta$. Define $\beta_2 := k_{a1}/(2\delta)$. Substituting (4.11-4.12) along with these substitutions in (4.13) and solving the expression for D, we obtain

$$D = \frac{R_T/2 - (C_4 + C_5)}{1 + \beta_2 i} \approx \frac{R_T/2}{1 + (\beta_2 \delta) i}, \tag{4.14}$$

assuming that the total amount of TetR is much higher than the number of operators ($C_4 + C_5 < O_T \ll R_T$).

Define $\beta_3 := (k_{d2} + 2\delta)/k_{a2}$. By setting the left hand side of equations (4.9-4.10), one obtains the identity

$$C_4 + C_5 = \frac{1 + \beta_3 D^{-1}}{1 + \beta_3 D^{-1} + \beta_3 D^{-2}} O_T,$$

from which we can deduce that the total amount of free promoters ptet to be

$$O = \frac{\beta_3^2 D^{-2}}{1 + \beta_3 D^{-1} + \beta_3^2 D^{-2}} O_T. \tag{4.15}$$

From Table 4.1, we can calculate the values for $\beta_2^{-1} = 2\delta/k_{a1} = 10^{-9}M = 1\text{nM}$ and $\beta_3 = (2\delta + k_{d2})/k_{a2} = 9.2\text{pM}$.

Define $\beta_1 := \dfrac{R_T}{2\beta_3}$. Combining both expressions (4.14) and (4.15), one obtains the expression

$$O(i) = \frac{(1+\beta_2 i)^2}{(1+\beta_2 i)^2 + (1+\beta_2 i)\beta_1 + \beta_1^2} O_T, \tag{4.16}$$

which is a monotonically increasing function of i with $\lim_{i\to\infty} O(i) = O_T$ and $O(0) = O_T(1+\beta_1+\beta_1^2)^{-1} \approx 0$, since $\beta_1 \gg 1$. It is possible to calculate the Hill constant through the response coefficient, as shown in [85]. In order to obtain that, note that $i_{0.9} = \dfrac{R_T}{0.1\beta_2\beta_3}$ and $i_{0.1} = \dfrac{R_T}{2.5\beta_2\beta_3}$, which gives $n = 1.36$. With these in hand, we obtain the input Hill function

$$O(i) \approx \frac{(i/i_{1/2})^n}{1+(i/i_{1/2})^n}.$$

In the simulations, we let $u = i/i_{1/2}$ and employ

$$O(u) = \frac{u^n}{1+u^n}, \text{ with } n = 1.36. \tag{4.17}$$

4.2.2 Circuit Model

The remainder of the circuit can be modelled by the chemical equations presented in Table 4.3. To derive this model, the following assumptions were made. Since the LacI repressor in dimer form bind to the DNA slower than its tetramer form [86]. Further, since the affinity of the tetrameric form is strong enough so that LacI is found *in vivo* essentially in its tetrameric form [87], we assume that only tetramers bind to the DNA. Additionally, free LacI monomers are present in insignificant quantities [88] and the affinity between LacI monomers to form dimers is very strong [86]. Based on these assumptions, we model the formation of LacI tetramers as a one step expression system from the promoter.

Table 4.3: Reactions for circuit model (Section 4.2.2).

Description	Reaction
Expression of LacI (tetramer represented by L)	$O \xrightarrow{\alpha_1} O+L$
LacI decay	$L \xrightarrow{\delta} \emptyset$
LacI binding to client operator (p) to form complex C_1	$L+p \underset{k'_{off}}{\overset{k'_{on}}{\rightleftharpoons}} C_1$
Decay of LacI bound to client operator	$C_1 \xrightarrow{\delta} p$
LacI binding to reporter operator (p_0) to form complex C_2	$L+p_0 \underset{k_{off}}{\overset{k_{on}}{\rightleftharpoons}} C_2$
Decay of LacI bound to reporter operator	$C_2 \xrightarrow{\delta} p$
GFP expression	$p_0 \xrightarrow{\alpha_2} p_0+GFP$
GFP decay	$GFP \xrightarrow{\delta} \emptyset$

Let p_T denote the concentration of the total amount of reporter operator sites and λ denote the ratio between the amount of client operator sites and the amount of reporter operator sites. Assuming that the total concentration of these promoters are constants, i.e., $p_0 + C_2 = p_T$ and $p + C_1 = \lambda p_T$ with p_T and λ constants, the resulting ODE model is given by

$$\dot{L} = \alpha_1 O(u) - \delta L - k'_{\text{on}} L(\lambda p_T - C_1) - k_{\text{on}}(p_T - C_2) + k'_{\text{off}} C_1 + k_{\text{off}} C_2 \tag{4.18}$$

$$\dot{C}_1 = k'_{\text{on}} L(\lambda p_T - C_1) - \delta C_1 - k'_{\text{off}} C_1 \tag{4.19}$$

$$\dot{C}_2 = k_{\text{on}} L(p_T - C_2) - \delta C_1 - k_{\text{off}} C_2 \tag{4.20}$$

$$\dot{G} = \alpha_2(p_T - C_2) - \delta G. \tag{4.21}$$

In this model, the isolated system is obtained by setting $\lambda = 0$ and $O(u)$ is the expression given in (4.17). Notice that due to the presence of the GFP reporters, our circuit already suffers from a baseline retroactivity.

In order to extract qualitative data from this model, we nondimensionalize the system using the transformations $(\ell, c_1, c_2, g) = (L, C_1, C_2, G)/p_T$. We will also de-

fine the nondimensional time variable by $\tau := \delta t$. Let the dissociation constant be $K_{d3} := k_{\text{off}}/k_{\text{on}}$, and define the nondimensional constants $\Gamma := k_{\text{off}}/\delta$, $\kappa_{D3} := K_{d3}/p_T$, $\eta_3 := k'_{\text{off}}/k_{\text{off}}$, $\zeta_3 = k'_{\text{on}}/k_{\text{on}}$ and $\kappa_t := \alpha_1/(\delta p_T)$. With these, one obtains the nondimensional system

$$\frac{d\ell}{d\tau} = \kappa_t \frac{u^n}{1+u^n} - \ell - \frac{\Gamma\zeta_3}{\kappa_{D3}}\ell(\lambda - c_1) - \frac{\Gamma}{\kappa_{D3}}\ell(1-c_2) + \eta_3\Gamma c_1 + \Gamma c_2 \tag{4.22}$$

$$\frac{dc_1}{d\tau} = -c_1 - \eta_3\Gamma c_1 + \frac{\Gamma\zeta_3}{\kappa_{D3}}\ell(\lambda - c_1) \tag{4.23}$$

$$\frac{dc_2}{d\tau} = -c_2 - \Gamma c_2 + \frac{\Gamma}{\kappa_{D3}}\ell(1-c_2) \tag{4.24}$$

$$\frac{dg}{d\tau} = -g + \alpha_2(1-c_2). \tag{4.25}$$

Here, p_T is the concentration of circuit plasmids in the cell while the parameter λ gives the ratio between the concentrations of client and the circuit plasmids. Note that at steady state, the total amount of tetramers is $\ell_T^* := \ell^* + c_1^* + c_2^* = \kappa_t$. Table 4.1 contains the values employed in the simulations. With the exception of the rate represented by $\eta_3\Gamma$, the rates related to association/dissociation interactions are at least one order of magnitude faster than the expression and decay reactions. Therefore, the retroactivity effect from the reporter is well modelled by the reduced model (2.8) while the retroactivity effect from the clients is well modelled by the degenerate model (2.19).

4.3 Single container experiments

4.3.1 Growth Conditions and Sample Preparation

The media used in the experiment is the M9 media supplemented with 0.4% glucose, 0.2% casamino acids, 40mg/l tryptophan, 100μg/ml ampicilin, and 34μg/ml chloramphenicol. Cells were inoculated into fresh media from plate or freezer stocks, and incubated at 30°C until mid-log phase (spectrophotometry reading of 0.15 at

600nm with 1cm pathlength). At that point the cells were quickly washed by pelleting and resuspension in fresh media, and diluted 7/8-fold. Care was taken to preserve the cells in log phase. These diluted cultures were then placed in a plate reader/incubator (Synergy MX) at 30°C and mild agitation in all experiments. Doubling time under these conditions was of approximately 100min. In longer experiments, cells were kept in mid-log phase via dilutions. No impact on the growth rate was observed due to dilutions, addition or removal of anyhdrotetracycline (atc).

4.3.2 Dynamic effects of retroactivity: Induction.

To measure the effect of retroactiviy in an induction experiments, cells prepared as per Section 4.3.1 were grown two generations in the plate reader, at which point cells were induced. Figure 4.2(a)-(b) shows the response of GFP to sudden application of atc for both the isolated and connected systems. The effect of retroactivity is basically a time delay. This can be qualitatively explained by recalling that the value of the dissociation constant k_d for LacI binding to its operator sites is extremely small and that the binding reactions are much faster that protein production and decay (see the Appendix for the exact values). In fact, LacI is sequestered by the operator sites as soon as it is produced. Only when the operator sites are filled, any additional LacI produced is free to take part in other reactions, and, in particular, in those of the reporter. Hence, before LacI can rise (GFP can decrease), there is a time delay, which is the time it takes for LacI to fill the operator sites. This time delay, monotonically increases with the relative amount λ of these sites. The reader is referred to next section for a precise mathematical explanation.

Figure 4.2(c) shows the mean values of the response times and their standard deviation for isolated and connected systems. The response time of the connected system increases in average by 40% with respect to the one of the isolated system.

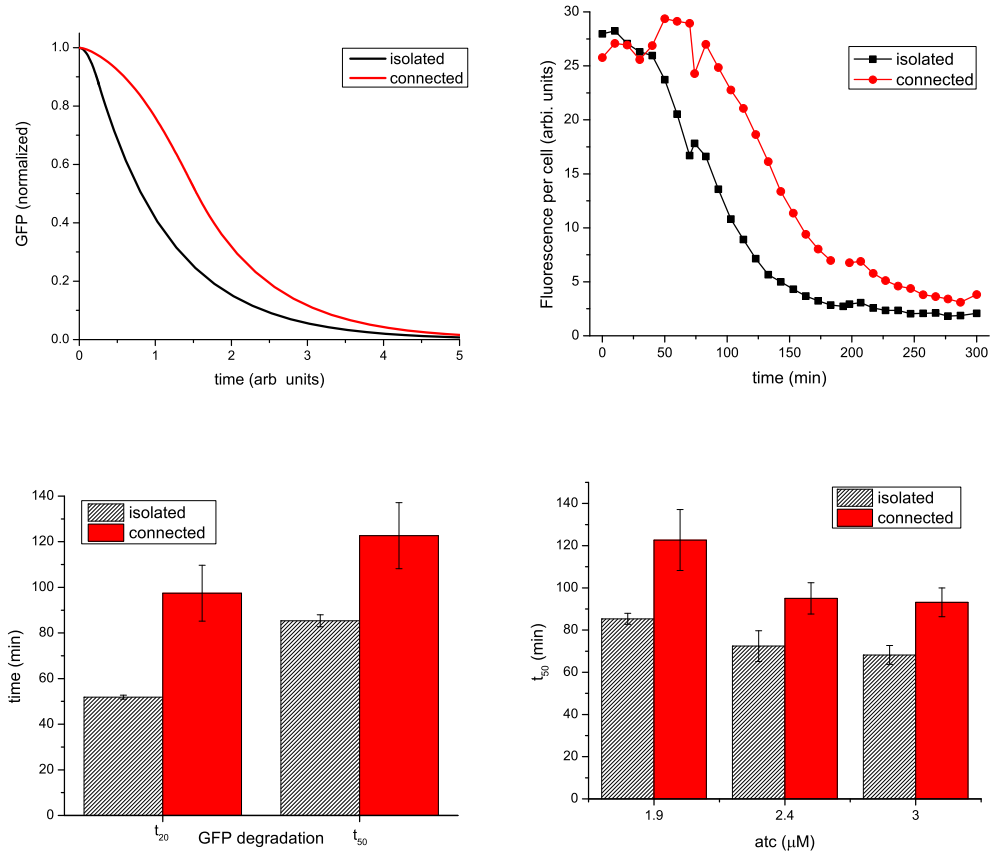

Figure 4.2: **Retroactivity delays the response to sudden input stimulation.** (a) Simulations from the model in equations (4.4). The units in this simulation are nondimensionalized. Parameters used in this simulation are given in the Appendix. (b) Experimental results show good agreement with the model. Retroactivity increases the response time to induction: upon the addition of 1.9μM atc, the average half-life of GFP (t_{50}) post-induction goes from 85±2min to 122±14min (43% change). (c) Response times are to 1.9 μM of atc. The slow response mainly occurs in the early stages of induction and can be quantified by calculating the t_{20}, the time it takes to remove 20% of the GFP. The t_{20} presents an average delay of 40min, slightly higher than the 37min delay in the half-life value (t_{50}). (d) Higher levels of atc can decrease the t_{50}, but the delay caused by retroactivity persists (see the Appendix for more data).

The minimal and maximal increases are of 24% and of 64%, respectively. Figure 4.2(d) shows that increasing the amount of atc, the response times for both isolated and connected systems decrease. However, the delay caused by retroactivity persists. This implies that the dynamic effect of retroactivity cannot be removed nor attenuated by choosing higher input values, that is, it cannot be pre-compensated. The desired speed of response of LacI (the one of the isolated system) cannot be

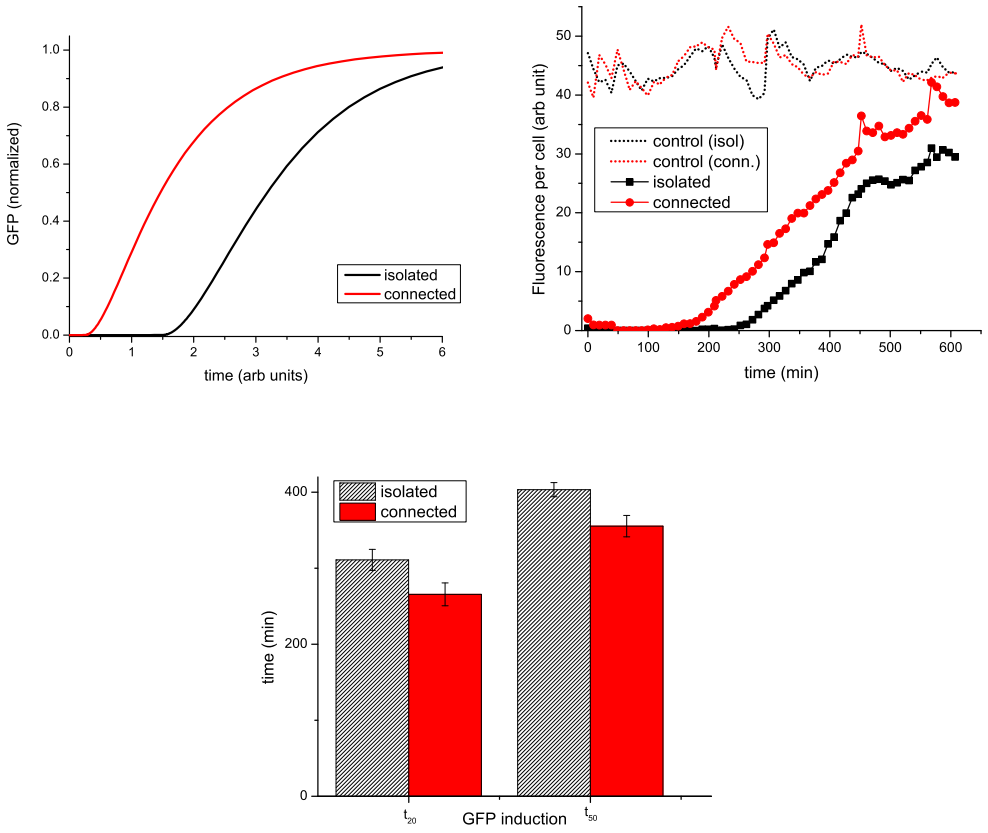

Figure 4.3: **Retroactivity speeds up the response to sudden removal of input stimulation.** (a) Simulation of the model in equation (4.4) illustrates the effect of retroactivity on the response to removal of atc. The atc input is removed at time zero. (b) Experimental results validate the model prediction. The connected system shows an anticipation, with respect to the isolated system, of about 50min in the response to removal of inducer from cultures pre-induced with 3μM atc for 400min. Specifically, the t_{50} went down from 403±9min in the isolated system to 355±15min in the connected system. The dotted lines show the maximal unrepressed steady state values of GFP for connected and isolated systems. (c) The increase in the speed of response occurs mainly in the early stages, indicating a time delay between the connected and isolated systems.

achieved by selecting different input values in the connected system. In order to keep the speed of response of the output in the connected system close to the one of the isolated system, feedback control is required. Through feedback control, one can design circuits that are effectively insulated from retroactivity and behave the same whether connected or isolated [13].

4.3.3 Dynamic effects of retroactivity: De-induction.

To measure the response to wash, cells were induced with 3uM atc. After 4 generations (400 minutes), the inducer was removed by pelleting and resuspension of the cells in fresh media. Figure 4.3 shows the response of GFP to sudden removal of atc for both the isolated and connected systems.

Surprisingly, the connected system responds faster (by about 50min) than the isolated system when atc is suddenly removed. This apparently counter-intuitive result can be explained as follows. In the isolated system, the only mechanism by which free LacI can be removed is through dilution and/or degradation. In the connected system there is an additional mechanism by which free LacI can be removed. Since the complex C_2 of LacI bound to operator sites also dilutes but the operator sites themselves do not dilute or degrade, free LacI can be removed by binding to the operator sites. The continuous dilution of LacI in complexes C_2 guarantees the presence of free operator sites during the de-induction, which can in turn binds to more free LacI. If the operator sites were protecting LacI from degradation and the system had no dilution (no growth), we should have observed a slower response in the connected system just like in the induction experiment.

Hence, because of retroactivity a sign-sensitive delay arises: when the input stimulation is suddenly applied, the connected system presents a delay of about 40%. By contrast, when the input stimulation is suddenly removed, the connected system presents an anticipation of the response of about 50min.

4.3.4 Effects of retroactivity on the steady state transfer curve.

To obtain the steady state transfer curve, we performed a series of experiments in which the steady state value of GFP was recorded in response to different constant

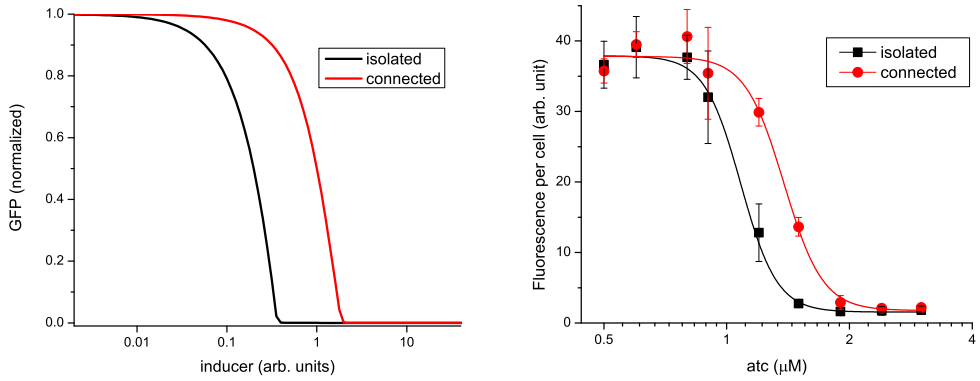

Figure 4.4: **Retroactivity increases the point of half maximal induction u_{50}.** (a) Normalized simulation results obtained from the model in equations (4.4). The parameter values for the simulations are given in the Appendix. (b) Experimental data showing an increase of 30% of the u_{50}. Experimental data was fitted using non-linear regression on a repression-type Hill function model.

values of atc.

In each experiment, cells were kept in the plate reader for one generation at which point different levels of atc were added to the individual wells. Cells reached steady state after approximately one generation. The steady-state level was preserved for at least another generation, at which point the cells moved into a late log phase.

Results are shown in Figure 4.4 (see the following section for the full time traces). The shape of the transfer curve is well characterized by the point of half maximal induction, called u_{50}, and by the apparent Hill coefficient n_H. The u_{50} corresponds to the value of the input stimulation for which the output response is 50% of the maximal. As seen in Figure 4.4, the experimental data showed an increase of about 30% in the u_{50}, going from 1.08±0.02μM in the isolated system to 1.38±0.03μM in the connected system. There was no significant change in the apparent Hill coefficient n_H (9.7±1.3 for the isolated system and 9.1 ± 1.5 for the connected system). When the input stimulation atc increases, LacI is produced but it is immediately sequestered by the high affinity operator sites, so that more atc must be applied in order to have

enough LacI that is available for the reporter system.

Note that for values of atc exceeding 1.9 μM, the steady state value of the circuit is not appreciably changed by retroactivity while the temporal dynamics is substantially impacted by retroactivity. This illustrates a concrete case in which understanding the extent of modularity requires studying the temporal dynamics.

The increase of the u_{50} can lead to fairly unpredictable results when the module is connected. In fact, based on the response of the module characterized in isolation as seen from the black plot of Figure 4.4(b), one expects that the maximal change of the output y is obtained by changing the input u about 1.08μM. Hence, one would design the system upstream of the transcription module so that it outputs u in a range about 1.08μM to lead to the maximal change in y. This process is sometimes referred to as input/output matching. Unfortunately, once y connects to downstream clients, a change in the input u about 1.08μM leads to almost no response in y because the true transfer curve is the red one of Figure 4.4(b). This problem can be overcome by accounting for the increase of u_{50} due to retroactivity when one performs input/output matching. This is in net contrast with the dynamic effects of retroactivity, which cannot be removed or attenuated by adjusting the input stimulation in the connected system.

4.4 Supporting data

4.4.1 Strains and Plasmids

In all experiments, the strain employed was the strain KL-323 [89], obtained from the Coli Genetic Stock Center at Yale University [90]. This strain was chosen due to its mutation in the *lacI* and *recA* genes. The absence of endogenous LacI is desirable to prevent cross talk with the LacI expressed by our circuit. The mutation in the *recA* gene increases the stability of our circuit by preventing recombination between

homologous regions on the gene and on the plasmids. Full genotype of this strain is given by a K-12 with mutations *F-, secA209(aziR), pro-48, lacZ118(Oc), lacI22, , trpA9605(Am), his-85(Am), gyrA19(NalR), recA1, rpsL171(strR), metE70, trpR55.*

The circuit plasmid, labeled pRET5, was assembled by inserting 3 genes in a pACYC184 plasmid. The genes inserted were the reporter gene P_{lac}*:gfp-lva*, the output gene P_{tet}*:lacI-lva* and P_{const}*:tetR-lva* were built from parts obtained from either the Registry of Biological Parts or amplified from the *E. coli* K-12 genome. Parts were then sequentially inserted into the backbone in a manner that preserved the chloramphenicol resistance but disrupted the tetracycline resistance gene. Sequential inclusion of genes allowed phenotypical screening of the construct. Expression of *tetR-lva* is controlled by promoter J23114 (constitutive) and ribossome binding site (RBS) B0034 [75]. Expression of *lacI-lva* is controlled by promoter R0040 (P_{tet}) and RBS B0033. Expression of *gfp-lva* is controlled by promoter sequence that regulates expression of LacZ in wild type cells.

The plasmid employed to emulate loads, labeld pUCblk, is a plasmid derived from a pUC18 plasmid in which the entire *lacZ*α gene was removed and a by a LacI symmetric operator site (O^{sym}) [81] was inserted. The control plasmid is a pUC18 plasmid in which the *lacZ*α gene was simply removed. In both plasmids, the *bla* gene which confers resistance to ampicilin was preserved. Both plasmids were obtained as a courtesy from Prof. Alexander J. Ninfa Lab at University of Michigan, Ann Arbor.

4.4.2 Dataset from retroactivity experiments

In order to show the reproducibility of the results obtained in our dynamic experiments, we illustrate in Figures 4.6 and 4.7 the variability measured in our data. Figure 4.6(a) shows the variance in t_{50} values among different clones of the isolated and connected systems. In order to obtain this data, four distinct colonies of each

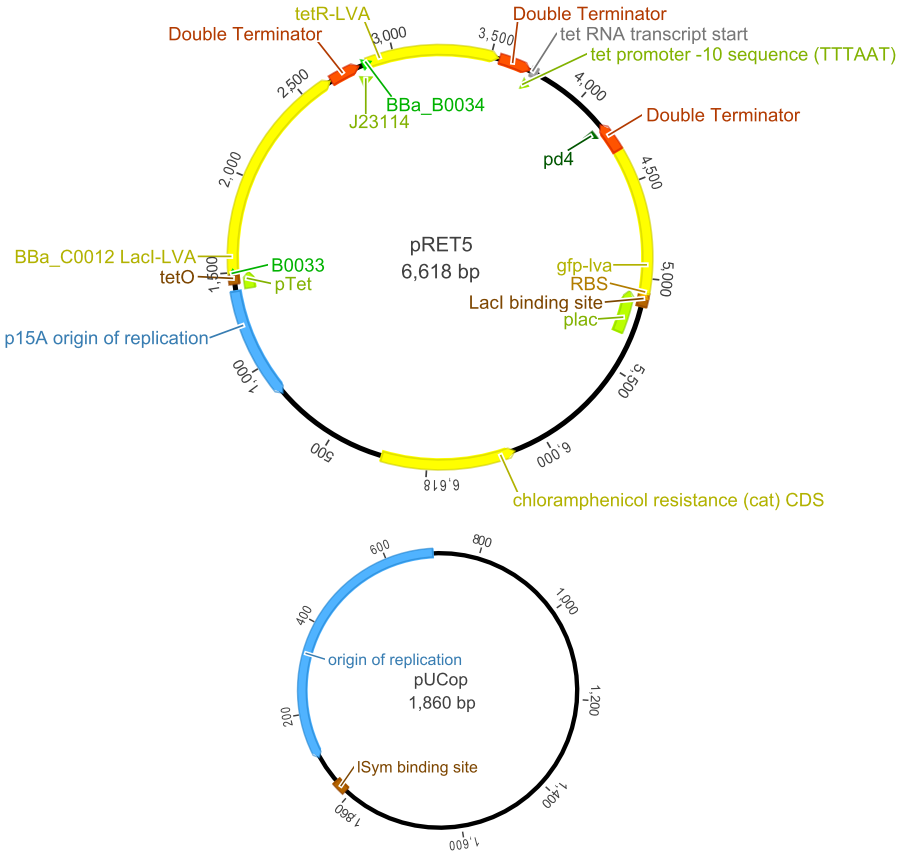

Figure 4.5: **Diagram of the plasmids containing the circuit (pRET5) and load (pUCop).** Details of assembly are given in the text. Full DNA sequence is given in the Appendix.

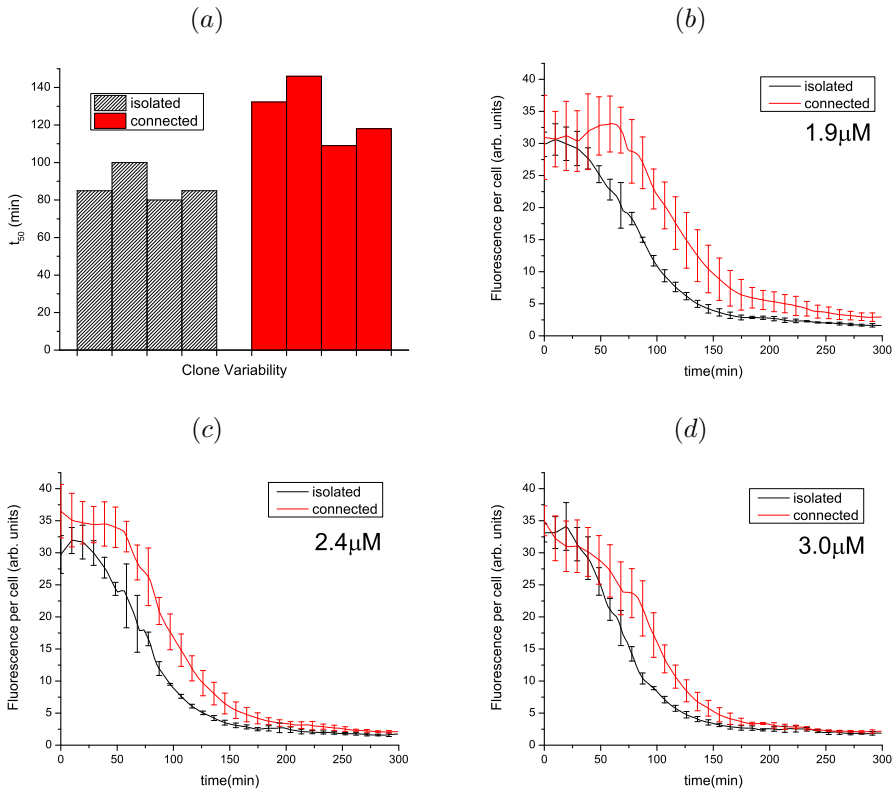

Figure 4.6: **Variability of the results for the induction experiments.** (a) This plot shows the t_{50} for four clones of isolated and connected systems when induced with $2.0\mu M$ atc. (b-d) Each plot shows point wise average of data coming from three different induction experiments with different concentrations of atc. The error bars represents one standard deviation around the average.

system (isolated and connected) were picked and then induced with 2.0μM atc. Figures 4.6(b-d) illustrate the significance of the delay in response to induction due to the presence of clients. In each plot, we show a point wise average along with error bars representing one standard deviation around the average. Figure 4.7 illustrates the significance of the anticipation of the response in wash experiments. In this plot we show a point wise average along with error bars representing one standard deviation around the average.

Figure 4.8 shows samples of time courses of experiments used to obtain the steady state data. Note that the amount of atc required to obtain full induction of LacI (and full removal of GFP) is higher in the connected system. In order to obtain the

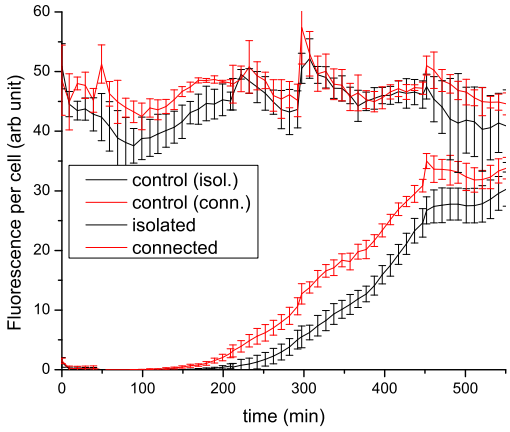

Figure 4.7: **Variability of the results for the wash experiments.** This plot shows point wise average of data coming from six different de-induction (wash) experiments. The error bars represent one standard deviation around the average.

statistics shown in the manuscript, this experiment was repeated three times.

4.4.3 Plasmid Copy Number Quantification

In order to obtain an estimation of the copy number of the circuit plasmids and of the client and blank plasmids, we performed (1) a cell counting assay and (2) a densitometry analysis with plasmid DNA extracted from samples. In both experiments, samples were in the same conditions as the experimental ones.

To obtain the cell density in the samples, samples were serially diluted and plated and the plates with isolated colonies were counted. Cell density was obtained by employing linear regression over the data obtained from this procedure. The resulting cell density obtained was of $3.59 \pm 0.08 \times 10^7$cells/ml in a culture presenting OD 0.1 at 600nm through a 1cm path length.

Since, as shown in [91], miniprep kits methods of DNA extraction are capable of providing consistent yields over a wide range of vector length and total mass, plasmid DNA was extracted employing a commercial kit (Qiagen Miniprep Kit). Samples were concentrated by 40-fold into $250\mu l$ suspensions prior to lysis. This procedure

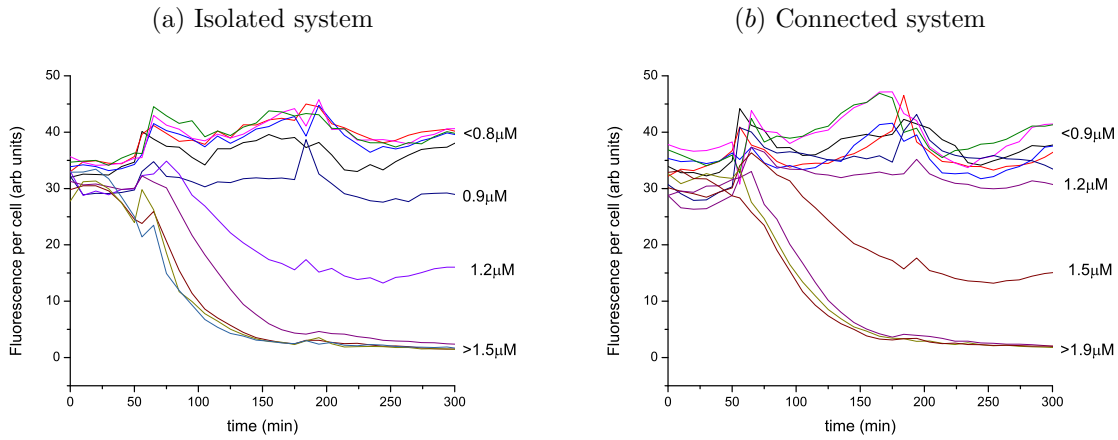

Figure 4.8: **Sample of time courses used to obtain data for steady state experiments.** These plots illustrate the evolution of the induction response for different levels of atc in the isolated and connected systems. Cells were monitored until a steady state value was reached. This experiment was reproduced three times in order to obtain the steady state data results shown in the manuscript.

provided us with few hundred nanograms of mixture of the pACYC184-based circuit and the pUC18-based client plasmids in circular form. Since both plasmids contain a single *EcoRI* restriction site, the entire DNA was linearized by digestion with *EcoRI-HF* (NEB) to prevent over/underestimation due to DNA trapping [92]. The two DNA plasmids were then separated through electrophoresis in 1.2% agarose gel, along with DNA standards of sizes comparable to the length of the linearized vectors. The mass of DNA sample was then estimated through interpolation. Figure 4.9 shows data related to the densitometric analysis and the linear regression curve for interpolation.

The mass obtained was then divided by the molecular weight of the DNA to obtain the copy number of DNA. Additionally, the copy number was divided by the number of cells from which the sample was extracted in order to obtain the number of plasmids per cell. The results are given in Table 4.4.

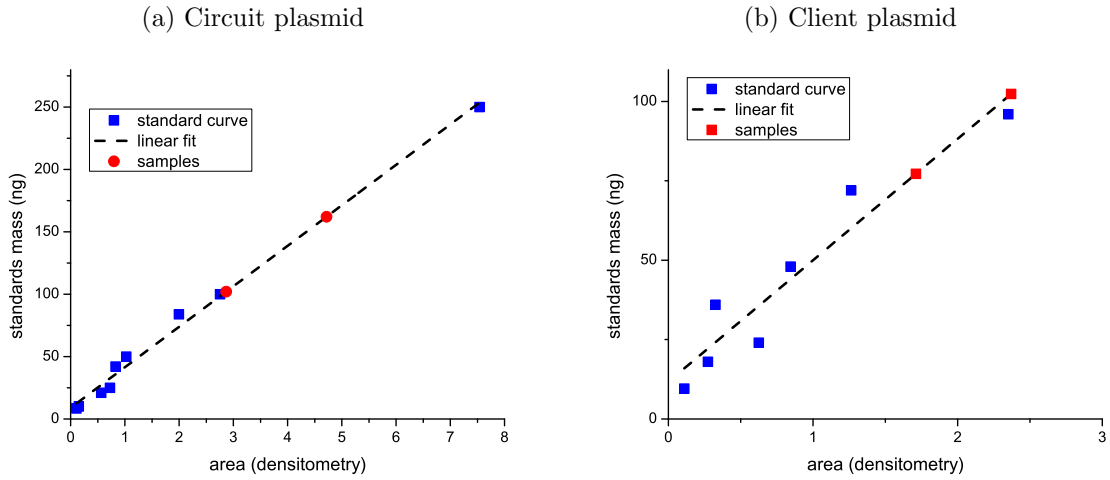

Figure 4.9: **Densitometric fitting used to estimate DNA mass from samples.** Blue points show the standards, the dashed line gives the results of linear regression. (a) Mass estimation of circuit plasmid. The red points are samples of circuit plasmid obtained from isolated and connected systems, with the isolated system having higher mass. Since the vector length of the plasmid circuit is 6.6kb, standards employed in the linear regression had length ranging around 6-8kb. (b) Mass estimation of client plasmid. The red points are samples of blank plasmid from the isolated system and client plasmid from the connected system, with the blank having higher mass. Since the vector length of these plasmids is 1.7kb, the standards employed in the linear regression had length ranging around 1-3kb.

Table 4.4: **Results from plasmid quantitation.** Second and third columns relate to amounts found in 250μl of 40x concentrated sample. The ratio given is between the client plasmid and circuit plasmid amounts, represented in the models by λ.

System	DNA (ng)	Plasmids (moles)	OD 600 (1cm)	Copy number (plasmids/cell)
Isolated	**ratio: 2.4**			
circuit	162	2.7×10^{-14}	0.216	28.8
client (blank)	102	9.1×10^{-14}	0.216	70.58
Connected	**ratio: 2.9**			
circuit	102	2.3×10^{-14}	0.188	20.8
client	77	6.8×10^{-14}	0.188	61.2

CHAPTER V

Conclusion

5.1 Summary of Results

In this dissertation we have introduced analytical tools to evaluate the effect of retroactivity on biomolecular systems that employ a transcription factor as an output.

The results show that the impact of retroactivity to downstream load can alter both the steady state behavior and the dynamic response. The impact depends on whether or not the transcription factor is stabilized when bound to the DNA. When the bound transcription factor is protected from decay, retroactivity slows its dynamics and does not impact the steady state behavior. In contrast, if the decay rate of bound protein is the same as of the unbound protein, retroactivity changes the steady state response, and presents a sign-sensitive dynamic response: it responds faster to de-induction and slower to induction experiments. We also discuss these effects can be included in the design of a biomolecular oscillator.

We also provide a framework to design insulation devices based on a separation of timescales. Through a nested application of Tikhonov's theorem, we provide structural and stability requirements that enable fast biomolecular systems to act as an insulation devices. A short analysis of the impact of large timescale separations

on the stochastic behavior is also provided. This analysis shows that while the use of large gains does not change the signal-to-noise ratio, it may change the frequency content of the noise.

We finally provide experimental validation of some of the analytical predictions present in this paper. Changes in the steady state response and in the dynamic behavior observed were consistent with the model provided for the case in which transcription factors bound to DNA decays at the same rate as the unbound ones. This can be explained by the fact that in growing *E. coli* cells, dilution is an important factor in the decay rate.

5.2 Discussion

The core mechanism for the retroactivity effects studied here is the sequestration of output signals by downstream loads. As such, the results found in this work should be contrasted with other studies related to sequestration effects. Results given in these studies focus on changes in the steady state with special attention given to the effect of "inhibition ultrasensitivity" [28, 29]. As a result, these studies employ large numbers of sequestering elements is large with a very strong affinity to the signalling molecules. Given our application, we focus on how sequestration presents itself in synthetic biology circuits. Therefore the number of sequestration elements is not taken to be large. As a result changes on the steady state behavior were, while significant, modest. No change significant change in sensitivity and a 30% change in the apparent dissociation constant was observed. Changes on the dynamic behavior on the other hand were significant, even with amounts of load consistent with regular synthetic biology usage.

This change in the dynamic behavior is important because it can disrupt the

timing of biomolecular circuits and cause system malfunction. We exemplify this by showing how the presence of load can alter periodic behavior of an activator repressor clock. It has been shown before that DNA binding sites can tune the behavior of a clock by changing its steady state behavior [45]. Here we present a method in which the changes are made exclusively by tuning the timescale separation employing DNA sites. This study also illustrates how to model retroactivity from transcription factors in complex systems by employing singular perturbation to reduce the additional dynamics from this effect. A method to measure the effect retroactivity to any output in complex gene networks inspired in Norton/Thevenin's theorem is given in [19].

Insulation devices for biomolecular systems were first suggested in [13]. The paradigm used, employing large amplification and feedback, was inspired in buffers for electrical circuits based on operational amplifiers. We generalize these results by studying conditions under which the separation of timescales is sufficient for insulation. The stability requirements in this study were based on Tikhonov's theorem. An approach to an analysis of insulation devices based on non-linear contraction theory can be found in [18]. While no insulation device *in vivo* several results showing insulation *in vitro* has been presented [26, 24, 25].

5.3 Future Work

The analysis of stochastic behavior of the circuits presented here can be expanded. Understanding how retroactivity affects the frequency content of the noise and studying the noise propagation through realization of insulation devices are important next steps. An experiment suggested by our results is tuning activator repressor clocks employing DNA binding sites. Due to the effect of the growth rate in how retroac-

tivity impacts the dynamics, we believe the appropriate system to test this approach are clocks in slow growing cells such as [39].

Another extension is to chart the effects of retroactivity on transcription factors used in synthetic biology. Transcription factors different from LacI may present different affinities and different decay properties. The resulting catalog would provide an additional parameter to choose the adequate transcription factors as output signals, in a manner similar to how fan-out specifications are employed in the design of digital circuits.

APPENDIX

APPENDIX A

Mathematical derivations

A.1 Linearization of systems with a retroactivity term

Consider the dynamic system in the following form

$$\dot{x} = S(x)[k + f(x)]. \tag{A.1}$$

Consider the input to be a sum of a bias with a perturbation: $k(t) = \bar{k} + \tilde{k}(t)$. Consider also $\bar{x}$ the steady state obtained when the input is $k(t) = k$ (which is assumed to exist), i.e., $\bar{k} + f(\bar{x}) = 0$. Let $y := x - \bar{x}$ be the output perturbation of the system, the linearization goal is to find how it responds to input $\tilde{k}$. Let $Q(x) = \dfrac{df(x)}{dx}$ and consider the exact and the truncated Taylor expansion around $\bar{x}$:

$$f(x) = f(\bar{x}) + f'(y) \text{ and } f'(y) = Q(\bar{x})y + \sum_{i=2}^{\infty} \frac{1}{i!} \frac{d^i f(x)}{dx^i}\bigg|_{x=\bar{x}} y^i \tag{A.2}$$

Rewrite the ODE as follows:

$$\begin{aligned} \dot{y} = \dot{x} &= S(x)[k(t) + f(x)] = S(\bar{x} + y)[\bar{k} + \tilde{k}(t) + f(\bar{x}) + f'(y)] \\ \dot{y} &= S(\bar{x} + y)[\tilde{k}(t) + f'(y)] = S(\bar{x} + y)\tilde{k}(t) + S(\bar{x} + y)f'(y) \end{aligned} \tag{A.3}$$

The linearization of this system around $\bar{x}$ then becomes

$$\begin{aligned} \dot{y} &= S(\bar{x})\tilde{k}(t) + \left(\frac{dS(\bar{x} + y)}{dy}\bigg|_{y=0} f'(0) + S(\bar{x}) \frac{df'(y)}{dy}\bigg|_{y=0} \right) y \\ \dot{y} &= S(\bar{x})\tilde{k}(t) + S(\bar{x})Q(\bar{x})y \end{aligned} \tag{A.4}$$

The dynamic for the output as a function of an input with bias $\bar{k}$ and perturbation $\tilde{k}$ will be then $x(t) = y(t) + \bar{x}$. The transfer function $G(s)$ of this system from $\tilde{k}$ to y is therefore

$$G(s) = \frac{S(\bar{x})}{s - S(\bar{x})Q(\bar{x})}, \tag{A.5}$$

which gives us a "DC gain" $G(0) = -Q(\bar{x})^{-1}$ and a pole at $p = S(\bar{x})Q(\bar{x})$.

A.2 Model of Hill functions

In this section we identify the Hill function approximations for the expression of proteins controlled by *(i)* an activator protein and *(ii)* a repressor and an activator protein. Consider first the expression of protein X whose expression rate is regulated by an activator protein A via the promoter p_R. These processes can be modelled by the following chemical reactions

$$\begin{aligned} p_R + mA &\underset{k_{b1}}{\overset{k_{a1}}{\rightleftharpoons}} C_1 \\ C_1 &\xrightarrow{\kappa_2} C_1 + X \\ p_R &\xrightarrow{\kappa_4} p_R + X, \end{aligned} \tag{A.6}$$

in which κ_2 is the expression level of the promoter bound to A, κ_4 is the basal expression level of the promoter, k_{a1} and k_{b1} are the association and dissociation rates of the promoter to A respectively and m models the cooperative binding of the activator protein. Assuming that there is a conservation of the total amount of promoter sites, modelled by the expression $p_R + C_1 = p_{R,T}$, the expression level from this promoter can be modelled by $g_2(A) = \kappa_2 C_1(A) + \kappa_4(p_{R,T} - C_1(A))$. The quasi-steady state value of C_1 can be obtained by identifying the equilibrium of the following ODE

$$\dot{C}_1 = k_{a1}(p_{R,T} - C_1)A^m - k_{b1}C_1. \tag{A.7}$$

Defining $K_{m1} = \sqrt[m]{k_{b1}/k_{a1}}$, we obtain

$$g_2(A) = \kappa_2 p_{R,T} \frac{A^m}{A^m + K_{m1}^m} + \kappa_4 p_{R,T} \frac{K_{m1}^m}{A^m + K_{m1}^m} = \frac{K_2 A^m + K_4 K_{m1}^m}{A^m + K_{m1}^m}, \tag{A.8}$$

in which $K_2 := \kappa_2 p_{R,T}$ and $K_4 := \kappa_4 p_{R,T}$.

Consider now the expression of a protein X whose expression rate is regulated by an activator protein A as well as by repressor protein R via the promoter p_A. We will assume that the binding is competitive. Expression can be modelled by the following chemical reactions

$$\begin{aligned} p_A + mA &\underset{k_{b1}}{\overset{k_{a1}}{\rightleftharpoons}} C_1 \\ p_A + nR &\underset{k_{b2}}{\overset{k_{a2}}{\rightleftharpoons}} C_2 \\ C_1 &\xrightarrow{\kappa_1} C_1 + X \\ p_A &\xrightarrow{\kappa_3} p_A + X, \end{aligned} \tag{A.9}$$

in which κ_1 is the expression level of the promoter bound to A, κ_3 is the basal expression level of the promoter, k_{a1} and k_{b1} are the association and dissociation rates of the promoter to A, respectively, k_{a2} and k_{b2} are the association and dissociation rates of the promoter to R, respectively, and m and n model the cooperative binding of the activator and repressor proteins, respectively. We assume that the repressor activity is perfect and therefore no expression can occur from the repressed promoter. Assuming that there is a conservation of the total amount of promoter sites, modelled by the expression $p_A + C_1 + C_2 = p_{A,T}$, the expression level from this promoter can be modelled by $g_1(A, R) = \kappa_1 C_1(A) + \kappa_3(p_{A,T} - C_1(A) - C_2(R))$. The quasi-steady state value of C_1 and C_2 can be obtained by identifying the equilibrium of the following ODE

$$\begin{aligned} \dot{C}_1 &= k_{a1}(p_{A,T} - C_1 - C_2)A^m - k_{b1}C_1 \\ \dot{C}_2 &= k_{a2}(p_{A,T} - C_1 - C_2)R^n - k_{b2}C_2 \end{aligned} \tag{A.10}$$

Defining $K_{m1} = (k_{b1}/k_{a1})^{1/m}$ and $K_{m2} = (k_{b2}/k_{a2})^{1/n}$, we obtain the expression

$$g_1(A,R) = p_{A,T}\frac{\kappa_1 K_{m2}^n A^m + \kappa_3 K_{m1}^m K_{m2}^n}{K_{m1}^m K_{m2}^n + K_{m2}^n A^m + K_{m1}^m R^n} \tag{A.11}$$

$$= \frac{K_1 K_{m2}^n A^m + K_3 K_{m1}^m K_{m2}^n}{K_{m1}^m K_{m2}^n + K_{m2}^n A^m + K_{m1}^m R^n}, \tag{A.12}$$

in which $K_1 := \kappa_1 p_{A,T}$ and $K_3 := \kappa_3 p_{A,T}$.

A.3 Nondimensionalization of the activator repressor clock

In this section, we identify a nondimensional model of the activator repressor clock having loads to activator and repressor, given in Figure 2.4d. The association and dissociation between transcription factor A and R and their respective additional binding sites q_A and q_R are model by the following dynamics

$$q_A + mA \underset{k'_{b1}}{\overset{k'_{a1}}{\rightleftharpoons}} D_1 \tag{A.13}$$

$$q_R + nR \underset{k'_{b2}}{\overset{k'_{a2}}{\rightleftharpoons}} D_2. \tag{A.14}$$

The model for this system can be obtained by adding the binding dynamics to the model given in [36] for the activator-repressor clock as

$$\begin{aligned}
\dot{A} &= -\delta_A A + g_1(A,R) + mk'_{b1}D_1 - mk'_{a1}A^m(q_{A,T} - D_1) \\
\dot{R} &= -\delta_R R + g_2(A) + nk'_{b2}D_2 - nk'_{a2}R^n(q_R - D_2) \\
\dot{D}_1 &= -k'_{b1}D_1 + k'_{a1}A^m(q_{A,T} - D_1) \\
\dot{D}_2 &= -k'_{b2}D_2 + k'_{a2}R^n(q_{R,T} - D_2),
\end{aligned} \tag{A.15}$$

in which $q_{A,T} := q_A + D_1$ and $q_{R,T} := q_R + D_2$ model the total amount of DNA bindings sites in the system, δ_A and δ_R model protein decay (due to either dilution or degradation) and functions f_1 and f_2 model expression rates and take the form of the standard Hill functions derived on Section A.2.

$$g_1(A,R) = \frac{K_1(A/K_{m1})^m + K_3}{1 + (A/K_{m1})^m + (R/K_{m2})^n} \text{ and } g_2(A) = \frac{K_2(A/K_{m1})^m + K_4}{1 + (A/K_{m1})^m}, \tag{A.16}$$

in which K_1 and K_2 are the maximal expression rates, K_3 and K_4 represent the basal expression, K_{m1} and K_{m2} is related to the affinity between the proteins and their respective binding sites and m and n are the Hill coefficients related to the multimerization of activator and repressor proteins, respectively. Define $G_1 := k'_{b1}/\delta_A$ and $G_2 := k'_{b2}/\delta_R$ to be non-dimensional constants modelling the timescale difference between complex dissociation and transcription factor degradations rates. Define additionally $K'_{m1} := \sqrt[m]{k'_{b1}/k'_{a1}}$ and $K'_{m2} = \sqrt[n]{k'_{b2}/k'_{a2}}$ as the apparent dissociation constant as defined in [51].

From this system, define the nondimensional variables $a := A/K_{m1}$, $r := R/K_{m2}$, $d = D_1/K'_{m1}$ and $d_2 = D_2/K'_{m2}$. Let $\sigma_1 = K'_{m1}/K_{m1}$ and let $\sigma_2 = K'_{m2}/K_{m2}$ describe the difference in affinity of the transcription factor to the promoter in the circuit or the additional DNA load. The differential equation is then reduced to

$$\begin{aligned}
\dot{a} &= -\delta_A a + \frac{\beta_1 a^m + \beta_2}{1 + a^m + r^n} + mG_1\delta_A\sigma_1 d_1 - mG_1\delta_A\sigma_1^{(1-m)} a^m(\bar{q}_A - d_1) \\
\dot{r} &= -\delta_R r + \frac{\beta_3 a^m + \beta_4}{1 + a^m} + nG_2\delta_R\sigma_2 d_2 - nG_2\delta_R\sigma_2^{(1-n)} r^n(\bar{q}_R - d_2) \\
\dot{d_1} &= -G_1\delta_A d_1 + G_1\delta_A\sigma_1^{-m} a^m(\bar{q}_A - d_1) \\
\dot{d_2} &= -G_2\delta_R d_2 + G_2\delta_R\sigma_2^{-n} r^n(\bar{q}_R - d_2),
\end{aligned} \tag{A.17}$$

in which $\beta_1 := K_1/K_{m1}$, $\beta_2 := K_A/K_{m1}$, $\beta_3 := K_2/K_{m2}$, $\beta_4 := K_R/K_{m2}$, $\bar{q}_A = q_{A,T}/K'_{m1}$ and $\bar{q}_R = q_{R,T}/K'_{m2}$.

From system (A.17), one can obtain non-dimensional models for the various systems described in Section 2.3. In particular, to obtain (2.23), $\bar{q}_R = \bar{q}_A = 0$; in (2.27) $\bar{q}_R = 0$ and $\sigma_1 = 1$; in (2.36) $\bar{q}_A = 0$ and $\sigma_2 = 1$ and finally in (2.42) $\sigma_1 = \sigma_2 = 1$.

A.4 Conditions for a unique and unstable equilibrium of an activator repressor clock

We next establish parameter conditions for which we can guarantee that there is a unique equilibrium of system (2.23).

Let $\bar{\beta}_1 = \beta_1/\delta_A$, $\bar{\beta}_2 = \beta_2/\delta_A$, $\bar{\beta}_3 = \beta_3/\delta_R$, $\bar{\beta}_4 = \beta_4/\delta_R$ and let

$$f(a,r) := -\delta_A a + f_1(a,r) \text{ and } g(a,r) := -\delta_R r + f_2(a). \tag{A.18}$$

Then, the nullclines are given by $f(a,r) = 0$ and $g(a,r) = 0$, which define r as a function of a in the following way:

$$f(a,r) = 0 \implies r = \left(\frac{\bar{\beta}_1 a^m + \bar{\beta}_2 - a(1+a^m)}{a}\right)^{1/n} \tag{A.19}$$

$$g(a,r) = 0 \implies r = \frac{\bar{\beta}_3 a^m + \bar{\beta}_4}{1+a^m}. \tag{A.20}$$

Proposition 7. *If $m = 1$, system (2.23) admits a unique stable equilibrium point. If $m = 2$, system (2.23) admits a unique unstable (not locally a saddle) equilibrium point if the following parameter relations are verified*

$$0 < \bar{\beta}_2 \leq \frac{\bar{\beta}_1^3}{27},\ L \leq \frac{\bar{\beta}_3 A_L^2 + \bar{\beta}_4}{1+A_L^2},\ l \geq \frac{\bar{\beta}_3 A_l^2 + \bar{\beta}_4}{1+A_l^2}, \tag{A.21}$$

and

$$\left.\frac{\delta_R}{\partial f_1/\partial a}\right|_{(a^*,r^*)} - \delta_A < 1, \tag{A.22}$$

in which

$$A_l = \frac{\bar{\beta}_1}{6}\left(1 - (cos(\phi/3) - \sqrt{3}sin(\phi/3))\right) \tag{A.23}$$

$$A_L = \frac{\bar{\beta}_1}{6} + \frac{\bar{\beta}_1}{3}cos(\phi/3) \tag{A.24}$$

$$\phi = atan\left(\frac{\sqrt{27\bar{\beta}_2(\bar{\beta}_1^3 - 27\bar{\beta}_2)}}{\frac{\bar{\beta}_1^3}{2} - 27\bar{\beta}_2}\right), \tag{A.25}$$

$$l = \sqrt[n]{\frac{\bar{\beta}_1 A_l^2 + \bar{\beta}_2 - A_l(1+A_l^2)}{A_l}},$$
$$L = \sqrt[n]{\frac{\bar{\beta}_1 A_L^2 + \bar{\beta}_2 - A_L(1+A_L^2)}{A_L}}.$$

Proof. The Jacobian at $S^* := (a^*, r^*)$ is given by the matrix

$$J(S^*) = \begin{pmatrix} \frac{\partial f}{\partial a} & \frac{\partial f}{\partial r} \\ \frac{\partial g}{\partial a} & \frac{\partial g}{\partial r}, \end{pmatrix},$$

in which the partial derivatives are computed at the equilibrium point S^*. For an unstable node or spiral to occur, it is sufficient that

$$(i)\ \mathrm{tr}(J(S^*)) > 0 \text{ and } (ii)\ \det(J(S^*)) > 0.$$

Case 1: $m = 1$. The nullcline $f(a, r) = 0$ has always negative slope, and therefore we always have only one equilibrium point. Furthermore, expression (A.19) with $m = 1$ leads to

$$\left.\frac{dr}{da}\right|_{f(a,r)=0} = -\frac{r^{-1+1/n}}{n}\frac{a^2+\bar{\beta}_2}{a^2} < 0.$$

Since $dr/da|_{f(a,r)=0} = -(\partial f/\partial a)/(\partial f/\partial r)$ by the implicit function theorem and since $\partial f/\partial r < 0$, it must be that $\partial f/\partial r < 0$. As a consequence, $\mathrm{tr}(J(S^*)) < 0$ because $\frac{\partial g}{\partial r} = -\delta_R < 0$. To show that both eigenvalues of $J(S^*)$ are negative, we are left to show that $\det(J(S^*)) > 0$. This is readily seen to be true as we have that

$$\left.\frac{dr}{da}\right|_{g(a,r)=0} = -\frac{\partial g/\partial a}{\partial g/\partial r} > \left.\frac{dr}{da}\right|_{f(a,r)=0} = -\frac{\partial f/\partial a}{\partial f/\partial r} < 0,$$

thus implying that $\frac{\partial f}{\partial a}\frac{\partial g}{\partial r} - \frac{\partial f}{\partial r}\frac{\partial g}{\partial a} = \det(J(S^*)) > 0$.

Case 2: $m = 2$. There is only possible configuration of the nullclines in which (a) we have a unique equilibrium and (b) the nullclines are intersecting with the same positive slope. The plots imply that

$$\frac{dr}{da}\Big|_{g(a,r)=0} = -\frac{\partial g/\partial a}{\partial g/\partial r} > \frac{dr}{da}\Big|_{f(a,r)=0} = -\frac{\partial f/\partial a}{\partial f/\partial r} > 0,$$

and thus that $\frac{\partial f}{\partial a}\frac{\partial g}{\partial r} - \frac{\partial f}{\partial r}\frac{\partial g}{\partial a} = \det(J(S^*)) > 0$. By relations (A.18), we have that $\partial g/\partial a = \partial f_2/\partial a$, $\partial g/\partial r = -\delta_R$, $\partial f/\partial a = (-\delta_A + \partial f_1/\partial a)$, and $\partial f/\partial r = -|\partial f_1/\partial r|$. If at the equilibrium point S^* the nullcline $f(a,r) = 0$ has negative slope, S^* is stable, as we have shown for the case $m = 1$. Therefore, we examine what additional conditions should be enforced to guarantee that the equilibrium point is unstable when the nullclines intersect both with positive slopes. Since condition (ii) is verified by the condition that the nullclines cross with positive slopes, we are left to provide conditions for which (i) is also true. To have that $\mathrm{tr}(J(S^*)) > 0$, we require that $(\frac{\partial f_1}{\partial a} - \delta_A) - \delta_R > 0$, which is verified if condition (A.22) holds.

We finally determine sufficient conditions on the parameters for having one crossing and such that the slopes of the two nullclines at the crossing are both positive (and thus (ii) is verified). This is performed by simple geometric considerations.

The values A_l and A_L of the location of the minimum and maximum of $f(a,r) = 0$ can be computed by computing the derivative with respect to A of expression

$$r^n = \frac{\bar{\beta}_1 a^2 + \bar{\beta}_2 - a(1+a^2)}{a}$$

obtained by (A.19) and equating it to zero, as the square root function is monotone. This way, we find a third order polynomial that has two positive roots if $0 < \bar{\beta}_2 \leq \frac{\bar{\beta}_1^3}{27}$, otherwise it has one positive and two complex roots. These roots are given by relations (A.25). Thus, by looking at the same figure, one deduces that if conditions (A.21) are satisfied, we have on equilibrium point only, and (ii) is verified. □

For having one equilibrium point only, we require the activator basal transcription rate, proportional to $\bar{\beta}_2$, to be sufficiently smaller then the maximal expression rate of the activator, which is proportional to $\bar{\beta}_1$. Also, $\bar{\beta}_2$ must be non-zero. Also, in case $\bar{\beta}_1 >> \bar{\beta}_2$, one can verify that $A_L \approx \bar{\beta}_1/2$ and thus $L \approx \sqrt[n]{\bar{\beta}_1^2/4}$. As a

consequence, conditions (A.21) require also that if $\bar{\beta}_1$ increases then so must do $\bar{\beta}_3$. This qualitatively implies that the maximal expression rate of the repressor must be larger than the maximal expression rate of the activator, when expressed in units of the affinity constant. Finally, $A_l \approx 0$ and $l \approx \sqrt[n]{\bar{\beta}_2/A_l}$. As a consequence, conditions (A.21) also imply that the smaller $\bar{\beta}_2$ becomes, the smaller $\bar{\beta}_3$ must be.

A.5 Proofs on stability of the slow manifolds found in the activator repressor clock

Proposition 8. *The stability of the slow manifold $d_1 = \psi_1(y)$ defined by setting $\epsilon = 0$ in system (2.29-2.31) is locally exponentially stable.*

Proof. The manifold $d_1 = \psi_1(y)$ is the unique solution of the algebraic equation

$$g(y, d_1) := -\delta_A d_1 + \delta_A (y - m d_1)^m (q_T - d_1) = 0.$$

Note that, since $0 \leq d_1 \leq q_T$, $0 \leq \psi_1(y) \leq q_T$.

To prove this proposition, we need to show that $\left.\dfrac{\partial g(y,d_1)}{\partial d_1}\right|_{d_1=\psi_1(y)} < 0$ [47].

$$\frac{\partial g(y,d_1)}{\partial d_1} = -\delta_A - m\delta_A (y - m d_1)^{m-1} (\bar{q}_A - d_1) - \delta_A (y - m d_1)^m.$$

Since $g(y, \psi_1(y)) = 0$, $y - m\psi_1(y) = \sqrt[m]{\dfrac{\psi_1(y)}{\bar{q}_A - \psi_1(y)}}$ and therefore

$$\left.\frac{\partial g(y,d_1)}{\partial d_1}\right|_{d_1=\psi_1(y)} = -\delta_A - m\delta_A \left(\frac{\psi_1(y)}{\bar{q}_A - \psi_1(y)}\right)^{\frac{m-1}{m}} (\bar{q}_A - \psi_1(y)) - \delta_A \frac{\psi_1(y)}{\bar{q}_A - \psi_1(y)} < 0,$$

since $0 \leq \psi_1(y) \leq \bar{q}_A$ for all values of y as shown above. □

Proposition 9. *The stability of the manifold $d_2 = \psi_2(y)$ defined by setting $\epsilon = 0$ in system (2.37) is locally exponentially stable.*

Proof. The proof of this result is similar to the proof of the previous proposition. Here we must show that $\left.\dfrac{\partial h(y,d_2)}{\partial d_2}\right|_{d_2=\psi_2(y)} < 0$ where the manifold $d_2 = \psi_2(y)$ is the

unique solution of equation

$$h(y, d_2) := -\delta_R d_2 + \delta_R (y - n d_2)^n (\bar{q}_R - d_2) = 0.$$

Since $0 \leq d_2 \leq \bar{q}_R$, $0 \leq \psi_2(y) \leq \bar{q}_R$. Additionally, from the definition of the manifold, $y - n\psi_2(y) = \sqrt[n]{\dfrac{\psi_2(y)}{q + R - \psi_2(y)}}$. Therefore

$$\begin{aligned}
\left.\frac{\partial h(y, d_2)}{\partial d_2}\right|_{d_2 = \psi_2(y)} &= -\delta_R - n\delta_R (y - n\psi_2(y))^{n-1} (\bar{q}_R - \psi_2(y)) - \delta_R (y - n\psi_2(y))^n \\
&= -\delta_R - n\delta_R \left(\frac{\psi_2(y)}{\bar{q}_R - \psi_2(y)}\right)^{\frac{n-1}{n}} (\bar{q}_R - \psi_2(y)) - \delta_R \frac{\psi_2(y)}{\bar{q}_R - \psi_2(y)} < 0.
\end{aligned}$$

□

Proposition 10. *The stability of the manifold* $(d_1, d_2) = (\psi_1(y_1), \psi_2(y_2))$ *defined by setting* $\epsilon = 0$ *in system (2.43) is locally exponentially stable.*

Proof. Define $g(y_1, d_1) := -\delta_A d_1 + \delta_A (y_1 - m d_1)^m (\bar{q}_A - d_1) = 0$ and $h(y_2, d_2) := -\delta_R d_2 + \delta_R (y_2 - n d_2)^n (\bar{q}_R - d_2) = 0$. The manifold $(d_1, d_2) = (\psi_1(y_1), \psi_2(y_2))$ is defined such that $g(y_1, \psi_1(y_1)) = 0$ and $h(y_2, \psi_2(y_2)) = 0$. To prove the local exponential stability of the manifold, we need to show that the Jacobian

$$J = \begin{bmatrix} \dfrac{\partial g(y_1, d_1)}{\partial d_1} & \dfrac{\partial g(y_1, d_1)}{\partial d_2} \\ \dfrac{\partial h(y_2, d_2)}{\partial d_1} & \dfrac{\partial h(y_2, d_2)}{\partial d_2} \end{bmatrix} = \begin{bmatrix} \dfrac{\partial g(y_1, d_1)}{\partial d_1} & 0 \\ 0 & \dfrac{\partial h(y_2, d_2)}{\partial d_2} \end{bmatrix}.$$

calculated at the manifold $(d_1, d_2) = (\psi_1(y_1), \psi_2(y_2))$ has negative eigenvalues. Since this is a diagonal matrix, the problem is reduced to proving that the two following inequalities hold:

$$\begin{aligned}
\left.\frac{\partial g(y_1, d_1)}{\partial d_1}\right|_{d_1 = \psi_1(y_1)} &< 0 \\
\left.\frac{\partial h(y_2, d_2)}{\partial d_2}\right|_{d_2 = \psi_2(y_2)} &< 0.
\end{aligned} \tag{A.26}$$

From the definition of the manifold,

$$0 \leq \psi_1(y_1) \leq \bar{q}_A \text{ and } 0 \leq \psi_2(y_2) \leq \bar{q}_R.$$

Additionally,

$$y_1 - \psi_1(y_1) = \sqrt[m]{\frac{\psi_1(y_1)}{\bar{q}_A - \psi_1(y_1)}} \text{ and } y_2 - \psi_2(y_2) = \sqrt[n]{\frac{\psi_2(y_2)}{\bar{q}_R - \psi_2(y_2)}}.$$

Therefore

$$\begin{aligned}
\left.\frac{\partial g(y_1, d_1)}{\partial d_1}\right|_{d_1=\psi_1(y_1)} &= -\delta_A - \delta_A \left(\frac{\psi_1(y_1)}{\bar{q}_A - \psi_1(y_1)}\right)^{\frac{m-1}{m}} (\bar{q}_A - \psi_1(y_1)) \\
&\quad - \delta_A \frac{\psi_1(y_1)}{\bar{q}_A - \psi_1(y_1)} < 0 \\
\left.\frac{\partial h(y_2, d_2)}{\partial d_2}\right|_{d_2=\psi_2(y_2)} &= -\delta_R - \delta_R \left(\frac{\psi_2(y_2)}{\bar{q}_R - \psi_2(y_2)}\right)^{\frac{n-1}{n}} (\bar{q}_R - \psi_2(y_2)) \\
&\quad - \delta_R \frac{\psi_2(y_2)}{\bar{q}_R - \psi_2(y_2)} < 0.
\end{aligned} \tag{A.27}$$

□

A.6 Proofs on orbital equivalence

Proposition 11. *Consider the following ordinary differential equations*

$$\dot{x} = f(x) \tag{A.28}$$

$$\dot{x} = g(x) = \mu(x) f(x), \tag{A.29}$$

in which $x \in \mathbb{R}^n$, $f : \mathbb{R}^n \to \mathbb{R}^n$ is Lipschitz continuous and $0 < a \leq \mu(x) \leq b < \infty$ is a Lipschitz continuous scalar function. Then, there exists a function $\alpha : \mathbb{R} \to \mathbb{R}$, monotonically increasing and bounded such that if $\phi(t)$, $t \in \mathbb{R}^n$ is a solution of (A.28) with initial condition $x = x_0$, then $\psi(t) := \phi(\alpha(t))$, is a solution of (A.29) with the same initial conditions. Furthermore, $\dfrac{d\alpha(t)}{dt} = \mu(\phi(\alpha(t)))$.

Proof. Since $\phi(t)$ is a solution of (A.28), for all $t > 0$, we have that $\dfrac{d\phi(t)}{dt} = f(\phi(t))$. Let $\alpha(t)$ be the solution of the ordinary differential equation

$$\frac{d\alpha}{dt} = \mu(\phi(\alpha)) \tag{A.30}$$

with initial condition $\alpha(0) = 0$. Let also $\psi(t)$ be defined as above. Since $g(x)$ is Lipschitz continuous, system (A.29) has an unique local solution at the point $\psi(t)$ whose tangent is given by $g(\psi(t))$. The vector tangent to $\psi(t)$ is given by

$$\frac{d\psi(t)}{dt} = \frac{d\phi(\alpha(t))}{dt} = \frac{d\phi(\alpha)}{d\alpha}\frac{d\alpha(t)}{dt} = f(\psi(t))\mu(\psi(t)) = g(\psi(t)) \tag{A.31}$$

for all t. Additionally, note that $\alpha(0) = 0$ and therefore $\psi(0) = \phi(0) = x_0$. It follows that $\psi(t)$ is the solution for (A.29) with initial condition $x = x_0$. □

The following proposition is used to show that the addition of load will increase the period.

Proposition 12. *Consider the ordinary differential equations (A.28-A.29) under the same conditions as in Proposition 11. Assume that (A.28) has a periodic solution $\phi(t)$ with period T. If $\mu(x) < 1$, then the solution of (A.29) is a periodic solution with period $T' > T$.*

Proof. From Proposition 11, we have that $\psi(t) := \phi(\alpha(t))$ is a solution for (A.29), in which $\alpha(t)$ satisfies the differential equation

$$\frac{d\alpha(t)}{dt} = \mu(\phi(\alpha(t))). \tag{A.32}$$

Since the solution $\alpha(t)$ is monotonic and unbounded and since $\alpha(0) = 0$, for all $T > 0$, there is $T' > 0$ such that $\alpha(T) = T'$. Since $\phi(T) = \phi(0)$, $\psi(T') = \psi(0)$, and hence ψ is periodic with period T'. From (A.32) and the fact that $\mu(x) < 1$,

$$T' = \alpha(T) = \int_0^T \mu(\phi(\alpha(t)))dt < \int_0^T 1dt = T. \tag{A.33}$$

□

A.7 Mechanistic Model for Stochastic Simulation

For the analysis employing the stochastic simulation algorithm [55], we considered a mechanistic model that includes all the reactions in Table A.1. Table A.2 gives the description the states.

This system is equivalent to the system 2.42 with $m = n = 2$. We consider a one-step model for protein expression and assume the rate of expression is a function of whether the promoter p_A and p_R are free, bound to an activator dimer and bound to a repressor dimer in the case of p_A. Additionally, we consider the dynamics of the dimerization of both transcription factors.

The degradation rate δ_R was the parameter chosen to generate a model for a functioning and a non-functioning clock. The total number of promoters in both simulations was $p_{A,T} = p_{R,T} = 5$. Changes in the number of binding sites q_A and q_R were used to generate retroactivity to the activator and repressor respectively.

A.8 DNA sequences

In this section, the DNA sequence of the plasmids used in this work are given. The circuit plasmid is labeled pRET5. The client plasmid, used to emulate the connected system is labeld pUCop. The control plasmid, used in the experiments with the isolated system is labeled pUCblk.

```
>pRET5
GAATTCCGGATGAGCATTCATCAGGCGGGCAAGAATGTGAATAAAGGCCGGATAAAACTTGTGCTTATTTTTCTTTACGG
TCTTTAAAAAGGCCGTAATATCCAGCTGAACGGTCTGGTTATAGGTACATTGAGCAACTGACTGAAATGCCTCAAAATGT
TCTTTACGATGCCATTGGGATATATCAACGGTGGTATATCCAGTGATTTTTTTCTCCATTTTAGCTTCCTTAGCTCCTGA
AAATCTCGATAACTCAAAAAATACGCCCGGTAGTGATCTTATTTCATTATGGTGAAAGTTGGAACCTCTTACGTGCCGAT
CAACGTCTCATTTTCGCCAAAAGTTGGCCCAGGGCTTCCCGGTATCAACAGGGACACCAGGATTTATTTATTCTGCGAAG
TGATCTTCCGTCACAGGTATTTATTCGGCGCAAAGTGCGTCGGGTGATGCTGCCAACTTACTGATTTAGTGTATGATGGT
GTTTTTGAGGTGCTCCAGTGGCTTCTGTTTCTATCAGCTGTCCCTCCTGTTCAGCTACTGACGGGGTGGTGCGTAACGGC
AAAAGCACCGCCGGACATCAGCGCTAGCGGAGTGTATACTGGCTTACTATGTTGGCACTGATGAGGGTGTCAGTGAAGTG
CTTCATGTGGCAGGAGAAAAAAGGCTGCACCGGTGCGTCAGCAGAATATGTGATACAGGATATATTCCGCTTCCTCGCTC
ACTGACTCGCTACGCTCGGTCGTTCGACTGCGGCGAGCGGAAATGGCTTACGAACGGGGCGGAGATTTCCTGGAAGATGC
CAGGAAGATACTTAACAGGGAAGTGAGAGGGCCGCGGCAAAGCCGTTTTTCCATAGGCTCCGCCCCCCTGACAAGCATCA
CGAAATCTGACGCTCAAATCAGTGGTGGCGAAACCCGACAGGACTATAAAGATACCAGGCGTTTCCCCCTGGCGGCTCCC
TCGTGCGCTCTCCTGTTCCTGCCTTTCGGTTTACCGGTGTCATTCCGCTGTTATGGCCGCGTTTGTCTCATTCCACGCCT
GACACTCAGTTCCGGGTAGGCAGTTCGCTCCAAGCTGGACTGTATGCACGAACCCCCCGTTCAGTCCGACCGCTGCGCCT
TATCCGGTAACTATCGTCTTGAGTCCAACCCGGAAAGACATGCAAAAGCACCACTGGCAGCAGCCACTGGTAATTGATTT
```

Table A.1: Reactions considered in the mechanistic model

Reaction	Description	Rate	Value
$2R \to R_2$	Repressor Dimerization	k_{ra}	200
$R_2 \to 2R$	Repressor Monomerization	k_{rb}	200
$2A \to A_2$	Activator Dimerization	k_{aa}	200
$A_2 \to 2A$	Activator Monomerization	k_{ab}	200
$p_R + A_2 \to C_3$	Activator Binding	k_{a1}	2000
$C_3 \to p_R + A_2$	Activator Dissociation	k_{b1}	2000
$C_3 \to C_3 + R$	Repressor Maximal Expression	κ_3	100
$p_R \to p_R + R$	Repressor Basal Expression	κ_4	.004
$p_A + A_2 \to C_1$	Activator Binding	k_{a1}	2000
$C_1 \to p_A + A_2$	Activator Dissociation	k_{b1}	2000
$p_A + R_2 \to C_2$	Repressor Binding	k_{a2}	2000
$C_2 \to p_A + R_2$	Repressor Dissociation	k_{b2}	2000
$C_1 \to C_1 + A$	Activator Maximal Expression	κ_1	100
$p_A \to p_A + A_2$	Activator Basal Expression	κ_2	.04
$A \to \emptyset$	Activator Monomer Degradation	δ_A	1
$R \to \emptyset$	Repressor Monomer Degradation	δ_R	.2 / .4
$A_2 \to \emptyset$	Activator Dimer Degradation	δ_A	1
$R_2 \to \emptyset$	Repressor Dimer Degradation	δ_R	.2 /.4
$q_A + A_2 \to D_1$	Activator-Load Binding	k_{a1}	2000
$D_1 \to q_A + A_2$	Activator-Load Dissociation	k_{b1}	2000
$q_R + R_2 \to D_2$	Repressor-Load Binding	k_{a1}	2000
$D_2 \to q_R + R_2$	Repressor-Load Dissociation	k_{b1}	2000

Table A.2: Species in mechanistic model

State	Species
R	Repressor Monomer
R_2	Repressor Dimer
A	Activator Monomer
A_2	Activator Dimer
p_R	Promoter Regulating Repressor Expression
p_A	Promoter Regulating Activator Expression
C_1	Promoter-Activator Complex, Activator Expression
C_2	Promoter-Repressor Complex, Activator Expression
C_3	Promoter-Activator Complex, Repressor Expression
q_A	Load with affinity to the activator
q_R	Load with affinity to the repressor
D_1	Activator-Load Complex
D_2	Repressor-Load Complex

AGAGGAGTTAGTCTTGAAGTCATGCGCCGGTTAAGGCTAAACTGAAAGGACAAGTTTTGGTGACTGCGCTCCTCCAAGCC
AGTTACCTCGGTTCAAAGAGTTGGTAGCTCAGAGAACCTTCGAAAAACCGCCCTGCAAGGCGGTTTTTTCGTTTTCAGAG
CAAGAGATTACGCGCAGACCAAAACGATCTCAAGAAGATCATCTTATTAATCAGATAAAATATTTCTAGAGTCCCTATCA
GTGATAGAGATTGACATCCCTATCAGTGATAGAGATACTGAGCACTACTAGAGTCACACAGGACTACTAGATGGTGAATG
TGAAACCAGTAACGTTATACGATGTCGCAGAGTATGCCGGTGTCTCTTATCAGACCGTTTCCCGCGTGGTGAACCAGGCC
AGCCACGTTTCTGCGAAAACGCGGGAAAAAGTGGAAGCGGCGATGGCGGAGCTGAATTACATTCCCAACCGCGTGGCACA
ACAACTGGCGGGCAAACAGTCGTTGCTGATTGGCGTTGCCACCTCCAGTCTGGCCCTGCACGCGCCGTCGCAAATTGTCG
CGGCGATTAAATCTCGCGCCGATCAACTGGGTGCCAGCGTGGTGGTGTCGATGGTAGAACGAAGCGGCGTCGAAGCCTGT
AAAGCGGCGGTGCACAATCTTCTCGCGCAACGCGTCAGTGGGCTGATCATTAACTATCCGCTGGATGACCAGGATGCCAT
TGCTGTGGAAGCTGCCTGCACTAATGTTCCGGCGTTATTTCTTGATGTCTCTGACCAGACACCCATCAACAGTATTATTT
TCTCCCATGAAGACGGTACGCGACTGGGCGTGGAGCATCTGGTCGCATTGGGTCACCAGCAAATCGCGCTGTTAGCGGGC
CCATTAAGTTCTGTCTCGGCGCGTCTGCGTCTGGCTGGCTGGCATAAATATCTCACTCGCAATCAAATTCAGCCGATAGC
GGAACGGGAAGGCGACTGGAGTGCCATGTCCGGTTTTCAACAAACCATGCAAATGCTGAATGAGGGCATCGTTCCCACTG
CGATGCTGGTTGCCAACGATCAGATGGCGCTGGGCGCAATGCGCGCCATTACCGAGTCCGGGCTGCGCGTTGGTGCGGAT
ATCTCGGTAGTGGGATACGACGATACCGAAGACAGCTCATGTTATATCCCGCCGTTAACCACCATCAAACAGGATTTTCG
CCTGCTGGGGCAAACCAGCGTGGACCGCTTGCTGCAACTCTCTCAGGGCCAGGCGGTGAAGGGCAATCAGCTGTTGCCCG
TCTCACTGGTGAAAAGAAAAACCACCCTGGCGCCCAATACGCAAACCGCCTCTCCCCGCGCGTTGGCCGATTCATTAATG
CAGCTGGCACGACAGGTTTCCCGACTGGAAAGCGGGCAGGCTGCAAACGACGAAAACTACGCTTTAGTAGCTTAATAACT
CTGATAGTGCTAGTGTAGATCTCTACTAGAGCCAGGCATCAAATAAAACGAAAGGCTCAGTCGAAAGACTGGGCCTTTCG
TTTTATCTGTTGTTTGTCGGTGAACGCTCTCTACTAGAGTCACACTGGCTCACCTTCGGGTGGGCCTTTCTGCGTTTATA
TACTAGAGTTTATGGCTAGCTCAGTCCTAGGTACAATGCTAGCTACTAGAGAAAGAGGAGAAATACTAGATGTCCAGATT
AGATAAAAGTAAAGTGATTAACAGCGCATTAGAGCTGCTTAATGAGGTCGGAATCGAAGGTTTAACAACCCGTAAACTCG
CCCAGAAGCTAGGTGTAGAGCAGCCTACATTGTATTGGCATGTAAAAAATAAGCGGGGCTTTGCTCGACGCCTTAGCCATT
GAGATGTTAGATAGGCACCATACTCACTTTTGCCCTTTAGAAGGGGAAAGCTGGCAAGATTTTTTACGTAATAACGCTAA
AAGTTTTAGATGTGCTTTACTAAGTCATCGCGATGGAGCAAAAGTACATTTAGGTACACGGCCTACAGAAAAACAGTATG
AAACTCTCGAAAATCAATTAGCCTTTTTATGCCAACAAGGTTTTTCACTAGAGAATGCATTATATGCACTCAGCGCTGTG
GGGCATTTTACTTTAGGTTGCGTATTGGAAGATCAAGAGCATCAAGTCGCTAAAGAAGAAAGGGAAACACCTACTACTGA
TAGTATGCCGCCATTATTACGACAAGCTATCGAATTATTTGATCACCAAGGTGCAGAGCCAGCCTTCTTATTCGGCCTTG
AATTGATCATATGCGGATTAGAAAAACAACTTAAATGTGAAAGTGGGTCCGCTGCAAACGACGAAAACTACGCTTTAGTA
GCTTAATAACACTGATAGTGCTAGTGTAGATCACTACTAGAGCCAGGCATCAAATAAAACGAAAGGCTCAGTCGAAAGAC
TGGGCCTTTCGTTTTATCTGTTGTTTGTCGGTGAACGCTCTCTACTAGAGTCACACTGGCTCACCTTCGGGTGGGCCTTT
CTGCGTTTATATACTAGTAGCGGCCGCTGCAGAAGCTTTAATGCGGTAGTTTATCACAGTTAAATTGCTAACGCAGTCAG
GCACCGTGTATGAAATCTAACAATGCGCTCATCGTCATCCTCGGCACCGTCACCCTGGATGCTGTAGGCATAGGCTTGGT
TATGCCGGTACTGCCGGGCCTCTTGCGGGATATCGTCCATTCCGACAGCATCGCCAGTCACTATGGCGTGCTGCTAGCGC
TATATGCGTTGATGCAATTTCTATGCGCACCCGTTCTCGGAGCACTGTCCGACCGCTTTGGCCGCCGCCCAGTCCTGCTC
GCTTCGCTACTTGGAGCCACTATCGACTACGCGATCATGGCGACCACACCCGTCCTGTGGATCCTCTACGCCGGACGCAT
CGTGGCCGGCATCACCGGCGCCACAGGTGCGGTTGCTGGCGCCTATATCGCCGACATCACCGATGGGGAAGATCGGGCTC
GCCACTTCGGGCTCATGATATAAACGCAGAAAGGCCCACCCGAAGGTGAGCCAGTGTGACTCTAGTAGAGAGCGTTCACC
GACAAACAACAGATAAAACGAAAGGCCCAGTCTTTCGACTGAGCCTTTCGTTTTATTTGATGCCTGGTTATTAAGCTACT
AAAGCGTAGTTTTCGTCGTTTGCAGCAGGCCTTTTGTATAGTTCATCCATGCCATGTGTAATCCCAGCAGCTGTTACAAA
CTCAAGAAGGACCATGTGGTCTCTCTTTTCGTTGGGATCTTTCGAAAGGGCAGATTGTGTGGACAGGTAATGGTTGTCTG
GTAAAAGGACAGGGCCATCGCCAATTGGAGTATTTTGTTGATAATGGTCTGCTAGTTGAACGCTTCCATCTTCAATGTTG
TGTCTAATTTTGAAGTTAACTTTGATTCCATTCTTTTGTTTGTCTGCCATGATGTATACATTGTGTGAGTTATAGTTGTA
TTCCAATTTGTGTCCAAGAATGTTTCCATCTTCTTTAAAATCAATACCTTTTAACTCGATTCTATTAACAAGGGTATCAC
CTTCAAACTTGACTTCAGCACGTGTCTTGTAGTTCCCGTCATCTTTGAAAAATATAGTTCTTTCCTGTACATAACCTTCG
GGCATGGCACTCTTGAAAAAGTCATGCTGTTTCATATGATCTGGGTATCTCGCAAAGCATTGAACACCATAACCGAAAGT
AGTGACAAGTGTTGGCCATGGAACAGGTAGTTTTCCAGTAGTGCAAATAAATTTAAGGGTAAGTTTTCCGTATGTTGCAT
CACCTTCACCCTCTCCACTGACAGAAAATTTGTGCCCATTAACATCACCATCTAATTCAACAAGAATTGGGACAACTCCA
GTGAAAAGTTCTTCTCCTTTACGCATCTAGTATTTCTCCTCTTTCTCTAGTATGTGTGAAATTGTTATCCGCTCACAATT
CCACACAACATACGAGCCGGAAGCATAAAGTGTAAAGCCTGGGGTGCCTAATGAGTGAGCTAACTCACATTAATTGCGTT
GCGCTCACTGCCCGCTTTCCAGTCGGGAAACCTGTCGTGCCAGCTGCATTAATGAATCGGCCAACGCGCGGGGAGAGGCG
GTTTGCGTATTGCTCGGGCAGCGTTGGGTCCTGGCCACGGGTGCGCATGATCGTGCTCCTGTCGTTGAGGACCCGGCTAG
GCTGGCGGGGTTGCCTTACTGGTTAGCAGAATGAATCACCGATACGCGAGCGAACGTGAAGCGACTGCTGCTGCAAAACG
TCTGCGACCTGAGCAACAACATGAATGGTCTTCGGTTTCCGTGTTTCGTAAAGTCTGGAAACGCGGAAGTCCCCTACGTG
CTGCTGAAGTTGCCCGCAACAGAGAGTGGAACCAACCGGTGATACCACGATACTATGACTGAGAGTCAACGCCATGAGCG
GCCTCATTTCTTATTCTGAGTTACAACAGTCCGCACCGCTGTCCGGTAGCTCCTTCCGGTGGGCGCGGGGCATGACTATC
GTCGCCGCACTTATGACTGTCTTCTTTATCATGCAACTCGTAGGACAGGTGCCGGCAGCGCCCAACAGTCCCCCGGCCAC
GGGGCCTGCCACCATACCCACGCCGAAACAAGCGCCCTGCACCATTATGTTCCGGATCTGCATCGCAGGATGCTGCTGGC
TACCCTGTGGAACACCTACATCTGTATTAACGAAGCGCTAACCGTTTTTATCAGGCTCTGGGAGGCAGAATAAATGATCA
TATCGTCAATTATTACCTCCACGGGGAGAGCCTGAGCAAACTGGCCTCAGGCATTTGAGAAGCACACGGTCACACTGCTT
CCGGTAGTCAATAAACCGGTAAACCAGCAATAGACATAAGCGGCTATTTAACGACCCTGCCCTGAACCGACGACCGGGTC
GAATTTGCTTTCGAATTTCTGCCATTCATCCGCTTATTATCACTTATTCAGGCGTAGCACCAGGCGTTTAAGGGCACCAA
TAACTGCCTTAAAAAAATTACGCCCCGCCCTGCCACTCATCGCAGTACTGTTGTAATTCATTAAGCATTCTGCCGACATG
GAAGCCATCACAGACGGCATGATGAACCTGAATCGCCAGCGGCATCAGCACCTTGTCGCCTTGCGTATAATATTTGCCCA
TGGTGAAAACGGGGGCGAAGAAGTTGTCCATATTGGCCACGTTTAAATCAAAACTGGTGAAACTCACCCAGGGATTGGCT
GAGACGAAAAACATATTCTCAATAAACCCTTTAGGGAAATAGGCCAGGTTTTCACCGTAACACGCCACATCTTGCGAATA
TATGTGTAGAAACTGCCGGAAATCGTCGTGGTATTCACTCCAGAGCGATGAAAACGTTTCAGTTTGCTCATGGAAAACGG
TGTAACAAGGGTGAACACTATCCCATATCACCAGCTCACCGTCTTTCATTGCCATACG

>pUCop sequenced map for pUCop
AAGCTTGTCGACAATTGTGAGCGCTCACAATTGGATCCGAATTCACATGTGAGCAAAAGGCCAGCAAAAGGCCAGGAACC
GTAAAAAGGCCGCGTTGCTGGCGTTTTTCCATAGGCTCCGCCCCCCTGACGAGCATCACAAAAATCGACGCTCAAGTCAG
AGGTGGCGAAACCCGACAGGACTATAAAGATACCAGGCGTTTCCCCCTGGAAGCTCCCTCGTGCGCTCTCCTGTTCCGAC
CCTGCCGCTTACCGGATACCTGTCCGCCTTTCTCCCTTCGGGAAGCGTGGCGCTTTCTCATAGCTCACGCTGTAGGTATC
TCAGTTCGGTGTAGGTCGTTCGCTCCAAGCTGGGCTGTGTGCACGAACCCCCCGTTCAGCCCGACCGCTGCGCCTTATCC
GGTAACTATCGTCTTGAGTCCAACCCGGTAAGACACGACTTATCGCCACTGGCAGCAGCCACTGGTAACAGGATTAGCAG
AGCGAGGTATGTAGGCGGTGCTACAGAGTTCTTGAAGTGGTGGCCTAACTACGGCTACACTAGAAGAACAGTATTTGGTA
TCTGCGCTCTGCTGAAGCCAGTTACCTTCGGAAAAAGAGTTGGTAGCTCTTGATCCGGCAAACAAACCACCGCTGGTAGC
GGTGGTTTTTTTGTTTGCAAGCAGCAGATTACGCGCAGAAAAAAAGGATCTCAAGAAGATCCTTTGATCTTTTCTACGGG
GTCTGACGCTCAGTGGAACGAAAACTCACGTTAAGGGATTTTGGTCATGAGATTATCAAAAAGGATCTTCACCTAGATCC
TTTTAAATTAAAAATGAAGGTTTTAAATCAATCTAAAGTATATATGAGTAAACTTGGNCTGACAGTTACCAATGCTTAAT
CAGTGAGGCACCTATCTCAGNGGATTNNNNNTATTTTCGTCANCATANTGCCTGACTCCCNTCGTGTAGATACTACGATA
CGGGAGGGCTTACCATCTGGCCCCAGTGCTGCAATGATACCGCGAGACCCCACGCTCCCCGGCTCCAGATTATCAGCAAT
AAACCAGCCAGCCGGGAAGGGCCGAGCGCAGAAGTGGTCTGCAACTTTATCCGCCTCCATCCAGTCTATTAATTGTTGCC
GGGAAGCTAGAGTAAGTAGTTCGCCAGTTAATAGTTTGCGCAACGTTGTTGCCATTGCTACAGGCATCGTGGTGTCACGC
TCGTCGTTTGGTATGGCTTCATTCAGCTCCGGTTCCCAACGATCAAGGCGAGTTACATGATCCCCCATGTTGTGCAAAAA
AGCGGTTAGCTCCTTCGGTCCTCCGATCGTTGTCAGAAGTAAGTTGGCCGCAGTGTTATCACTCATGGTTATGGCAGCAC
TGCATAATTCTCTTACTGTCATGCCATCCGTAAGATGCTTTTCTGTGACTGGTGAGTACTCAACCAAGTCATTCTGAGAA
TAGTGTATGCGGCGACCGAGTTGCTCTTGCCCGGCGTCAATACGGGATAATACCGCGCCACATAGCAGAACTTTAAAAGT
GCTCATCATTGGAAAACGTTCTTCGGGGCGAAAACTCTCAAGGATCTTACCGCTGTTGAGATCCAGTTCGATGTAACCCA
CTCGTGCACCCAACTGATCTTCAGCATCTTTTACTTTCACCAGCGTTTCTGGGTGAGCAAAAACAGGAAGGCAAAATGCC
GCAAAAAAGGGAATAAGGGCGACACGGAAATGTTGAATACTCATACTCTTCCTTTTTCAATATTATTGAAGCATTTATCA
GGGTTATTGTCTCATGAGCGGATACATATTTGAATGTATTTAGAAAAATAAACAAATAGGGGTTCCGCGCACATTTCCCC
GAAAAGTGCCACCTGACGTC

>pUCblk sequenced map for pUCop
AAGCTTGTCGACGGATCCGAATTCACATGTGAGCAAAAGGCCAGCAAAAGGCCAGGAACCGTAAAAAGGCCGCGTTGCTG
GCGTTTTTCCATAGGCTCCGCCCCCCTGACGAGCATCACAAAAATCGACGCTCAAGTCAGAGGTGGCGAAACCCGACAGG
ACTATAAAGATACCAGGCGTTTCCCCCTGGAAGCTCCCTCGTGCGCTCTCCTGTTCCGACCCTGCCGCTTACCGGATACC
TGTCCGCCTTTCTCCCTTCGGGAAGCGTGGCGCTTTCTCATAGCTCACGCTGTAGGTATCTCAGTTCGGTGTAGGTCGTT
CGCTCCAAGCTGGGCTGTGTGCACGAACCCCCCGTTCAGCCCGACCGCTGCGCCTTATCCGGTAACTATCGTCTTGAGTC
CAACCCGGTAAGACACGACTTATCGCCACTGGCAGCAGCCACTGGTAACAGGATTAGCAGAGCGAGGTATGTAGGCGGTG
CTACAGAGTTCTTGAAGTGGTGGCCTAACTACGGCTACACTAGAAGAACAGTATTTGGTATCTGCGCTCTGCTGAAGCCA
GTTACCTTCGGAAAAAGAGTTGGTAGCTCTTGATCCGGCAAACAAACCACCGCTGGTAGCGGTGGTTTTTTTGTTTGCAA
GCAGCAGATTACGCGCAGAAAAAAAGGATCTCAAGAAGATCCTTTGATCTTTTCTACGGGGTCTGACGCTCAGTGGAACG
AAAACTCACGTTAAGGGATTTTGGTCATGAGATTATCAAAAAGGATCTTCACCTAGATCCTTTTAAATTAAAAATGAAGG
TTTTAAATCAATCTAAAGTATATATGAGTAAACTTGGNCTGACAGTTACCAATGCTTAATCAGTGAGGCACCTATCTCAG
NGGATTNNNNNTATTTTCGTCANCATANTGCCTGACTCCCNTCGTGTAGATACTACGATACGGGAGGGCTTACCATCTGG
CCCCAGTGCTGCAATGATACCGCGAGACCCCACGCTCCCCGGCTCCAGATTATCAGCAATAAACCAGCCAGCCGGGAAGG
GCCGAGCGCAGAAGTGGTCTGCAACTTTATCCGCCTCCATCCAGTCTATTAATTGTTGCCGGGAAGCTAGAGTAAGTAGT
TCGCCAGTTAATAGTTTGCGCAACGTTGTTGCCATTGCTACAGGCATCGTGGTGTCACGCTCGTCGTTTGGTATGGCTTC
ATTCAGCTCCGGTTCCCAACGATCAAGGCGAGTTACATGATCCCCCATGTTGTGCAAAAAAGCGGTTAGCTCCTTCGGTC
CTCCGATCGTTGTCAGAAGTAAGTTGGCCGCAGTGTTATCACTCATGGTTATGGCAGCACTGCATAATTCTCTTACTGTC
ATGCCATCCGTAAGATGCTTTTCTGTGACTGGTGAGTACTCAACCAAGTCATTCTGAGAATAGTGTATGCGGCGACCGAG
TTGCTCTTGCCCGGCGTCAATACGGGATAATACCGCGCCACATAGCAGAACTTTAAAAGTGCTCATCATTGGAAAACGTT
CTTCGGGGCGAAAACTCTCAAGGATCTTACCGCTGTTGAGATCCAGTTCGATGTAACCCACTCGTGCACCCAACTGATCT
TCAGCATCTTTTACTTTCACCAGCGTTTCTGGGTGAGCAAAAACAGGAAGGCAAAATGCCGCAAAAAAGGGAATAAGGGC
GACACGGAAATGTTGAATACTCATACTCTTCCTTTTTCAATATTATTGAAGCATTTATCAGGGTTATTGTCTCATGAGCG
GATACATATTTGAATGTATTTAGAAAAATAAACAAATAGGGGTTCCGCGCACATTTCCCCGAAAAGTGCCACCTGACGTC

BIBLIOGRAPHY

BIBLIOGRAPHY

[1] M. S. Levin, *Combinatorial Engineering of Decomposable Systems.* Springer, 1998.

[2] T. H. Cormen, C. E. Leiserson, R. L. Rivest, and C. Stein, "Dynamic Programming," in *Introduction to Algorithms*, 2nd ed. MIT Press, 2001, ch. 15, pp. 323–369.

[3] A. Snyder, "Encapsulation and Inheritance in Object-Oriented Programming Languages," in *Readings in Object-Oriented Database Systems*, S. B. Z. Zdonic and D. Maier, Eds. Morgan Kaufmann, 1990, ch. 1, pp. 84–90.

[4] D. Self, "Line Outputs," in *The Design of Active Crossovers.* Focal Press, 2011, ch. 15.

[5] A. K. Maini, *Digital Electronics: Principles, Devices and Applications.* John Wiley & Sons, Inc., 2007.

[6] E. Andrianantoandro, S. Basu, D. K. Karig, and R. Weiss, "Synthetic biology: new engineering rules for an emerging discipline." *Molecular systems biology*, vol. 2, p. 2006.0028, Jan. 2006.

[7] P. Schwille, "Bottom-up synthetic biology: engineering in a tinkerer's world." *Science (New York, N.Y.)*, vol. 333, no. 6047, pp. 1252–4, Sep. 2011.

[8] R. P. Shetty, D. Endy, and T. F. Knight, "Engineering BioBrick vectors from BioBrick parts." *Journal of biological engineering*, vol. 2, p. 5, Jan. 2008.

[9] P. E. M. Purnick and R. Weiss, "The second wave of synthetic biology: from modules to systems." *Nature reviews. Molecular cell biology*, vol. 10, no. 6, pp. 410–22, Jun. 2009.

[10] H. M. Sauro, "Modularity defined." *Molecular systems biology*, vol. 4, p. 166, Jan. 2008.

[11] S. Cardinale and A. P. Arkin, "Contextualizing context for synthetic biology - identifying causes of failure of synthetic biological systems." *Biotechnology journal*, vol. 7, no. 7, pp. 856–66, Jul. 2012.

[12] J. Saez-Rodriguez, A. Kremling, and E. D. Gilles, "Dissecting the puzzle of life: modularization of signal transduction networks," *Computers and Chemical Engineering*, vol. 29, no. 3, pp. 619–629, Feb. 2005.

[13] D. Del Vecchio, A. J. Ninfa, and E. D. Sontag, "Modular cell biology: retroactivity and insulation." *Molecular systems biology*, vol. 4, no. 161, p. 161, Jan. 2008.

[14] A. Faanes and S. Skogestad, "Buffer Tank Design for Acceptable Control Performance," *Industrial & Engineering Chemistry Research*, vol. 42, no. 10, pp. 2198–2208, May 2003.

[15] R. C. Li, *RF Circuit Design(Google eBook).* John Wiley & Sons, 2012.

[16] C. F. Taylor, *Internal Combustion Engine in Theory and Practice: Vol. 2 - 2nd Edition, Revised: Combustion, Fuels, Materials, Design.* MIT Press, 1985.

[17] P. Kokotovic, H. K. Khalil, and J. O'Reilly, *Singular Perturbation Methods in Control*. SIAM, 1999.

[18] D. Del Vecchio and J. Slotine, "A Contraction Theory Approach to Singularly Perturbed Systems," *IEEE Transactions on Automatic Control*, vol. 1, no. c, pp. 1–1, 2012.

[19] A. Gyorgy and D. Del Vecchio, "Retroactivity to the Input and Thevenin's Theorem for Complex Gene Transcription Networks," *Decision and Control, 2012 (to appear)*, 2012.

[20] K. H. Kim and H. M. Sauro, "Fan-out in gene regulatory networks," *Journal of biological engineering*, vol. 4, no. 1, p. 16, Jan. 2010.

[21] H. R. Ossareh, A. C. Ventura, S. D. Merajver, and D. Del Vecchio, "Long signaling cascades tend to attenuate retroactivity." *Biophysical journal*, vol. 100, no. 7, pp. 1617–26, Apr. 2011.

[22] P. Liu, I. G. Kevrekidis, and S. Y. Shvartsman, "Substrate-dependent control of ERK phosphorylation can lead to oscillations." *Biophysical journal*, vol. 101, no. 11, pp. 2572–81, Dec. 2011.

[23] Y. Kim, Z. Paroush, K. Nairz, E. Hafen, G. Jiménez, and S. Y. Shvartsman, "Substrate-dependent control of MAPK phosphorylation in vivo." *Molecular systems biology*, vol. 7, p. 467, Feb. 2011.

[24] P. Jiang, A. C. Ventura, E. D. Sontag, A. J. Ninfa, D. Del Vecchio, and S. D. Merajver, "Load-induced modulation of signal transduction networks." *Science signaling*, vol. 4, no. 194, p. ra67, Jan. 2011.

[25] A. C. Ventura, P. Jiang, L. Van Wassenhove, D. Del Vecchio, S. D. Merajver, and A. J. Ninfa, "Signaling properties of a covalent modification cycle are altered by a downstream target." *Proceedings of the National Academy of Sciences of the United States of America*, vol. 107, no. 22, pp. 10 032–7, Jun. 2010.

[26] E. Franco, E. Friedrichs, J. Kim, R. Jungmann, R. Murray, E. Winfree, and F. C. Simmel, "Timing molecular motion and production with a synthetic transcriptional clock." *Proceedings of the National Academy of Sciences of the United States of America*, vol. 108, no. 40, pp. E784–93, Oct. 2011.

[27] N. E. Buchler and M. Louis, "Molecular titration and ultrasensitivity in regulatory networks." *Journal of molecular biology*, vol. 384, no. 5, pp. 1106–19, Dec. 2008.

[28] N. E. Buchler and F. R. Cross, "Protein sequestration generates a flexible ultrasensitive response in a genetic network." *Molecular systems biology*, vol. 5, no. 272, p. 272, Jan. 2009.

[29] T.-H. Lee and N. Maheshri, "A regulatory role for repeated decoy transcription factor binding sites in target gene expression." *Molecular systems biology*, vol. 8, no. 576, p. 576, Jan. 2012.

[30] A. Burger, A. M. Walczak, and P. G. Wolynes, "Abduction and asylum in the lives of transcription factors." *Proceedings of the National Academy of Sciences*, vol. 107, no. 9, pp. 4016–21, Mar. 2010.

[31] R. Guantes and J. F. Poyatos, "Dynamical principles of two-component genetic oscillators." *PLoS computational biology*, vol. 2, no. 3, p. e30, Mar. 2006.

[32] A. Relógio, P. O. Westermark, T. Wallach, K. Schellenberg, A. Kramer, and H. Herzel, "Tuning the mammalian circadian clock: robust synergy of two loops." *PLoS computational biology*, vol. 7, no. 12, p. e1002309, Dec. 2011.

[33] E. Conrad, A. E. Mayo, A. J. Ninfa, and D. B. Forger, "Rate constants rather than biochemical mechanism determine behaviour of genetic clocks." *Journal of the Royal Society, Interface / the Royal Society*, vol. 5 Suppl 1, pp. S9–15, Aug. 2008.

[34] J. Dunlap, "The Molecular bases for circadian clocks," *Cell*, vol. 96, pp. 271–290, 1999.

[35] H. Ukai and H. R. Ueda, "Systems biology of mammalian circadian clocks." *Annual review of physiology*, vol. 72, no. 6, pp. 579–603, Jan. 2010.

[36] D. Del Vecchio, "Design and Analysis of an Activator-Repressor Clock in E. Coli," in *American Control Conference, 2007. ACC '07.* IEEE, Jul. 2007, pp. 1589–1594.

[37] A. J. Ninfa, M. R. Atkinson, D. Forger, S. Atkins, D. Arps, S. Selinsky, D. Court, N. Perry, and A. E. Mayo, "A Synthetic Biology Approach to Understanding Biological Oscillations : Developing a Genetic Oscillator for Escherichia coli," in *Bacterial Circadian Programs*, J. L. Ditty, Ed. Springer-Verlag, 2009, pp. 301–329.

[38] M. R. Atkinson, M. A. Savageau, J. T. Meyers, and A. J. Ninfa, "Development of genetic circuitry exhibiting toggle switch or oscillatory behavior in \it {E}scherichia coli \rm," *Cell*, vol. 113, pp. 597–607, 2003.

[39] M. Tigges, T. T. Marquez-Lago, J. Stelling, and M. Fussenegger, "A tunable synthetic mammalian oscillator." *Nature*, vol. 457, no. 7227, pp. 309–12, Jan. 2009.

[40] T. Danino, O. Mondragón-Palomino, L. S. Tsimring, and J. Hasty, "A synchronized quorum of genetic clocks." *Nature*, vol. 463, no. 7279, pp. 326–30, Jan. 2010.

[41] J. Hasty, M. Dolnik, V. Rottsch?fer, and J. J. Collins, "Synthetic Gene Network for Entraining and Amplifying Cellular Oscillations," *Physical Review Letters*, vol. 88, pp. 148 101.1–148 101.4, 2002.

[42] J. Stricker, S. Cookson, M. R. Bennett, W. H. Mather, L. S. Tsimring, and J. Hasty, "A fast, robust and tunable synthetic gene oscillator." *Nature*, vol. 456, no. 7221, pp. 516–9, Nov. 2008.

[43] J. M. G. Vilar, H. Y. Kueh, N. Barkai, and S. Leibler, "Mechanisms of noise-resistance in genetic oscillators." *Proceedings of the National Academy of Sciences of the United States of America*, vol. 99, no. 9, pp. 5988–92, Apr. 2002.

[44] C. H. Ko and J. S. Takahashi, "Molecular components of the mammalian circadian clock." *Human molecular genetics*, vol. 15 Spec No, no. suppl_2, pp. R271–7, Oct. 2006.

[45] E. M. Ozbudak, M. Thattai, H. N. Lim, B. I. Shraiman, and A. Van Oudenaarden, "Multistability in the lactose utilization network of Escherichia coli." *Nature*, vol. 427, no. 6976, pp. 737–40, Feb. 2004.

[46] U. Alon, *An introduction to systems biology. {D}esign principles of biological circuits.* Chapman-Hall, 2007.

[47] H. K. Khalil, *Nonlinear Systems.* Prentice Hall, 2002.

[48] M. R. Atkinson, M. A. Savageau, J. T. Myers, and A. J. Ninfa, "Development of Genetic Circuitry Exhibiting Toggle Switch or Oscillatory Behavior in Escherichia coli," *Cell*, vol. 113, no. 5, pp. 597–607, May 2003.

[49] Y. A. Kuznetsov, *Elements of Applied Bifurcation Theory.* New York, NY: Springer-Verlag, 2004.

[50] N. Barkai and S. Leibler, "Circadian clocks limited by noise." *Nature*, vol. 403, no. 6767, pp. 267–8, Jan. 2000.

[51] C. R. Cantor and P. R. Schimmel, *Biophysical Chemistry: The Behavior of biological macromolecules.* W. H. Freeman, 1980.

[52] S. Wiggins, *Introduction to Applied Nonlinear Dynamical Systems and Chaos*. Springer-Verlag, 1990.

[53] V. K. Mutalik and K. V. Venkatesh, "A theoretical steady state analysis indicates that induction of Escherichia coli glnALG operon can display all-or-none behavior." *Bio Systems*, vol. 90, no. 1, pp. 1–19, 2007.

[54] M. Stamatakis and N. V. Mantzaris, "Comparison of deterministic and stochastic models of the lac operon genetic network." *Biophysical journal*, vol. 96, no. 3, pp. 887–906, Feb. 2009.

[55] D. T. Gillespie, "Exact Stochastic Simulation of Coupled Chemical Reactions," *The Journal of Physical Chemistry*, vol. 81, pp. 2340–2361, 1977.

[56] J. J. Hornberg, B. Binder, F. J. Bruggeman, B. Schoeber, R. Heinrich, and H. V. Westerhoff, "Control of {MAPK} signaling: from complexity to what really matters," *Oncogene*, vol. 24, pp. 5533–5542, 2005.

[57] J. M. Rohwer, N. D. Meadow, S. Roseman, H. V. Westerhoff, and P. W. Postma, "Understanding glucose transport by the bacterial phosphoenolpyruvate:glycose phosphotransferase system on the basis of kinetic measurements in vitro." *The Journal of biological chemistry*, vol. 275, no. 45, pp. 34 909–21, Nov. 2000.

[58] J. Elf, G.-W. Li, and X. S. Xie, "Probing transcription factor dynamics at the single-molecule level in a living cell." *Science (New York, N.Y.)*, vol. 316, no. 5828, pp. 1191–4, May 2007.

[59] M. Dunaway, J. S. Olson, J. M. Rosenberg, O. B. Kallai, R. E. Dickerson, and K. S. Matthews, "Kinetic studies of inducer binding to lac repressor.operator complex." *The Journal of biological chemistry*, vol. 255, no. 21, pp. 10 115–9, Nov. 1980.

[60] E. Klipp, R. Herwig, A. Kowald, C. Wierling, and H. Lehrach, *Systems Biology in Practice*. Wiley-VCH, 2005.

[61] A. Kumar, P. Christofides, and P. Daoutidis, "Singular perturbation modeling of nonlinear processes with non explicit time-scale multiplicity," *Chemical Engineering Science*, vol. 53, pp. 1491–1504, 1998.

[62] A. Ciliberto, F. Capuani, and J. J. Tyson, "Modeling Networks of coupled enzymatic reactions using the total quasi-steady state approximation," *PLOS Computational Biology*, vol. 3, no. 3, pp. 463–472, 2007.

[63] B. Alberts, A. Johnson, J. Lewis, M. Raff, K. Roberts, and P. Walter, *Molecular Biology of the Cell*. Garland Science, 2002.

[64] C. F. Huang and J. E. Ferrell, "Ultrasensitivity in the mitogen-activated protein kinase cascade," *Proc. Natl. Acad. Sci.*, vol. 93, no. 19, pp. 10 078–10 083, 1996.

[65] J. Keener and J. Sneyd, *Mathematical Physiology: I: Cellular Physiology*, 2nd ed. Springer, Oct. 2008.

[66] M. A. Shea and G. K. Ackers, "The \text{O}_R Control System of Bacteriophage Lambda A Physical-Chemical Model for Gene Regulation," *J. Mol. Biol.*, vol. 181, pp. 211–230, 1985.

[67] T. Mizuno, "His-Asp phosphotransfer signal transduction." *Journal of biochemistry*, vol. 123, no. 4, pp. 555–63, Apr. 1998.

[68] S. Jagadeesen, P. Mann, C. W. Schink, and P. I. Higgs, "A novel "four-component" two component signal transduction mechanism regulates developmental progression in Myxococcus xanthus." *The Journal of biological chemistry*, Jun. 2009.

[69] J. Stülke and W. Hillen, "Coupling physiology and gene regulation in bacteria: the phosphotransferase sugar uptake system delivers the signals." *Die Naturwissenschaften*, vol. 85, no. 12, pp. 583–92, Dec. 1998.

[70] S. Sastry, *Nonlinear Systems: Analysis, Stability, and Control*, 1st ed. Springer, Jun. 1999.

[71] N. G. van Kampen, *Stochastic Processes in Physics and Chemistry*, third edit ed. North Holland, 2007.

[72] J. Hespanha and A. Singh, "Stochastic Models for Chemically Reacting Systems Using Polynomial Stochastic Hybrid Systems," *Int. J. on Robust Control, Special volume on Control at Small Scales: volume 1*, vol. 15, pp. 669–689, 2005.

[73] C. W. Gardiner, *Handbook of Stochastic Methods: For Physics, Chemistry and the Natural Sciences*. Springer, 1996.

[74] D. T. Gillespie, "The chemical Langevin equation," *The Journal of Chemical Physics*, vol. 113, no. 1, pp. 297–306, 2000.

[75] "Registry of Biological Parts." [Online]. Available: http://partsregistry.org/Main_Page

[76] H. E. Kubitschek and J. A. Friske, "Determination of bacterial cell volume with the Coulter Counter," *Journal of Bacteriology*, vol. 168, no. 3, pp. 1466–7, Dec. 1986.

[77] J. M. Flynn, I. Levchenko, M. Seidel, S. H. Wickner, R. T. Sauer, and T. A. Baker, "Overlapping recognition determinants within the ssrA degradation tag allow modulation of proteolysis," *Proceedings of the National Academy of Sciences*, vol. 98, no. 19, 2001.

[78] J. B. Andersen, C. Sternberg, L. K. Poulsen, S. P. Bjorn, M. Givskov, and S. Molin, "New unstable variants of green fluorescent protein for studies of transient gene expression in bacteria." *Applied and environmental microbiology*, vol. 64, no. 6, pp. 2240–6, Jun. 1998.

[79] P. Schubert, K. Pfleiderer, and W. Hillen, "Tet repressor residues indirectly recognizing anhydrotetracycline." *European Journal of Biochemistry*, vol. 271, no. 11, pp. 2144–52, Jun. 2004.

[80] D. Hansen and W. Hillen, "Tryptophan in alpha-helix 3 of Tet repressor forms a sequence-specific contact with tet operator in solution," *Journal of Biological Chemistry*, vol. 262, no. 25, pp. 12 269–74, Sep. 1987.

[81] C. M. Falcon and K. S. Matthews, "Operator DNA sequence variation enhances high affinity binding by hinge helix mutants of lactose repressor protein." *Biochemistry*, vol. 39, no. 36, pp. 11 074–83, Sep. 2000.

[82] H. Backes, C. Berens, V. Helbl, S. Walter, F. X. Schmid, and W. Hillen, "Combinations of the alpha-helix-turn-alpha-helix motif of TetR with respective residues from LacI or 434Cro: DNA recognition, inducer binding, and urea-dependent denaturation." *Biochemistry*, vol. 36, no. 18, pp. 5311–22, May 1997.

[83] P. Orth, D. Schnappinger, and W. Hillen, "Structural basis of gene regulation by the tetracycline inducible Tet repressor-operator system," *Nature Structural Biology*, pp. 215–219, 2000.

[84] D. Nevozhay, R. M. Adams, K. F. Murphy, K. Josic, and G. Balázsi, "Negative autoregulation linearizes the dose-response and suppresses the heterogeneity of gene expression." *Proceedings of the National Academy of Sciences*, vol. 106, no. 13, pp. 5123–8, Mar. 2009.

[85] A. Goldbeter and D. E. Koshland, "An amplified sensitivity arising from covalent modification in biological systems," *Proceedings National Academy of Sciences*, vol. 78, no. 11, pp. 6840–6844, 1981.

[86] M. Hsieh and M. Brenowitz, "Comparison of the DNA Association Kinetics of the Lac Repressor Tetramer, Its Dimeric Mutant LacIadi, and the Native Dimeric Gal Repressor," *Journal of Biological Chemistry*, vol. 272, no. 35, pp. 22 092–22 096, Aug. 1997.

[87] J. K. Barry and K. S. Matthews, "Thermodynamic analysis of unfolding and dissociation in lactose repressor protein." *Biochemistry*, vol. 38, no. 20, pp. 6520–8, May 1999.

[88] M. M. Levandoski, O. V. Tsodikov, D. E. Frank, S. E. Melcher, R. M. Saecker, and M. T. Record, "Cooperative and anticooperative effects in binding of the first and second plasmid Osym operators to a LacI tetramer: evidence for contributions of non-operator DNA binding by wrapping and looping." *Journal of Molecular biology*, vol. 260, no. 5, pp. 697–717, Aug. 1996.

[89] E. A. Birge and K. Low, "Detection of transcribable recombination products following conjugation in Rec+, RecB and RecC strains of Escherichia coli K12," *Journal of Molecular Biology*, vol. 83, no. 4, pp. 447–457, Mar. 1974.

[90] "Coli Genetic Stock Center." [Online]. Available: http://cgsc.biology.yale.edu/index.php

[91] T. Schmidt, K. Friehs, and E. Flaschel, "Rapid determination of plasmid copy number," *Journal of Biotechnology*, vol. 49, pp. 219–229, 1996.

[92] S. J. Projan, S. Carleton, and R. P. Novick, "Determination of Plasmid Copy Number by Fluorescence Densitometry," *Plasmid*, vol. 9, pp. 182–190, 1983.